Politechnika Krakowska im. Tadeusza Kościuszki

Wydział Inżynierii Środowiska i Energetyki

Rozprawa doktorska

MODELING ANALYSIS HEAT LOSSES IN DISTRICT HEATING NETWORK

mgr inż. Dariusz Jakubek

Promotor: dr hab. inż. Marzena Nowak-Ocłoń

Kraków, 2023

Pragnę podziękować mojej promotor
dr hab. inż. Marzenie Nowak-Ocłoń
za okazaną pomoc, cenne uwagi, cierpliwość i życzliwość.

Serdeczne podziękowania
prof. dr hab. inż. Pawłowi Ocłoń
za zainteresowanie się problematyką mojej pracy doktorskiej,
które z czasem przerodziło się w owocną współpracę.
Dariusz Jakubek

Nomenclature

b distance between the pipes axes, m

D external diameter, m

d internal diameter, m

DN nominal diameter,

H depth of foundation, m

h heat transfer coefficient, W/(m^{2}K)

R thermal resistance, (mK)/W

r radius, m

s thickness of the pipe, m

L length, m

q heat losses, W/m

T number of days of the heating season, days

t temperature, °C

NPV Net present value, PLN

NPVR net present value ratio, PLN

IRR internal rate of return)

DPBT dynamic payback time)

Greek symbols

λ thermal conductivity, W/(mK)

Subscripts

d domain

gr ground

is insulation

o summer

r	return
s	supply
w	winter

1. The historical and technical development of district heating systems

The most basic building heating systems have been powered by fuel, which can be burned in many different ways. The types of fuel used include wood, charcoal, coal, natural gas, and oil. In the beginning, the fuel was burned in open fireplaces, but enclosed stoves became more popular from the XIX century onwards. The burned fuel was used to heat up water or to produce steam which circulated in a closed cycle around the building supplying radiators.

Based on the definition [1], the district heating system (DH) is the way heat is distributed and produced in a centralized location through insulated pipes for various heating requirements, like space heating or hot water. The development process first began in large buildings among housing estates and was subsequently extended to individual homes. The acceleration of the development process in the United Kingdom was caused by a massive number of natural gas sources across the country. For that reason soon even large apartments were equipped with individual boilers. However, Central and Eastern European countries, including Denmark, Sweden, Germany, and the USSR, moved to district heating (DH).

One of the first district heating systems that supplied hot water to housing estates is mentioned by historians in fourteenth century France [2]. The hot water was obtained from an underground thermal bath, similar to the solutions commonly used in Rome. In the United States, the steam system was established in the late 1880s and successfully pawed the way for modern DH. Intriguingly, early DH steam systems were not used for providing hot water to home estates, but rather the steam was used for powering generators before electricity networks appeared. The most recognized district heating system in the United States is based on steam. It is considered to be the first generation of district heating. For dozens of years, steam distribution was the most developed technology. Steam was considered as a good heat carrier due to high heat content, what is more, it’s available from boilers or steam power plants. Steam-based system fuelled by coal used concrete ducts. Inside of the concrete duct typically were placed two pipes. One larger pipe was responsible for supply, and small return pipe. Corrosion is the main difficulty with return pipes, hence condensate return pipes are mostly disconnected. Modernisation and installing new condensation pipes are considered as too expensive, therefore condensate is drained at customer’s location. Typical temperature of the steam is up to 300 °C, and the pressure is up to 20 bar. High temperature inside of the channels and their poor insulation cause large heat losses during the distribution process.

Nowadays, the first generation of DH is outdated but still some of system are still in use for instance in Paris or New York. In relation to the supply capacity, the largest network is located in New York City, which was launched in 1882. In the meantime, the development of DH systems in Europe was completely different. Hot water has numerous advantages over steam systems. For instance:

- Reducing the environmental impact
- Lowering distribution loses
- Ability to integrate with additional heat sources

The impact to the environment is related to lower CO_2 emissions. An example of an additional heat source is solar thermal collectors. Steam systems in the largest cities were gradually converted to or replaced by water systems. At an early stage, engineers successfully implemented other sources of heat. Waste incinerators partly handle the disposal problem. The first notable example is located in Copenhagen, which has been supplying heat to hospitals since 1903.

Since 1970, there has been a rapid growth of DH in the United Kingdom due to a government research program. In 1979, *Energy Paper 35* was established, which concluded that there are no technical limits for the DH city-wide system. That technology could represent a low-cost heating energy system for cities. A major incentive for the development of DH systems in European countries was the price of fuel. The Organization of the Petroleum Exporting Countries (OPEC) increased the price of oil, hence countries with limited access to natural fossil fuels were facing the problem of natural alternatives like Sweden or Denmark[3-5].

Since 1930 to 1970 the second generation of DH was common [3-5]. As a carrier of heat was used water whose temperature was 160 $-$ 220 °C $[320 - 420\ F]$ and saturated pressure from 5 – 25 bar $[75 - 367\ psig]$. Main components of typical second generation network were tube-and-shell heat exchangers, concrete dusts, steel water pipes. There are numerous of advantages over system based on steam, like:

- Reduction of the risks and their consequences in case of failure
- Simple way of metering heat consumption
- Better energy quality and energy usage

Systems which based on water have closed circuits, therefore they require little make up and constantly blow down is not required. Comparing that to the steam systems they are losing 1,5% to 3,0% of boiler power output due to required blow downs. What is more uneven firing in steam system causes extensive heat loses through boiler. In Soviet Union countries open system was commonly used. It allowed consumers to use hot water directly from network. Another example of second generation system was in Iceland. Due to numerous geothermal energy sources, the heat obtained from free geothermal energy.

The main characteristic which differentiate third generation from the previous is material and labour of components. In this generation the components (pre insulated pipes) are buried directly into the ground. All components like valves, pre insulated pipes, T-pipes are prefabricated in factories therefore, components are reproducible and reliable. What is more the initial shape is applied during production. As a final product the curved pipes or prefabricated joints are obtained as required in the project. 3rd generation is commonly called "Scandinavian", the reason of that is due to commercialization in named country. It was introduced in 1970 but generally used since 1980 up to 2010. Water under the pressure was used as heat carrier. The operating temperatures were below 110°C. Focusing on new technology was triggered by oil crises in the 70s. As alternative of fuel biomass and waste were used.

Applying the 3rd generation allows for reducing the operation and investment costs. As a principal development is reducing the operating temperature. Lower temperature leads to savings on distribution due to smaller heat transfer losses, along with the opportunity to use other renewable heat sources. Manufacturing development of pre-insulated pipes and their insulation have huge influence on lifetime and maintenance of the district heating network.

This generation has usually steel media pipes, however the cupper and PEX material was also used. Transmission tubes were insulated with polyurethane insulation merged to the core. To stop diffusion, the aluminium foil were used as barrier. Outer layer coast is made out of PEHD (grade material PE 80 is minimum). The TwinPipe system was introduced in 3rd generation of DH. Thanks for this concept the overall network investment and installation cost was reduced in comparison to separate pipelines.

The next 4th generation of the DH operate on even lower temperatures than the previous generation. Reduced temperature in the system not only increases the efficiency of

the system but reliability and flexibility also. Ability to integrate this system to district cooling and fossil free energy sources, HVAC systems in not negligible. The new generation is an integrated system where gas, electricity, heating and cooling are working together to achieve an optimal solution. The concept assumes to use any kind of thermal energy like CHP, surplus heat from industry, additional heat from waste, solar thermal and fluctuating electricity via electric boilers or heat pumps[6-7].

2. Introduction

The European Union (EU) has for many years undertaken numerous activities related to improving the environment by reducing pollutants and improving energy efficiency. The district heating system (DHS) is one of the most popular systems for covering the energy demand and energy for domestic hot water in buildings in urban areas. It shows a great potential for future low carbon energy systems with a more efficient use of energy sources, including renewable energy sources.

In Poland, district heating supplies 40% of the heat demand and its length is 21,701 km (URE data for 2019). Polish heating systems are fundamentally different from similar infrastructures in other European countries. The structure of the heating network in a given city is usually very individual, which means that modernisation concepts must be developed individually, taking into account local conditions. Reducing heat losses through transmission creates the most effective system and enables the use of the most efficient heat source (Mathiesen et al. [8]).

Many authors have analysed different models for energy efficient district heating networks. One such method is proposed by Dobos et al. in their paper [9], where the proposed non-linear model predictive controller (NMPC) model aims to adapt the current heat demand to the customer's needs and distribute the appropriate amount of heat in the network.There is observed a significant increase in using TwinPipe pre-insulated in district heating system (DHS) installations. Bøhm and Kristjansson [10] compared the pair of single pipes and the main advantage of them is lower cost of building the network. They found that also shape of the insulation has tremendous impact in heat losses. The egg-shaped TwinPipe can reduce the heat loss up to 37% in comparison to traditional pre-insulated pair of pipes and 7% compared to TwinPipes.

Chen et al. [11] in order to bridge the gap between measured and theoretical heat losses, they developed a combined model based on a theoretical heat loss determination model and

an artificial neural network model. The results show that the predicted heat losses using the developed combined model reproduce the measured data well. Moreover, compared with the original pipe diameter and insulation layer thickness, the optimized pipe diameter and insulation layer thickness values using the proposed combined model are increased

Chicherin et al. [12] proposed new model to evaluate heat losses and the demand of 4th generation DH. The result of this model showed the positive effect of modernization thermal insulation.

Usman and Kim's study [13] used a computational fluid dynamics method to evaluate the optimal insulation thickness based on material and excavation costs in South Korea. In a study of a micro-hybrid district heating system with a fuel cell fueled by natural gas, a heat pump, and solar panels, they calculated heat losses in a 500-meter pipe supplying hot water at 60°C in polyethylene, ethylene propylene rubber, and polyurethane insulation using ANSYS Fluent 17.2. It was shown that heat loss is minimal when PU foams are used. A cost estimation analysis showed an optimum insulation thickness of 32 mm.

The common method of reducing heat loss is reduction of network operating temperature. was proposed in papers by Pirouti et al. [14] and Neirotti et al. [15]

This development of future DH was discussed by Lund et al [17] to the so-called low-temperature DH (the part of the 4^{th} generation DH) using also smart energy systems. The integration of district heating into a future smart energy system based on renewable energy sources also by using 4^{th} generation DH was mentioned by Lund et al [18]. Wirtz et al [19] proposed the 5^{th} generation DH which temperature is lower than 50°C. It will use waste heat, heat and cold storage facilities and renewable energy installations. To make this system more effective there is proposed the model by Quaggiotto et al [20] to management of predictive control operation for DH network.

The potential of fifth generation district heating and cooling (5GDHC) networks was studied in his work by Bilardo et al [21]. They analyzed the energy benefits of connecting several users in a bidirectional fifth generation network based on the integration of reversible heat pumps with on-site renewable generation and waste energy recovery. An integrated 5GDHC network model with buildings along with their energy characteristics was developed to meet the energy needs of a district consisting of users with different energy profiles throughout the year. The integration of established technologies with fifth generation thermal networks has been emphasized, keeping in mind the future development of near-zero energy districts (nZED).

Gross at all [22] in their work presented the DHS working in different temperature low (60 °C) and ultra-low (20 °C). In their examples are calculated the heat losses in the pipes. The results show a heat loss reduction in ultra-low temperature networks due to lower network working temperatures (20 °C) of about 80% compared to a low-temperature network.

Zhu et al. [23] in order to reduce heat loss in a district heating system, booster heat pumps (BHPs) were applied to utilize low-temperature heat sources in district heating. In the experimental study, the thermal behavior, steady-state heat loss of the BHP device was analyzed for cases with different feed water temperature and different flow rate on the user side

Krawczyk [24] described real disadvantageous which are associated with reduction of the working temperature in network system. There are also two other solutions for reducing the heat losses in transportation. The first is using the thicker layers of thermal insulation or heating networks with a lower thermal conduction coefficient of thermal insulation, however both solutions require financial outlays. The economic considerations of this solution were presented in their another work by Krawczyk and Teleszewski [25].

Kim et al.[26] examine the effect of operating temperature conditions on the degradation of the thermal insulated of the pipe and how it works due to the large fluctuation in the operating temperature.

Wang et al.[27] proposes new model to estimate onsite heat losses of a general pipe network with hourly measurements of heat sources and substations. This method can get a detailed heat loss profile along each pipe. Sartor and Dewalef [28] presented the model for design and optymalized DH system which consider their the dynamic behavior. The calculations take into account heat losses and pipe and have been validated experimentally. Another dynamic model proposed Zhang W. et al.[29] in which is the temperature distribution is analytically expressed as a linear superposition of the source states and initial conditions. As a result, the regularity of the temperature distribution borne by independent sources can be clearly distinguished.

Teleszewki et al. [30] in their work analyzed the heat loss and reduction of annual air pollutant emissions of a quadruple preinsulated district heating network by comparing this solution with an existing preinsulated network consisting of four single preinsulated pipes and a variant consisting of two double preinsulated pipes. In order to determine the heat loss, a simplified two-dimensional heat conduction model was developed using a Fortran computer program. The results of numerical simulations indicate that the use of TwinPipe for the

construction of pre-insulated quadruple pipe networks contributed to a significant reduction in heat loss compared to the existing single pre-insulated network (up to 57.1%), while reducing the thermal insulation area of the cross-section of the pre-insulated pipe by 21.4%.

Zhang Z. et al.[31] in their work, they proposed an ultra-short term optimal energy management planning considering the characteristics of a district heating network. Based on graph theory, a district heating network model suitable for optimal system planning was developed. Considering the transient temperature characteristics of the thermal medium, the theoretical basis for evaluating the transient and steady-state heat transfer characteristics of the pipeline depending on the scheduling period and pipeline length was derived.

Triebs and Tsatsaronis [32] in their work analyzed the problem of mismatch between the heat demand and the required heat supply due to heat losses as well as the unsteady behavior of the district heating network. Standard load profiles for district heating systems were developed and used to account for transients in the network without the need for a complex physical model. Compared to the direct prediction method, the proposed approach shows a 5% decrease in mean square error with an increase in peak load estimation accuracy of 7 percentage points. The proposed method is best coupled with loss allocation methods based on a fixed proportion of actual load or on grid supply and return temperatures. The proposed method and published dataset are intended to produce annual load profiles for district heating networks for which data are lacking to serve as input parameters for long-term dispatching or investment problems.

Zheng et al.[33] in their work, they established a coupled thermo-hydraulic simulation model of a real large-scale district heating network with multiple heat sources in Tianjin, and then the actual operation data of the district heating network was monitored to validate the model. The operating conditions and energy consumption of the DHN during the heating period were analyzed using the proposed model. As the heating load increases, the heat loss ratio (HLR) and energy and heating consumption ratio (EHR) decrease. The results show that the relative errors of hydraulic and thermal simulation are within ±8% and ±5%, respectively.

Nowak-Ocłoń et al.[34] analysis the thermal and economic effect of using the pre-insulated pipes and proves the most-cost effective TwinPipe system in DH. The TwinPipe system was found to be the most economically viable. These pipes are more expensive, but heat losses occurring during their use are much smaller in comparison with pre-insulated pipes. Short return time of such an investment (6-7 years) with 100 m of installed pipe and a positive NPV value make this type of pipe the best investment for district heating networks.

Ocłoń et al.[35] in their work, they determined the heat loss of a pre-insulated pipe and a TwinPipe in a district heating network. They compared the heat loss calculated using analytical solution (1D model) and numerical model (2D model) based on finite element method. The developed numerical model considered the undisturbed ground temperature at different depths. This made it possible to investigate the effect of temperature distribution at different depths on heat loss in the district heating network. Different insulation variants were considered, including standard, plus and plus-plus types for pre-insulated pipes.

After analysing the literature we have noticed a lack of "quick" and simple calculations taking into account the actual heat losses in DHN which allow to analyse and choose the appropriate insulation thickness when designing new connections of installations or modernisation of existing networks designed for high parameters, which should be adjusted to lower parameters as it is required by heat sources based on RES.

In this work, heat losses calculated on the basis of the 1D model (analytical model), 2D model based on finite element method (numerical method) are presented, and the results of these calculations are compared with the results obtained on the experimental bench.

The main novelty in this work is the presented algorithm, which can be helpful in thermal optimization of heating system design, as well as in its modernization.

3. Aim and scope of the work

A review of the literature to date indicates a variety of approaches to modelling flow and heat processes occurring in District Heating Networks (DHN).

The aim of this study is to create a model that allows a quick and short term calculation of heat losses in district heating networks and thus to find optimal insulation thicknesses for two types of pipes used in district heating networks - single pre-insulated pipes and the TwinPipe system. It is also possible to determine the temperature distribution in the pipe area of district heating networks. The knowledge of heat transfer losses in the two most common types of pipes: the preinsulated parallel pipes and TwinPipe discussed makes it possible to model their optimum insulation thicknesses at the design stage.

The scope of the work includes the creation of a mathematical model, its computational and experimental verification. The first step will be to compare the results of the one-dimensional (1D) mathematical model with those of the two-dimensional (2D) model. This will be followed by the construction of a test stand, the results of which will be verified with the results of the calculation of the unit heat loss of single pre-insulated parallel pipes and TwinPipe underground pipes. The experimental temperature distribution around the pipes in the ground for both cases will be compared with the results of the CFD simulations.

Economic calculations of the cost-effectiveness of single parallel pre-insulated pipe and double pre-insulated pipes (TwinPipe) will also be carried out based on actual daily flow and return temperature data of the urban district heating network throughout the year using the proposed heat loss model..

4. Thesis

The implemented mathematical model of heat losses in the heating network allows for proper design of heating system network. The CFD simulation and analytical calculation of different sizes of pipes may reflect heat transfer losses in terms of economic aspects.

5. Analytical model

This chapter proposes a mathematical model to analyse the flow and thermal phenomena occurring in the pipes of a district heating network. The analytical model is a one-

dimensional model; the medium flowing in them is single-phase water at a given temperature. The model is presented for two types: pre-insulated parallel single pipe and TwinPipes.

5.1 Heat losses through pre-insulated single parallel pipe.

The calculation of the heat losses of the DHN located in ground is determined by following equation [36]

$$q = \frac{\Delta t}{\sum R} \qquad \left[\frac{W}{m}\right] \qquad (5.1)$$

where:

Δt – the difference temperature between temperature of the factor in the pipe and the ground temperature [K],

$\sum R$ – the sum of the thermal resistance $\left[\frac{mK}{W}\right]$

Figure 5.1 presents the model of pre-insulated pipe. The pipe is made of three main elements: conduct pipe, insulation and shield pipe.

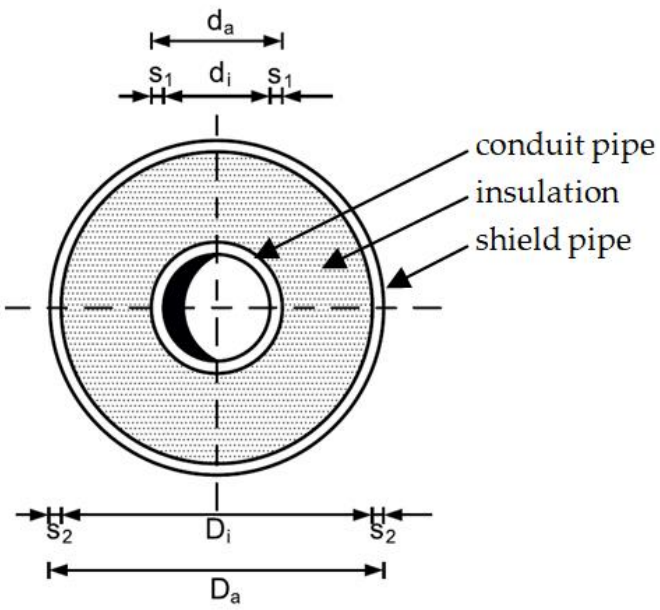

Figure 5.1. The model of the underground pre-insulated single pipe.

The total of the linear thermal resistance of heat transfer $\sum R$ in equation (1) there are resistances resulting from [36]:

$$\sum R = R_{h1} + R_{pipe} + R_{gr} \qquad \left[\frac{mK}{W}\right] \qquad (5.2)$$

- heat transfer resistance from heating fluid to inner surface of pipe R_{h1}

- heat transfer resistance through the pipe R_{pipe}

- heat transfer resistance through the ground R_{gr}

The thermal resistance of heat transfer through the pipe in equation (2) is calculating by the formula for thermal resistance multilayer pipe [36]:

$$R_{pipe} = R_{ST} + R_{IS} + R_{SH} \qquad \left[\frac{mK}{W}\right] \qquad (5.3)$$

where:

- heat transfer resistance through the conduit pipe steel R_{ST}

- heat transfer resistance through the insulation R_{IS}

- heat transfer resistance through the shield pipe R_{SH}

The thermal resistances of heat transfer in equation (3) is calculated by formula:

$$R_{ST} = \frac{1}{2\Pi\lambda_{ST}} ln \frac{d_a}{d_i} \qquad \left[\frac{mK}{W}\right] \qquad (5.4)$$

$$R_{IS} = \frac{1}{2\Pi\lambda_{IS}} ln \frac{D_i}{d_a} \qquad \left[\frac{mK}{W}\right] \qquad (5.5)$$

$$R_{SH} = \frac{1}{2\Pi\lambda_{SH}} ln \frac{D_a}{D_i} \qquad \left[\frac{mK}{W}\right] \qquad (5.6)$$

where:

D_i – internal cylindrical diameter of the shield pipe with a thickness s_2

D_a – outer cylindrical diameter of the shield pipe with a thickness s_2

d_i – internal cylindrical diameter of the conduit pipe with a thickness s_1

d_a – outer cylindrical diameter of the conduit pipe with a thickness s_1

R_{ST} – thermal resistance of the conduit pipe steel

R_{IS} – thermal resistance of the insulation

R_{SH} – thermal resistance of the shield pipe

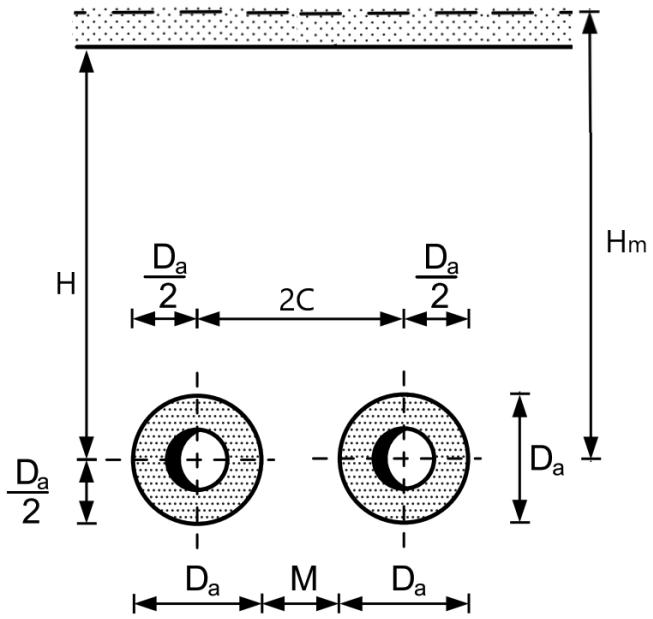

Figure 5.2. The model of the underground pre-insulated two pipes (supply and return).

In the Fig 5.2. is presented model of the underground pre-insulated supply and return pipes arranged in parallel with each other. The overall linear thermal resistance of heat transfer $\sum R$ in this case is presented by:

$$\sum R = R_{h1} + R_{pipe} + R_{gr} + R_{RR} \qquad \left[\frac{mK}{W}\right] \tag{5.7}$$

The thermal resistance of the soil in accordance with the Forgheimer principle is determined as follows:

$$R_{gr} = \frac{1}{2\Pi\lambda_{gr}} \ln\left[2\frac{H_m}{D_a} + \sqrt{4\left(\frac{H_m}{D_a}\right)^2 - 1}\right] \qquad \left[\frac{mK}{W}\right] \qquad \text{where } \frac{H}{D_a} < 2{,}0 \tag{5.8}$$

$$R_{gr} = \frac{1}{2\Pi\lambda_{gr}} \ln\frac{4H_m}{D_a} \qquad \left[\frac{mK}{W}\right] \qquad \text{where } \frac{H}{D_a} \geq 2{,}0 \tag{5.9}$$

The value of H_m(in Fig. 5.2) is determined as follows:

$$H_f = \frac{\lambda_{gr}}{h_{air}} \quad [\text{m}] \quad (5.10)$$

$$H_m = H_f + H \quad [\text{m}] \quad (5.11)$$

h_{air}–heat transfer coefficient from the ground surface to the outside air [W/m^{2}K]

The resistance to mutual influence is determined from the following formula:

$$R_{RR} = \frac{1}{2\Pi\lambda_{gr}} \ln[1 + \sqrt{4\left(\frac{H_m}{a^2}\right)^2}] \quad \left[\frac{mK}{W}\right] \quad (5.12)$$

The resistance of heat transfer thought the heating fluid to inner surface of pipe is determined by the formula:

$$R_{h1} = \frac{1}{\Pi h_f d_i} \quad \left[\frac{mK}{W}\right] \quad (5.13)$$

h_f – heat transfer coefficient from heating fluid to inner surface of pipe [W/m^{2}K]

The unit heat loss in the supply and return pipes are determined by the formula:

- supply:

$$q_s = \frac{(t_s - t_{gr})(R_{h1} + R_{pipe} + R_{gr}) + (t_r - t_{gr})R_{RR}}{(R_{h1} + R_{pipe} + R_{gr}) \cdot (R_{h1} + R_{pipe} + R_{gr}) - R_{RR}^2} \quad (5.14)$$

- return:

$$q_r = \frac{(t_r - t_{gr})(R_{h1} + R_{pipe} + R_{gr}) + (t_s - t_{gr})R_{RR}}{(R_{h1} + R_{pipe} + R_{gr}) \cdot (R_{h1} + R_{pipe} + R_{gr}) - R_{RR}^2} \quad (5.15)$$

5.2 The heat transfer of the soil

Soil thermal conductivity is influenced by many factors such as density, porosity, water content, texture, mineralogy, organic matter content, soil structure and soil temperature. Numerous correlations for the thermal conductivity of soil have been proposed in the literature and are listed in Table 5.1.

Table 5.1. A summary of correlations for the thermal conductivity of soil in literature

Author	*Correlations*	*Limitation*
Kersten, [37]	• <u>silt and clay soils</u>: Unfrozen: $\lambda_{gr} = [0.9 \log w - 0.2]10^{0.01 \cdot \rho_b}$ Frozen: $\lambda_{gr} = 0.01(10)^{0.022 \cdot \rho_b} + 0.085(10)^{0.008 \cdot \rho_b}$ • <u>sandy soils:</u> Unfrozen: $\lambda_{gr} = [0.7 \log w + 0.4]10^{0.01 \cdot \rho_b}$ Frozen: $\lambda_{gr} = 0.076(10)^{0.013 \cdot \rho_b} + 0.032(10)^{0.0146 \cdot \rho_b}$ $\rho_b -$ density w – moisture content	only one influencing factor ρ_b, only for frozen and unfrozen silt and sandy soils
Gemant, [38]	$$\frac{1}{\lambda_{gr}} = \frac{[\frac{1-a}{a}]^{4/3}\arctan[\frac{\lambda_s - \lambda_w}{\lambda_w}]^{1/2}}{(\frac{h}{2})^{1/3}[\lambda_w(\lambda_s - \lambda_w)]^{1/2}} + \frac{1-z_w}{\lambda_s a} f\left\{\frac{b^2}{a}\right\}$$ where: $\lambda_s -$ thermal conductivity of soil skeleton $\lambda_w -$ thermal conductivity of water $h -$ the apex water (water collected around the contact points) $h_0 -$ water absorbed as a film around the soil particles $f\left\{\frac{b^2}{a}\right\}$, a b, z - shape functions given by Gemant $$a = 0.078\sqrt{s}$$ $$h = 0.16 \cdot 10^{-3} sw - h_0$$ $$z_w = \left(\frac{1-a}{a}\right)^{2/3}\left(\frac{h}{2}\right)^{1/3}$$ $$b^2 = \left(\frac{a}{1-a}\right)^{2/3}\left(\frac{h}{2}\right)^{2/3}$$	for only unfrozen sandy soils based on idealized geometrical model of soil
van Rooyen, et al.	$$\frac{1}{\lambda_{gr}} = A10^{-BS_r} + s$$	limited to unfrozen sands and gravels with saturation levels

[39]	where: $S_r -$ degree of saturation $A, B, s -$ function of dry density, mineral type, granulometry, respectively	between 1.5 % and 10 %
de Vries et al. [40]	$$\lambda_{gr} = \frac{x_f \lambda_f + F x_s \lambda_s}{x_f + F x_s}$$ where: f, s – fluid and solid phases respectively $x -$ volume fraction $$F = \frac{1}{3}\sum_i \left[1 + \left(\frac{\lambda_s}{\lambda_f} - 1\right) g_i\right]^{-1}, \qquad i = a, b, c$$ g – shape factors, usually used to fit empirical data	applicable to unfrozen coarse soils with saturations between 10% to 20%
Johansen [41]	$$\lambda_{gr} = \left(\lambda_{sat} - \lambda_{dry}\right) \times K_e + \lambda_{dry}$$ where: λ_{sat} – saturated soil thermal conductivity • unfrozen soils $\lambda_{sat} = \lambda_s^{(1-P)} \lambda_w{}^P$ $P -$ porosity • saturated, frozen soils containing some unfrozen water $^{(1-P)} 2.2^P 0.269^{w_u}$ w_u $-$ fractional volume of unfrozen water λ_{dry} – dry soil thermal conductivity • dry natural soils: $\lambda_{dry} = \frac{0.135\rho_d + 64.7}{2700 - 0.947\rho_d} \pm 20\%$ $\rho_d -$ dry density • crushed rock material $\lambda_{dry} = 0.039 P^{-2.2} \pm 25\%$ Kersten coefficient K_e - dimensionless • coarse unfrozen soil: $K_e = 0.7 log\mathrm{S} + 1.0$ • fine unfrozen soil: $K_e = log\mathrm{S} + 1.0$ • any type of frozen soil: $K_e = \mathrm{S}$ S - saturation	limited to saturations greater than 20%

Campbell, [42]	$k_{gr} = A + B\theta - (A - D)exp[-(C\theta)^E]$ where: θ – volumetric water content *A, B, C, D, E* - soil-dependent coefficients obtained by curve fitting $A = 0.65 - 0.78\rho_b + 0.60{\rho_b}^2$ ρ_b - soil bulk density $B = 1.06\rho_b$ $C = 1 + 2.6{c_{clay}}^{-0.5}$ c_{clay} - clay mass fraction $D = 0.03 + 0.10{\rho_b}^2$ $E = 4$	the parameters in the model are difficult to obtain the function is not suitable for a large variety of soil textures
Ewen and Thomas [43]	Kersten coefficient K_e were modified: $K_e = 1 - exp(-\xi S_r)$ where: ξ - fitted parameter and n = 8.9 was given based on their data	Application model to unsaturated sand
Côté and Konrad, et al. [44]	(based on Johansen model) - Kersten coefficient K_e were modified: $K_e = \frac{\kappa S_r}{1 + (\kappa - 1)S_r}$ where: $\kappa -$ texture-dependent factor $S_r -$ unfrozen and frozen soils of different textures/grain sizes κ = 4.60, for gravel and coarse sand, κ =3.55, medium and fine sand κ =1.90, silty and clayed soils κ = 0.60, organic fibrous soils, Conducted an empirical relationship between λ_{dry} and *P* $\lambda_{dry} = \chi 10^{-\eta P}$ where: χ – parameters based on particle shape: $\chi = 1.70$ and $\eta = 1.80$ - for crushed rocks $\chi = 0.75$ and $\eta = 1.20$ - for mineral soils $\chi = 0.30$ and $\eta = 0.87$ - for organic fibrous soil	The calculation of Ke does not always take soil saturation into account. Especially when the soil is fine-textured and the water content is low.
Lu S. et al. 2007, [45]	Kersten coefficient K_e were modified: $K_e = exp\{\gamma[1 - {S_r}^{(\gamma - 1.33)}]\}$ where:	Unknown influence of soil type on dry conductivity

	$\gamma -$ soil texture-dependent parameter γ = 0.96, for coarse textured sand, γ =0.27, for fine textured sand Conducted an empirical relationship between λ_{dry} and P $$\lambda_{dry} = aP + b$$ a, b - empirical parameters that can be determined by fitting the dry soil data, a = 0.56 and b = 0.51 for 0.2<P<0.6	
Chen, et al [46]	$$\lambda_{gr} = {\lambda_w}^P {\lambda_s}^{1-P}[(1-b)S_r + b]^{cP}$$ where: b, c - model parameters b = 0.0022; c = 0.78	Limited applicability
Lu Y.L et al [47]	$$\lambda_{gr} = \lambda_{dry} + exp(-\theta^{-\mu}) \quad for\ \theta > 0$$ where: μ, θ – shape dependent parameter $\mu = 0.67c_{clay} + 0.24$ $\theta = 1.97c_{sand} + 1.87\rho_b - 1.36c_{sand}\rho_b - 0.95.$	The model clearly overestimates the values of λ over the whole range of range of water contents
Nikolaev et al. [48]	$$\lambda_{gr}(S_{r,}\,T) = \lambda_{dry_{22}\circ C} + (\lambda_{sat_{22}\circ C} - \lambda_{dry_{22}\circ C})K_e(S_{r,}\,T)$$	Correlation assessed on the basis of complete data covering all temperatures and all water contents.
Nikoosokhan et al. [49]	The developed model of Johansen: $\lambda_{sat} = 0.53c_{sand} + 0.1\gamma_d$ $\lambda_{dry} = 0.087c_{sand} + 0.019\gamma_d$ where $\gamma_d = g\rho_b$ $g -$ gravity acceleration	developed a model, using soil volumetric water content, sand content, and dry soil specific weight
Su et al. [50]	The development model of Lu (2007) $$\omega = cc_{clay} + dc_{silt} + ec_{sand} + fc_{om}$$ where: c, d, e, f - weighting factors; c = −0.5863, d = 0.9451, e = 0.1080, f = 0.0567	many factors infuencing λ, each factor is mutually constrained improved the expression of the shape factor
He et al. [51]	Kersten coefficient K_e were modified: $$K_e = \begin{cases} 0 & S_r = 0 \\ \left[Aexp\left({S_r}^{-B}\right)\right]^{-1} & S_r > 0 \end{cases}$$	lack of correlation formulas for determining model parameters

	where: A, B – fitting parameters $\lambda_{gr} = \begin{cases} \lambda_{dry} & S_r = 0 \\ \lambda_{dry} + (\lambda_{sat} - \lambda_{dry}) & \\ \dfrac{}{A\ exp\left(P{S_r}^{-B}\right)} & S_r > 0 \end{cases}$	
Ren et al [52]	Kersten coefficient K_e were modified: $K_e = exp(\alpha - \theta^{-\beta})$ where: α, β – the shape factors $\alpha = gc_{sand} + hc_{silt} + ic_{om} + j$ $\beta = pc_{clay} + rc_{om}$ *g, h, i, j, p, r* – the weighting factors of the physical parameter's	the influence of organic matter content and particle composition is considered
Xiong et al [53]	The development model of Campbell (1985) $\lambda_{gr} = P + QS_r{}^R + Sexp[S_r(1 - S_r)]$ where: P, Q, R - physical properties of the soil (porosity, composition, and texture $P = \lambda_{dry} = a + bm$ $Q = \lambda_{sat} - \lambda_{dry}$ $S = c(S_r - S_r{}^2)$	improved the agreement between calculated and measured data

Xiong et al [53] described a new mathematical model between soil thermal conductivity and saturation. The improved model was compared to other models and measured data of different types of soils (starting from sand up to clay). In conclusion, improved proposed model can be used in terms of determination of soil thermal conductivity. Ren et al [52] showed that new empirical model is suitable for studying thermal conductivities of soils of different textures. Published database was used the new estimation was evaluated along with nine other models. Models were analysed compared. He et al [51], developed new model to simulate effective soil thermal conductivity of soils of various soil textures and water contents. New function for calculating dry soil thermal conductivity is presented. The results proves that new model has best performance among seven tested models (with root-mean-square error of 0.059 W m^{-1}°C^{-1}, and Nash-Sutcliffe efficiency of 0.994). Nikoosokhan et al [49] developed simple model for predicting soil thermal conductivity from sand content and dry densities. It is relationship between thermal conductivity saturated and non-saturated based on content X_s and dry density y_d. The proposed model describes ground thermal

conductivity λ_{gr} across the entire water content range for soils of various textures. Lu et al. [47] presented simple empirical model for estimation of thermal conductivity. The main difference is simplicity of the model, which requires only two input parameters: soil porosity and volumetric water content. The RMSEs of thermal conductivity estimations for new model is similar to more complex models. Chen et al. [46] during laboratory tests found that thermal conductivity increases with saturation degree and decrease with porosity. Empirical equation of thermal conductivity was expressed as function of porosity and saturation degree. Côté and Konrad et al. [44] develop a generalized thermal conductivity model for moist soils. Presented model integrates well effects of porosity, saturation, mineral content and grain – size distribution. Nearly 220 experimental results were analyzed to develop empirical relationship to assess the thermal conductivity of dry soils.

Ewen et al. [43], paper focused on thermal probe experimental determination of thermal conductivity of unsaturated soil. During investigation it is proven that two criteria cannot be satisfied (reduction of run time – migration of migration is limited and extension of the run time to obtain accuracy of the method). The alternative approach proposed, theoretically can satisfied both criteria simultaneously. Campbell et al. [42], thermal conductivity depends on its bulk density, water content , quartz content, and organic matter content. The parameters in the model are difficult to obtain, function is not suitable for large variety of soil textures. Kersten et al. [37], developed his method for calculating thermal conductivity in soil materials by fitting mathematical expressions to the extensive experimental data. Presented model consist two equations of frozen and un-frozen soil materials.

There exists various soil thermal conductivity models, are above mentioned. However, for the present calculations the constant value of soil thermal conductivity is selected $\lambda_{gr} = 2.2\ \left[\frac{W}{mK}\right]$.

5.3 Heat losses formulas for TwinPipe pipe – analytical model

The model of the TwinPipe system is presented in Fig. 5.3.

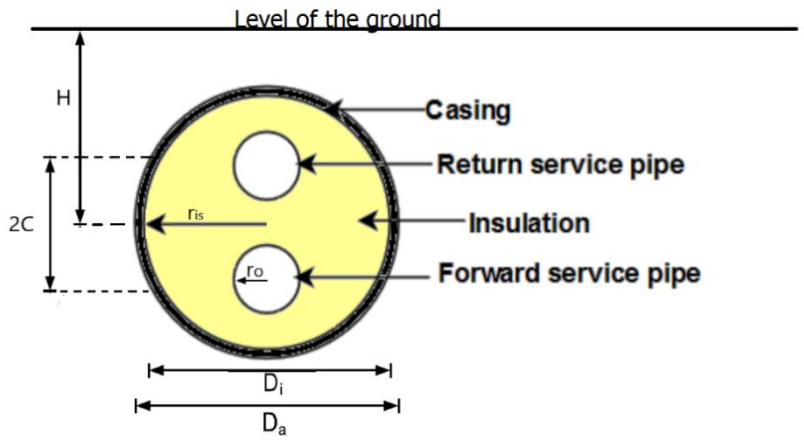

Figure 5.3. The model of the underground TwinPipe system

The calculation based on multipole superposition method for symmetric states. The correlation of heat loss between supply and return pipe is shown on equation (15-17) [54]:

- supply:

$$q_s = q_{sm} + q_a \tag{5.16}$$

-return:

$$q_r = q_{sm} - q_a \tag{5.17}$$

The total heat losses are in this case:

$$q_s + q_r = 2q_{sm} \tag{5.18}$$

The component of heat losses in the symmetrical state is:

$$q_{sm} = \frac{t_{sm} - T_E}{R_{sm}} \tag{5.19}$$

where:

T_E – temperature of the ground[°C]

t_{sm} – temperature of the fluid in a symmetrical state [°C]

$$t_{sm} = \frac{t_s + t_r}{2} \quad [°C] \tag{5.20}$$

t_s – the average temperature in the supply pipe

t_r – the average temperature in the return pipe

R_{sm} – resistance of heat transfer in the symmetrical state is calculated by:

$$R_{sm} = \frac{1}{2\pi\lambda_{is}h_s} \tag{5.21}$$

The coefficient of heat loss for the symmetrical state is calculated according to the formula

$$\frac{1}{h_s} = 2 \cdot \frac{\lambda_{is}}{\lambda_{gr}} \cdot \ln\left(\frac{2H}{r_{is}}\right) + \ln\left(\frac{{r_{is}}^2}{2Cr_o}\right) + \sigma \cdot \ln\left(\frac{{r_{is}}^4}{{r_{is}}^4 - C^4}\right) - \frac{\left(\frac{r_o}{2C} - \frac{2\sigma r_o C^3}{{r_{is}}^4 - C^4}\right)^2}{1+\left(\frac{r_o}{2C}\right)^2 + \sigma\left(\frac{2r_o {r_{is}}^2 C}{{r_{is}}^4 - C^4}\right)^2} \tag{5.22}$$

where the dimensionless parameter σ will be used in the following:

$$\sigma = \frac{\lambda_{is} - \lambda_{gr}}{\lambda_{is} + \lambda_{gr}} \tag{5.23}$$

The component of heat losses in the symmetrical state is:

$$q_a = \frac{t_a}{R_a} \tag{5.24}$$

where:

t_a – temperature of the fluid in a symmetrical state [°C]

$$t_a = \frac{t_s - t_r}{2} \qquad [°C] \tag{5.25}$$

t_s – the average temperature in the supply pipe

t_r – the average temperature in the return pipe

R_a – resistance of heat transfer in the symmetrical state is calculated by:

$$R_a = \frac{1}{2\pi\lambda_{is}h_a} \tag{5.26}$$

The coefficient of heat loss for the asymmetrical state is calculated according to the formula [37-39]

$$\frac{1}{h_a} = \ln\left(2\frac{C}{r_o}\right) + \sigma \cdot \ln\left(\frac{{r_{is}}^2 + C^2}{{r_{is}}^2 - C^2}\right) - \frac{\left(\frac{r_o}{2C} - \gamma\frac{Cr_o}{4H^2} + \frac{2\sigma r_o {r_{is}}^2 C}{{r_{is}}^4 - C^4}\right)^2}{1 - \left(\frac{r_o}{2C}\right)^2 - \gamma\frac{r_o}{2H} + 2\sigma {r_o}^2 {r_{is}}^2 \frac{{r_{is}}^4 + C^4}{\left({r_{is}}^4 - C^4\right)^2}} - \gamma\left(\frac{C}{2H}\right)^2 \tag{5.22}$$

where the dimensionless parameter γ will be used in the following:

$$\gamma = \frac{2\cdot(1-\sigma^2)}{1-\sigma(\frac{r_{is}}{2H})^2} \tag{5.23}$$

6. Numerical modelling of heat transfer

6.1 Finite element formulation in heat conduction

A three-dimensional heat conduction equation is solved to determine the maximum temperature within the heating network $T = T(x, y, z)$. The heating network is composed of layers tube (*t*), insulation (*ins*) and an ground (*gr*), is considered. The convective heat transfer occurs between the fluid flowing inside the supply (s) and return (r) tubes.

$$\begin{cases} \frac{\partial}{\partial x}\left[\lambda_t \frac{\partial T(x,y,z)}{\partial x}\right] + \frac{\partial}{\partial y}\left[\lambda_t \frac{\partial T(x,y,z)}{\partial y}\right] + \frac{\partial}{\partial z}\left[\lambda_t \frac{\partial T(x,y,z)}{\partial z}\right] = 0, & \text{for the tube domain,} \\ \frac{\partial}{\partial x}\left[\lambda_{ins} \frac{\partial T(x,y,z)}{\partial x}\right] + \frac{\partial}{\partial y}\left[\lambda_{ins} \frac{\partial T(x,y,z)}{\partial y}\right] + \frac{\partial}{\partial z}\left[\lambda_{ins} \frac{\partial T(x,y,z)}{\partial z}\right] = 0, & \text{for the insulation domain,} \\ \frac{\partial}{\partial x}\left[\lambda_{gr} \frac{\partial T(x,y,z)}{\partial x}\right] + \frac{\partial}{\partial y}\left[\lambda_{gr} \frac{\partial T(x,y,z)}{\partial y}\right] + \frac{\partial}{\partial z}\left[\lambda_{gr} \frac{\partial T(x,y,z)}{\partial z}\right] = 0, & \text{for the ground domain,} \end{cases} \tag{6.1}$$

where,

x, *y*, *z* – are Cartesian coordinates of the specified point that belongs to heat transfer domain,

λ – is a thermal conductivity specified for the different computational domains, i.e.:

- for the tube wall material λ_t = 30 W/(m K),
- for the insulation material λ_{ins} = 0.042 W/(m K),
- for the soil layer λ_{gr} = 2.2 W/(m K),

In last decades numerous research provide information related to the earth temperature and thermal diffusivity . The solar radiation constantly transfer energy to soil surface of the Earth, thus the temperature distribution of soil depends on depth. Due to level of complexity this phenomena, it is assumed that soil is certain area is homogenous and physical properties do not change over time. Also, surface of the soil supposed to be flat therefore the heat flows in a direction perpendicular to the surface.

Kusuda and Achenbach [55], 63 sets of underground installations through 48 states of the United States of America have been complied and analysed. Data obtained were used to compute phase angle of earth temperature (least–squares method used) and annual average amplitude. The monthly average temperature at depth intervals form 2 to 10 feet and minimum and maximum integrated average temperatures in this region were calculated for each station for a selected value of thermal diffusivity using the results of the least-squares analysis. The results were compared with corresponding values of air and temperature of the ground water temp.

Carson in [56] performed Fourier analyses based on soil and air temperature data collected by Meteorology Group. The coefficients obtained provide phase and amplitude variations with depth of the annual soil temperature cycles. Also based on the information given, the pattern of variation of the heat-transfer processes in the soil is exposed.

Penrod, et al in [57] and [58] described geophysical studies which include recording of the solar energy received on horizontal surface and measurement of the temperature of the soil (clay soil with sod) at various depths. The solar energy was determined by pyrheliometer assembled on the top the University of Kentucky at the elevation 1026.6 feet. Temperature of the soil was recorded by thermocouples buried at depths of 0, 2, 4, 6, 8, 10 feet. The soil temperature were recorded at 2 hour intervals since 1952 to 1956.

The oscillation of soil temperature near surface has been discussed widely over the years in various texts [59-61]. The surface of the temperature at any point x and time t is provided by heat conduction equation:

$$\rho C \frac{\partial T(x,t)}{\partial t} = \nabla \cdot [\lambda \nabla T(x,t)] \tag{6.2}$$

where:

ρ – is a average soil density (Kg/m^3)

C – soil specific heat capacity (J/KgK)

λ – soil thermal conductivity (W/mK)

Depending on content of the water and heterogeneity the soil parameters vary. Thermal conductivity λ is affected by soil anisotropy. Principle components are aligned with the coordinate system, such that the off-diagonal components of this tensor are $K_{ij} = 0$ for $i \neq j$

The equation mentioned above is a subject to:

$$T(x,0) = T_m \tag{6.3}$$

Márquez et al [62] concentrated on methodology and instrumentation system for the indirect measurement of the thermal diffusivity of a soil at certain depth based on measured temperature. The harmonic function describes annual monthly average soil temperature at the surface and dedicated depth. The function is presented as follows:

$$T_{soil\ surface}(t) = T_m - T_p cos(\omega t - \varphi) \tag{6.4}$$

where:

T_m- annual average temperature of soil in the stable layer; it is commonly set to the average temperature of air, practically the average temperature in the place (°C).

T_p - amplitude (°C); the peak deviation of the function from zero. In this case the annual amplitude of the monthly average temperature cycle in the place.

t - time coordinate (s). To set a starting time (t = 0), it begins to run from 1 January at 0 s. This way of measuring the time obviously result in a phase shift since the beginning of the sinusoid in general will not coincide with t = 0.

ω - angular frequency (rad/s). The rate of change of the function argument in units of radians per second; $\omega=2\pi/T$, where T is the period of the sinusoid; in this case the annual temperature cycle,

φ - Phase (rad). When φ is non-zero, the entire waveform appears to be shifted in time by the amount φ/ω seconds. A negative value represents a delay, and a positive value represents an advance.

Undisturbed ground temperature distribution T_g (y_d) is calculated from Kusuda and Achenbach [47] ground temperature model

$$t_g(y_d,\tau) = t_{mean} - t_{amp} e^{-y_d\sqrt{\frac{\omega}{2\alpha}}} \cos(\omega\tau - \varphi - y_d\sqrt{\frac{\omega}{2\alpha}}) \tag{6.5}$$

where T_{mean} is annual average temperature of soil stable layer, assumed as 8 ^{o}C**,** T_{amp} is the temperature amplitude, assumed as 12 ^{o}C, τ in (s), is the time coordinate starting from 1st January and ending at 31 December; α is soil thermal diffusivity assumed as 2 x 10^{-6} m^2/s; ω

is angular frequency equal to $\omega = 2\pi/T$, where T is the period of sinusoid (one year) i.e. T = 3.1557 x 10^7 s; φ is a phase shift, where the wave form appears to be shifted in time by φ/ ω seconds. In this study the shift of 10 days is assumed i.e. φ/ ω = 8.64 x 10^5 s.

6.2 Linear triangular element

The temperatures within a finite element is approximated by values of nodal temperatures and their shape function according to x, y coordinates. The shape of function is used to determine components of element vectors and matrices. Two-dimensional heat conduction equation for solids is given as [48]:

$$\frac{\partial}{\partial x}\left(\lambda_x \frac{\partial T}{\partial x}\right) + \frac{\partial}{\partial y}\left(\lambda_y \frac{\partial T}{\partial y}\right) + \dot{q}_v = 0 \tag{6.6}$$

To solve the equation the, initial and boundary conditions are needed:

$$T|_{\Gamma_T} = T_b \tag{6.7}$$

$$\left(\lambda_x \frac{\partial T}{\partial x} n_x + \lambda_y \frac{\partial T}{\partial y} n_y\right)\Big|_{\Gamma_q} = q_b \cdot n = q_{bn} \tag{6.8}$$

$$\left(\lambda_x \frac{\partial T}{\partial x} n_x + \lambda_y \frac{\partial T}{\partial y} n_y\right)\Big|_{\Gamma_h} = q_b \cdot n = h\left(T_{cz} - T|_{\Gamma_h}\right) \tag{6.9}$$

where:

$\lambda_x, \lambda_y -$ thermal conductivities in x and y directions, respectively

$\dot{q}_v -$ heat flux density on the edge Γ_q

$T_b -$ temperature set on the edge Γ_T

$\alpha -$ heat transfer coefficient on the edge Γ_α

$T_{cz} -$ temperature of the fluid

The heat flux q_b is acting in the inward direction. The normal vector n components equal to:

$$n_x = cos\varphi \qquad\qquad n_y = cos\left(\frac{\pi}{2} - \varphi\right) = sin\varphi \tag{6.10}$$

where:
$\varphi -$ is angle between normal vector $\boldsymbol{n}$ and horizontal direction.

The boundary conditions can be written in matrix and vectors form as follows:

The thermal conductivity matrix:

$$[\lambda] = \begin{bmatrix} \lambda_x & 0 \\ 0 & \lambda_y \end{bmatrix} \tag{6.11}$$

The vector of temperature derivatives with respect x and y directions:

$$\{g\} = \begin{Bmatrix} \frac{\partial T}{\partial x} \\ \frac{\partial T}{\partial y} \end{Bmatrix} \tag{6.12}$$

The heat flux vector components:

$$\begin{Bmatrix} q_x \\ q_y \end{Bmatrix} = -[\lambda]\{g\} \tag{6.13}$$

Components of heat flux vector:

$$q = -\lambda_x \frac{\partial T}{\partial x} i - \lambda_y \frac{\partial T}{\partial y} j = q_x i + q_y j \quad n = n_x i + n_y j \tag{6.14}$$

The unit vectors i, j in x and y –direction, respectively. After multiplying heat flux vector q and normal vector n the normal component of heat flux is obtained:

$$q_n = -q \cdot n = -\left(-\lambda_x \frac{\partial T}{\partial x} n_x - \lambda_y \frac{\partial T}{\partial y} n_y\right) \tag{6.15}$$

6.3 Galerkin finite element formulation

The boundary conditions were formulated for entire Ω area [64-66]. Thanks for Garlekin formulation boundary conditions are defined to single finite element Ω^e. The assumption that three boundary conditions are on edge of the element like for entire structure. The temperature distribution within the domain of the e-th finite element approximates by using shape function $N^e(x, y)$:

$$T^e(x, y) = \sum_{j=1}^{n} T_j^e \cdot N_j^e(x, y) = [N^e]\{T^e\} \tag{6.16}$$

where:

$n -$ is a number of finite element nodes

$T_j^e -$ temperature of j-th node

$N_i^e -$ shape function

To calculate temperature in T_j^e, $j = 1, \dots, n$ the Garlekin method is applied. The transient heat conduction equation is multiplied by shape function $N^e(x, y)$, and integrated over the entire finite element area Ω^e.

$$\int_{\Omega^e} \left[\frac{\partial}{\partial x}\left(\lambda_x \frac{\partial T^e}{\partial x}\right) + \frac{\partial}{\partial y}\left(\lambda_y \frac{\partial T^e}{\partial y}\right) + q_v\right] N_i^e(x, y)\, dx\, dy = 0 \tag{6.17}$$

Acc. To Green theorem the equation is evaluated.

$$\int_{\Omega^e} \left(\frac{\partial G}{\partial x} - \frac{\partial F}{\partial y}\right) dx\, dy = \oint_{\Gamma^e} (F dx + G dx) \tag{6.18}$$

Integration is done all over the element edge Γ^e in counter clockwise direction after consideration:

$$F = -\lambda_y \frac{\partial T^e}{\partial y} N_i^e \qquad\qquad G = -\lambda_x \frac{\partial T^e}{\partial x} N_i^e \tag{6.19}$$

$$\int_{\Omega^e} \left[\frac{\partial}{\partial x}\left(\lambda_x \frac{\partial T^e}{\partial x}\right) N_i^e + \frac{\partial}{\partial y}\left(\lambda_y \frac{\partial T^e}{\partial y}\right) N_i^e\right] dx\, dy = \int_{\Gamma^e} N_i^e \left(-\lambda_y \frac{\partial T^e}{\partial y} dx + \lambda_x \frac{\partial T^e}{\partial x} dy\right) \tag{6.20}$$

After transformation left side of the equation the following formula is obtained:

$$\int_{\Omega^e} \left[\frac{\partial}{\partial x}\left(\lambda_x \frac{\partial T^e}{\partial x}\right) N_i^e + \frac{\partial}{\partial y}\left(\lambda_y \frac{\partial T^e}{\partial y}\right) N_i^e\right] dx\, dy =$$

$$- \int_{\Omega^e} \left(\lambda_x \frac{\partial T^e}{\partial x}\frac{\partial N_i^e}{\partial x} + \lambda_y \frac{\partial T^e}{\partial y}\frac{\partial N_i^e}{\partial y}\right) dx\, dy + \int_{\Gamma^e} N_i^e \left(-\lambda_y \frac{\partial T^e}{\partial y} dx + \lambda_x \frac{\partial T^e}{\partial x} dy\right) \tag{6.21}$$

Further transformation

$$\int_{\Omega^e} \left(\lambda_x \frac{\partial T^e}{\partial x}\frac{\partial N_i^e}{\partial x} + \lambda_y \frac{\partial T^e}{\partial y}\frac{\partial N_i^e}{\partial y}\right) dx\, dy = \int_{\Omega^e} N_i^e q_v\, dx\, dy + \int_{\Gamma^e} N_i^e \left(-\lambda_y \frac{\partial T^e}{\partial y} dx + \lambda_x \frac{\partial T^e}{\partial x} dy\right) \tag{6.22}$$

$$-dx = ds \sin\varphi = n_y ds$$

$$dy = ds \sin\varphi = n_x ds$$

$$-\lambda_y \frac{\partial T^e}{\partial y} dx + \lambda_x \frac{\partial T^e}{\partial x} dy = \lambda_y \frac{\partial T}{\partial y} n_y ds + \lambda_x \frac{\partial T}{\partial x} n_x ds = -\dot{q} \cdot n = \dot{q}_n ds \tag{6.23}$$

$$\int_{\Omega^e} \left(\lambda_x \frac{\partial T^e}{\partial x}\frac{\partial N_i^e}{\partial x} + \lambda_y \frac{\partial T^e}{\partial y}\frac{\partial N_i^e}{\partial y}\right) dx\, dy = \int_{\Omega^e} N_i^e q_v\, dx\, dy + \int_{\Gamma_q^e} N_i^e \dot{q}_b ds + \int_{\Gamma_\alpha^e} N_i^e \alpha (T_{cz} - T^e) ds \tag{6.24}$$

After substitution the sum equation is obtained.

$$\int_{\Omega^e}\left(\lambda_x\frac{\partial N_i^e}{\partial x}\sum_{j=1}^{n}T_j^e\frac{\partial N_j^e}{\partial x}+\lambda_y\frac{\partial N_i^e}{\partial y}\sum_{j=1}^{n}T_j^e\frac{\partial N_j^e}{\partial y}\right)dx\,dy=\int_{\Omega^e}N_i^e q_v\,dx\,dy+\int_{\Gamma_q^e}N_i^e\dot{q}_b ds-$$

$$\int_{\Gamma_\alpha^e}N_i^e\alpha\sum_{j=1}^{n}T_j^e N_j^e\,ds+\int_{\Gamma_\alpha^e}N_i^e\alpha T_{cz}ds \tag{6.25}$$

The equation of *i*-th node is written as follow:

$$\sum_{j=1}^{n}\left(K_{c,ij}^e+K_{\alpha,ij}^e\right)T_j^e=f_{Q,i}^e+f_{q,i}^e+f_{\alpha,i}^e \tag{6.26}$$

6.4 Finite volume method in heat conduction

The two-dimensional equation for heat conduction in finite volume method is given as [67-69]:

$$c(T)\rho(T)\frac{\partial T}{dt}dV=-div\dot{q}+\dot{q}_v \tag{6.27}$$

where:

$d-$ the thickness of analysed material

$\dot{q}_v-$ internal heat sources

$\rho-$ density of material

$\lambda-$ thermal conductivity

$c-$ specific heat

The studied area is divided into small control volumes (CV) which size is: $\Delta x;\ \Delta y; d$ in Cartesian coordinate system (Fig. 6.1) or $\Delta r;\ \Delta\varphi$ in cylindrical coordinate system.

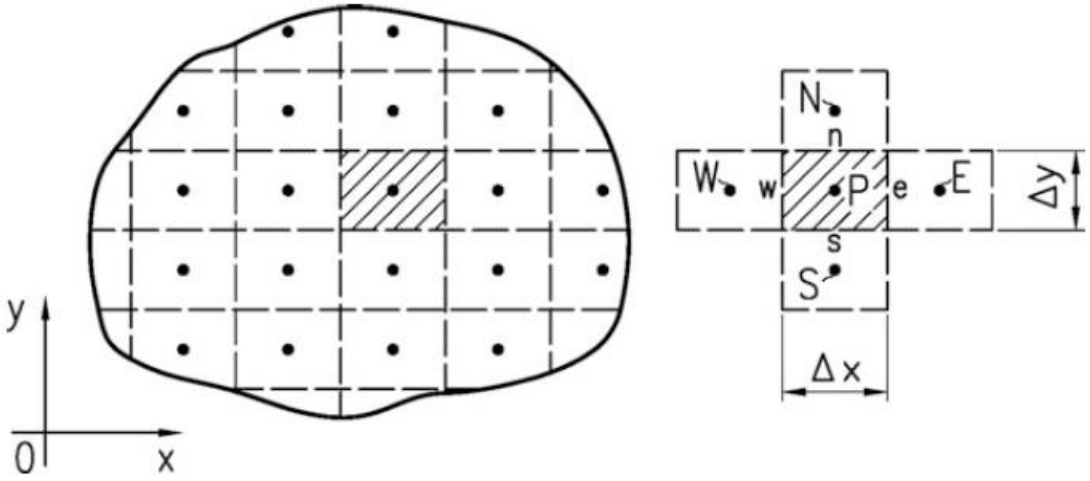

Figure 6.1. Cartesian coordinate system of two-dimensional examined area in finite volume method. Where N, W, P, E, S – center points of CV volumes; w, s, e, n – one wall of the boundary, $\Delta x;\ \Delta y$ – dimensions of CV cell [67-69].

After integration of the heat equation (xx) over the control volume, the calculation for single cell is following:

$$\int_{CV} c(T)\rho(T)\frac{\partial T}{dt}dV = -\int_{CV} div\dot{q} + \int_{CV} \dot{q}_v\, dV \tag{6.28}$$

Applying Green-Gauss-Ostrogradsky theorem on the right part of the equation gives:

$$n\dot{q} = 1|\dot{q}|\cos(n,q)^{\cdot} = \dot{q}_n \tag{6.29}$$

Based that, the direction of the heat flux vector $\dot{q}$ is pointing to inside of the area of the control volume and the angle between normal vector - n and $\dot{q}$ is 180° then heat is transported into the CV.

The equation (6.29) is simplified by substitution ΔV as the control volume:

$$\int_{\boldsymbol{CV}} c(T)\rho(T)\frac{\partial T}{dt}dV \approx \Delta V_c(T_p)\rho(T_p)\frac{dT_p}{dt} \tag{6.30}$$

The integral of the CV is replaced by ΔV

$$-\int_S\ n\dot{q}\, dS = \sum_{i=1}^{4} \dot{Q}_\iota \tag{6.31}$$

The heat flow transferred to the cell from 4 different directions. The dimensions of the rectangular volume that heat is transferred to the cell: $\Delta x\ \times \Delta y\ \times d$

$$-\int_{CV} \dot{q_v}\, dV = \Delta V \dot{q_v}\,(T_p) \tag{6.32}$$

The integral of the CV is replaced by ΔV

where:

$\dot{Q}_\iota -$ heat flow that is transferred from the neighbouring cell
$\dot{q} -$ heat flux vector directed to the inside of the control volume
$n -$ outward unit normal vector

Substituting the equations above the following formula is obtained:

$$\Delta V_c(T_p)\rho(T_p)\frac{dT_p}{dt} = \sum_{i=1}^{4} \dot{Q}_\iota + \Delta V \dot{q_v}\,(T_p) \tag{6.33}$$

6.5 Energy conservation equation in Cartesian coordinates

The centre points of the divided area are: W, N, E, S, P. The node P is surrounded by four boundaries: w, n, e, s from where the heat is transferred to the midpoint of the P control volume.

The heat flow for each boundary is calculated by following formula [70, 71]:

$$\dot{Q}_{W-P} = (\Delta y) d \dot{q}_{W-P} = (\Delta y) d \frac{\lambda(T_w)+\lambda(T_p)}{2} \frac{T_w - T_p}{\Delta x} \tag{6.34}$$

$$\dot{Q}_{N-P} = (\Delta x) d \dot{q}_{N-P} = (\Delta x) d \frac{\lambda(T_N)+\lambda(T_p)}{2} \frac{T_N - T_p}{\Delta y} \tag{6.35}$$

$$\dot{Q}_{E-P} = (\Delta y) d \dot{q}_{E-P} = (\Delta y) d \frac{\lambda(T_E)+\lambda(T_p)}{2} \frac{T_E - T_p}{\Delta x} \tag{6.36}$$

$$\dot{Q}_{S-P} = (\Delta x) d \dot{q}_{S-P} = (\Delta x) d \frac{\lambda(T_s)+\lambda(T_p)}{2} \frac{T_s - T_p}{\Delta x} \tag{6.37}$$

Considering the equations above the heat flow is calculated:

$$(\Delta x)(\Delta y) dc(T_p)\,\rho(T_p)\frac{dT_p}{dt} = (\Delta y) d \frac{\lambda(T_w)+\lambda(T_p)}{2} \frac{T_w - T_p}{\Delta x} + (\Delta x) d \frac{\lambda(T_N)+\lambda(T_p)}{2} \frac{T_N - T_p}{\Delta y} + (\Delta y) d \frac{\lambda(T_E)+\lambda(T_p)}{2} \frac{T_E - T_p}{\Delta x} + (\Delta x) d \frac{\lambda(T_s)+\lambda(T_p)}{2} \frac{T_s - T_p}{\Delta x} \tag{6.38}$$

To simplify this equation, the following notification is used.

$$\lambda_p = \lambda(T_p), \quad c_p = c(T_p), \quad a_p = \frac{\lambda_p}{c_p \rho_p} \tag{6.39}$$

$$\frac{dT_p}{dt} = a_p \left[\frac{\lambda_w + \lambda_p}{2\lambda_p} \frac{T_w - T_p}{(\Delta x)^2} + \frac{\lambda_n + \lambda_p}{2\lambda_p} \frac{T_N - T_p}{(\Delta y)^2} + \frac{\lambda_E + \lambda_p}{2\lambda_p} \frac{T_E - T_p}{(\Delta x)^2} + \frac{\lambda_S + \lambda_p}{2\lambda_p} \frac{T_S - T_p}{(\Delta y)^2} \right] + \frac{\dot{q}_{v,p}}{c_p \rho_p} \tag{6.40}$$

7. Laboratory device stab

The purpose of the district heating system is to provide the heat distribution generated in centralized location plants. Heating losses through transmission is the undesirable effect. Heating networks that used foam concrete installations had many disadvantages related to the fragility of the material, both during production, as well as transport and assembly. Research and development in the field of insulation have led to the conception of pre-insulated pipes. Due to the low heat losses during the transport of the hot medium, pre-insulated pipes began to be used on a large scale in Poland after 1989.

7.1. Construction of the laboratory device

The experimental laboratory stab is used to measure the amount of heat losses in municipal heating networks. The principle of operation is based on the flow of the working medium through the supply system (high temperature system) and the return system (low temperature system) with simultaneous temperature measurement at the beginning and at the end of the measuring section. For parallel measurements (single pre-insulated pipes), the soil temperature between the supply and return systems is recorded. The measuring system consists of 16 sensors. Water was used as the heat carrier. The working medium (demoralized water) was heated to the desired temperature in two independent open systems (electric storage heater) - No. 1 - Fig. 7.1. Each of the circuits has two separate temperature measurement sensors (No. 2), information about the liquid temperature goes to the temperature regulators (No. 3) which turn on or off the heater system. The refrigerant goes to the pumps forcing the liquid circulation (No. 4). Then, through an insulated pipeline - (No. 5), it goes to pre-insulated pipes (No. 6). Measurement of temperature at the inlet (No. 7), measurement of the external temperature of the pipeline at the outlet (No. 8) Measurement of the flow with a turbine sensor is located at the outlet of the pipeline (No. 9). Then the refrigerant goes to the accumulation tank (No. 1) - the whole cycle starts again.

In order to obtain laminar flow, the inlet section is 1 meter long. The high-temperature pipes (equivalent to the district heating supply line) were made of steel pipes with an internal diameter of 1 inch. The insulation for the discussed system was made of polyethylene cladding with an internal diameter of 28 mm and a thickness of 13 mm. Low temperature system (equivalent to the return line of the municipal heating network) made of flexible, reinforced rubber pipes with an internal diameter of 22 mm. The insulation for the return system was made of polyethylene cladding with an internal diameter of 23 mm and a thickness of 13 mm.

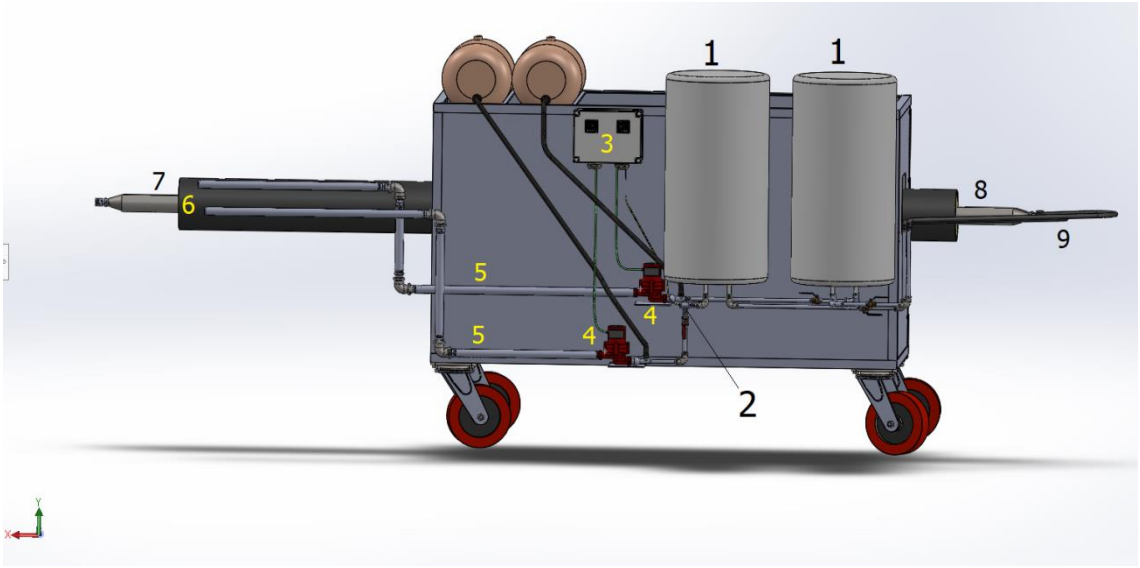

Figure 7.1 3D model of the test stand for heat loss in pre-insulated pipes of district heating networks.

7.2. Electrical circuits

Wiring diagram of the supply circuit (high temperature - Fig. 7.2b) and the return circuit (low temperature - Fig. 7.2a).

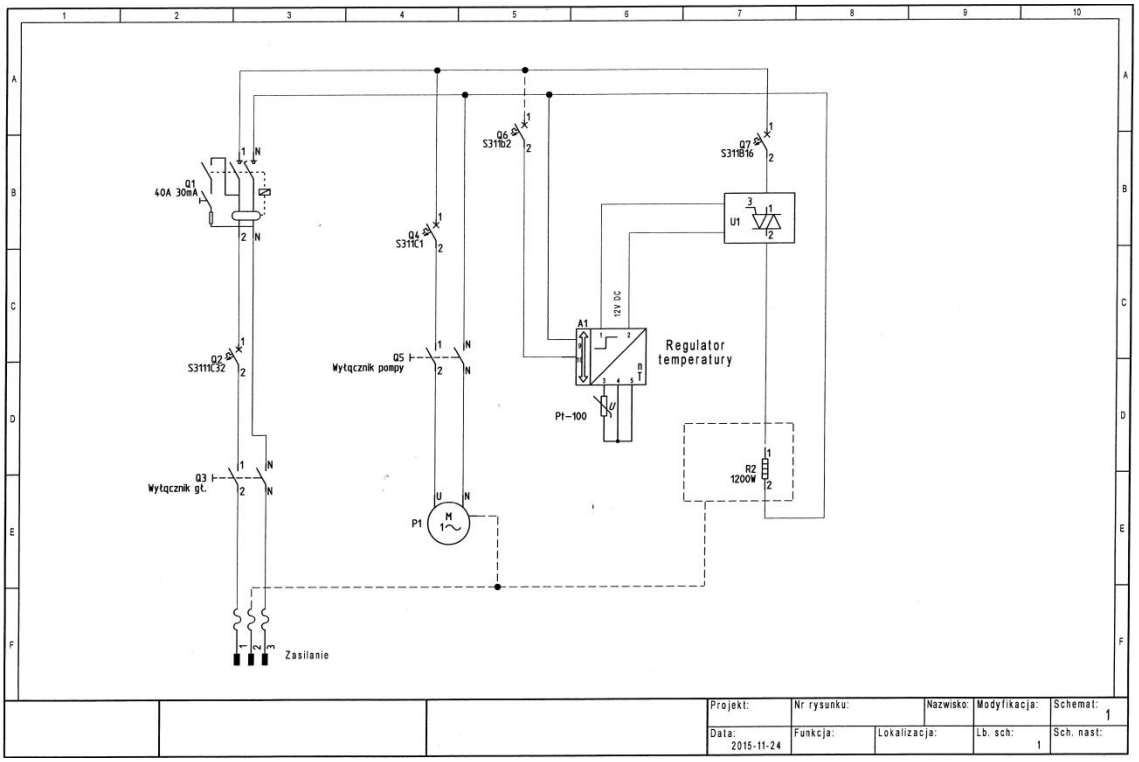

Figure 7.2a Electrical diagram of the return circuit: P1 - centrifugal pump; Q1 - Residual current circuit breaker; Q3 - pump switch; Q5 - pump switch; A1 - Temperature controller; U1 - solid state relay; R2 - Electric heater; U - temperature sensor: Pt-100

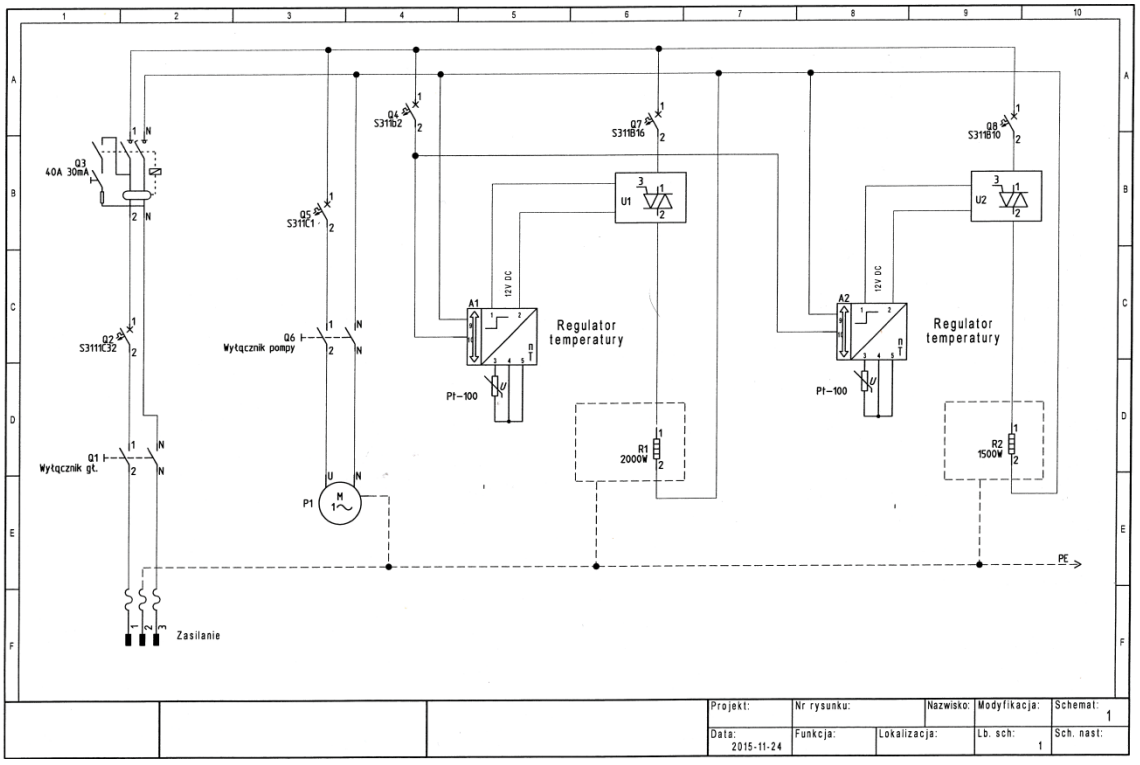

Figure 7.2b Electric diagram of the power supply system: P1 - centrifugal pump; Q1 - Residual current circuit breaker; Q3 - pump switch; Q5 - pump switch; A1, A2 - Temperature

controller; U1, U2 - semiconductor relay; R1, R2 - Electric heater; U - temperature sensor: Pt-100

7.3. Main electrical components

Parameters of the main electrical components as temperature controller, temperature sensor, electric heater (no 1 and no 2), are presented below

1. **Temperature controller :** model REX-C100FK02-M*AN
   - Accuracy: 0.5% lub +/- 3°C
   - Sampling time: 0.5s
   - Current-carrying capacity: 7A 250VAC/10A 125VAC/10A 125VDC/10A 28VDC
   - Temperature range: -199.9 – +1820°C
   - Working temperature: 0–50°C
   - Power supply: AC 220-230V

2. **Temperature sensor:**
   - Thermocouple type: K
   - Temperature range : -30 - 500°C
   - Cover: stainless steel
   - Cable fixing: glued sheath
   - Sheath diameter: 5 mm
   - Sheath length: 30 mm
   - Cable length: 1.5 m

3. **Electric heater No. 1 used:**
   - Storage capacity: 78 l
   - Max. working pressure: 6 bar
   - Heater power: 1500 W + 2000 W
   - Temp. adjustment range: 10-90°C
   - Heating time to 40°C: 1.6 hours
   - Heating time to 90°C: 5.0 h
   - Dimensions: 1310 x 365 mm

4. Electric heater No. 2 used:

- Storage capacity: 50 l
- Max. working pressure: 6 bar
- Heater power: 1200 W
- Temp. adjustment range: 10-90 ° C
- Heating time to 40°C: 1.6 hours
- Heating time to 90°C: 5.0 h
- Dimensions: 810 x 265 mm

7.4. Temperature measurement system

Temperature archiving was carried out by using two eight-channel AVT 5725 recorders and 16x DS18B20 sensors and included individual program. The photo below shows a partially assembled measuring system.

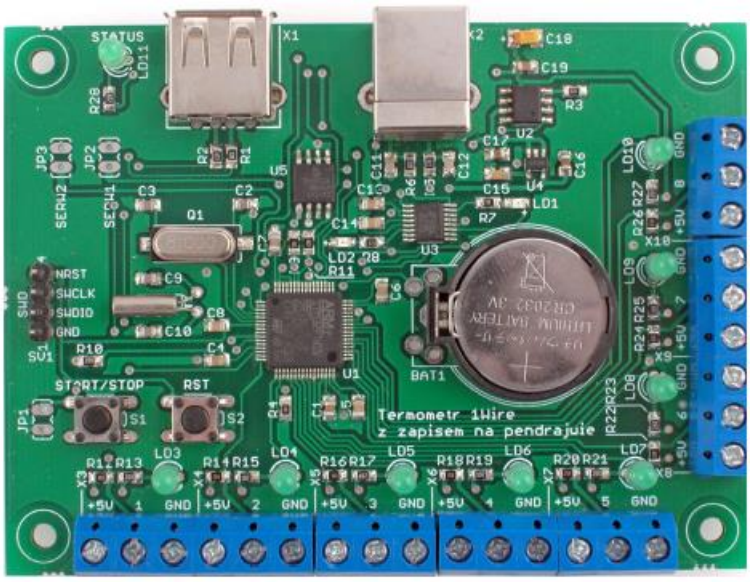

Figure 7.3 Partially assembled measuring system AVT5725 (1) and 4x DS18B20 sensors (2).

Temperature measurement is automatic with an interval of 2 seconds. The generated log is a text file in the form of columns containing the measurement date, time of measurement, and temperature reading for individual sensors. A fragment of the generated file is presented in Fig. 7.4 below.

MT_007 - Notepad

File Edit Format View Help

```
N:210604;Time:035017;T1=  33.0'C;T2=  28.4'C;T3=  19.0'C;T4=  18.8'C;T5=  19.5'C;T6=  20.3'C;T7=  52.5'C;T8=  21.1'C;
N:210604;Time:035019;T1=  34.2'C;T2=  28.8'C;T3=  19.0'C;T4=  18.8'C;T5=  19.5'C;T6=  20.3'C;T7=  53.7'C;T8=  21.4'C;
N:210604;Time:035021;T1=  35.3'C;T2=  29.1'C;T3=  19.0'C;T4=  18.8'C;T5=  19.5'C;T6=  20.3'C;T7=  54.5'C;T8=  21.6'C;
N:210604;Time:035023;T1=  36.3'C;T2=  29.5'C;T3=  19.0'C;T4=  18.8'C;T5=  19.5'C;T6=  20.3'C;T7=  55.3'C;T8=  21.8'C;
N:210604;Time:035025;T1=  37.2'C;T2=  29.8'C;T3=  19.0'C;T4=  18.8'C;T5=  19.5'C;T6=  20.3'C;T7=  56.0'C;T8=  22.0'C;
N:210604;Time:035027;T1=  38.2'C;T2=  30.1'C;T3=  19.0'C;T4=  18.9'C;T5=  19.5'C;T6=  20.3'C;T7=  56.5'C;T8=  22.2'C;
N:210604;Time:035029;T1=  39.1'C;T2=  30.3'C;T3=  19.0'C;T4=  18.9'C;T5=  19.5'C;T6=  20.3'C;T7=  57.1'C;T8=  22.4'C;
N:210604;Time:035031;T1=  40.0'C;T2=  30.6'C;T3=  19.0'C;T4=  18.9'C;T5=  19.5'C;T6=  20.3'C;T7=  57.5'C;T8=  22.6'C;
N:210604;Time:035033;T1=  40.9'C;T2=  30.8'C;T3=  19.0'C;T4=  18.9'C;T5=  19.5'C;T6=  20.3'C;T7=  57.9'C;T8=  22.8'C;
N:210604;Time:035035;T1=  41.7'C;T2=  31.0'C;T3=  19.0'C;T4=  18.9'C;T5=  19.5'C;T6=  20.3'C;T7=  58.3'C;T8=  23.0'C;
N:210604;Time:035037;T1=  42.5'C;T2=  31.2'C;T3=  19.0'C;T4=  18.9'C;T5=  19.5'C;T6=  20.3'C;T7=  58.5'C;T8=  23.2'C;
N:210604;Time:035039;T1=  43.3'C;T2=  31.4'C;T3=  19.0'C;T4=  18.9'C;T5=  19.5'C;T6=  20.3'C;T7=  58.8'C;T8=  23.5'C;
```

Figure 7.4. Extract of a file containing data from the AVT5725 recording system and 8x DS18B20 sensors.

7.5. Temperature measurement – reliability.

Verification of all temperature sensors is performed using Almemo 2890-9 data logger (Fig. 7.5) equipped with T type thermocouple. The point of reference was the boiling point of distilled water.

A B C

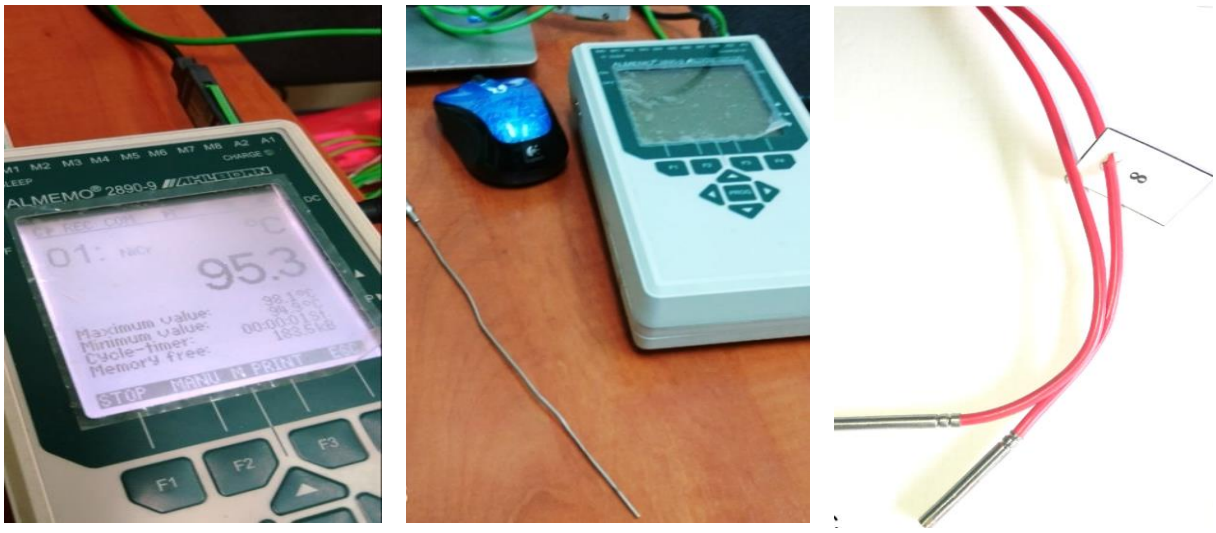

Figure 7.5 The precision measuring instrument used in the verification and calibration of the digital temperature sensors. A – example of measurement, B – Data logger Almemo 2890-9 equipped with T type thermocouple, C – digital thermometer used in recording data in laboratory stab.

The verification is performed according to the following procedure. All sensors are labelled and verified separately. The distilled water is constantly boiled, and temperature is measured by T-type thermocouple and successive digital thermometer. During that, the thermocouple and thermometers are at the same depth in reference from the bottom as well air gaps between them are minimised. Thermal equilibrium is achieved after a few minutes in

a specified position. The calibration is made to check the temperature stability and verify the measurement results to determine suspected records.

At the start of each test on single and double pipes, the single-point temperature verification is performed for sensors located at the beginning and the end of the supply and return of the pipe. A single-point calibration is performed before the start of collecting data. Locations of the sensors are indicated in Fig. 7.6 (3-6) and Fig. 7.7 (3-6, 9-12). The value of the temperature from the digital sensor is compared to the value from Almemo 2890-9 equipped with a T-type (Cu-CuNi) thermocouple to prove the tolerance condition of the loop.

7.6. Temperature measurement – arrangement of sensors

The location of the temperature sensors depends on the system used. Steel single pipes and their TwinPipe counterparts were tested. The temperature is measured at the inlet and outlet of the pre-insulated pipes and on the outer surface of the casing. For the variant with single pipes, two sections of pre-insulated pipes with a length of 3.0 m (length of the insulated surface) were mounted to the device. The diagram of the location of the temperature sensors is presented below (Fig. 7.6 and 7.7).

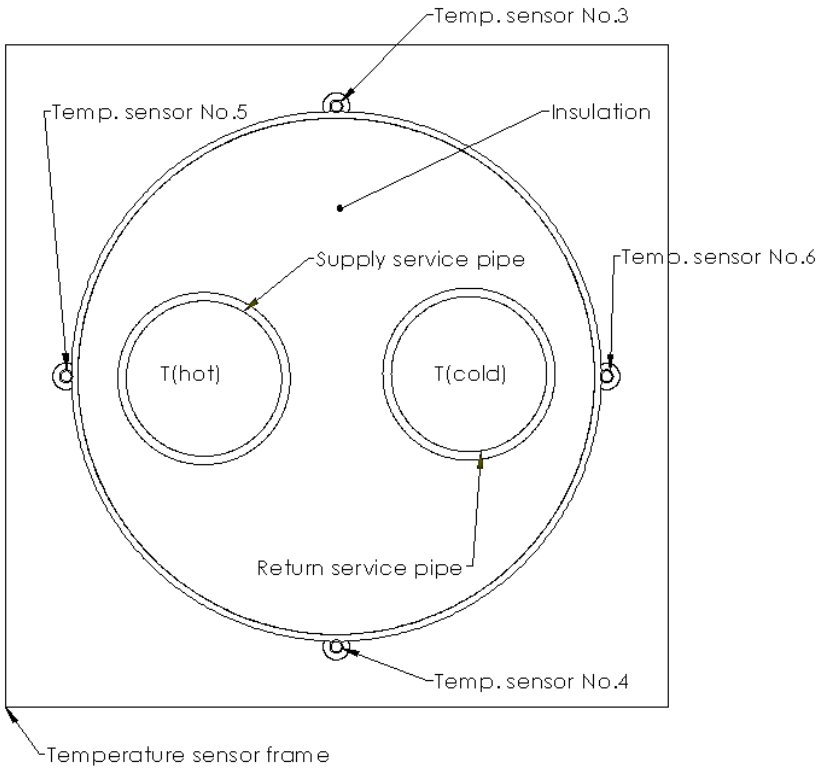

Figure 7.6. Arrangement of DS18B20 temperature sensors for TwinPipe configuration Sensors No. 3 - No. 6 are sensors recording the temperature on the external surface.

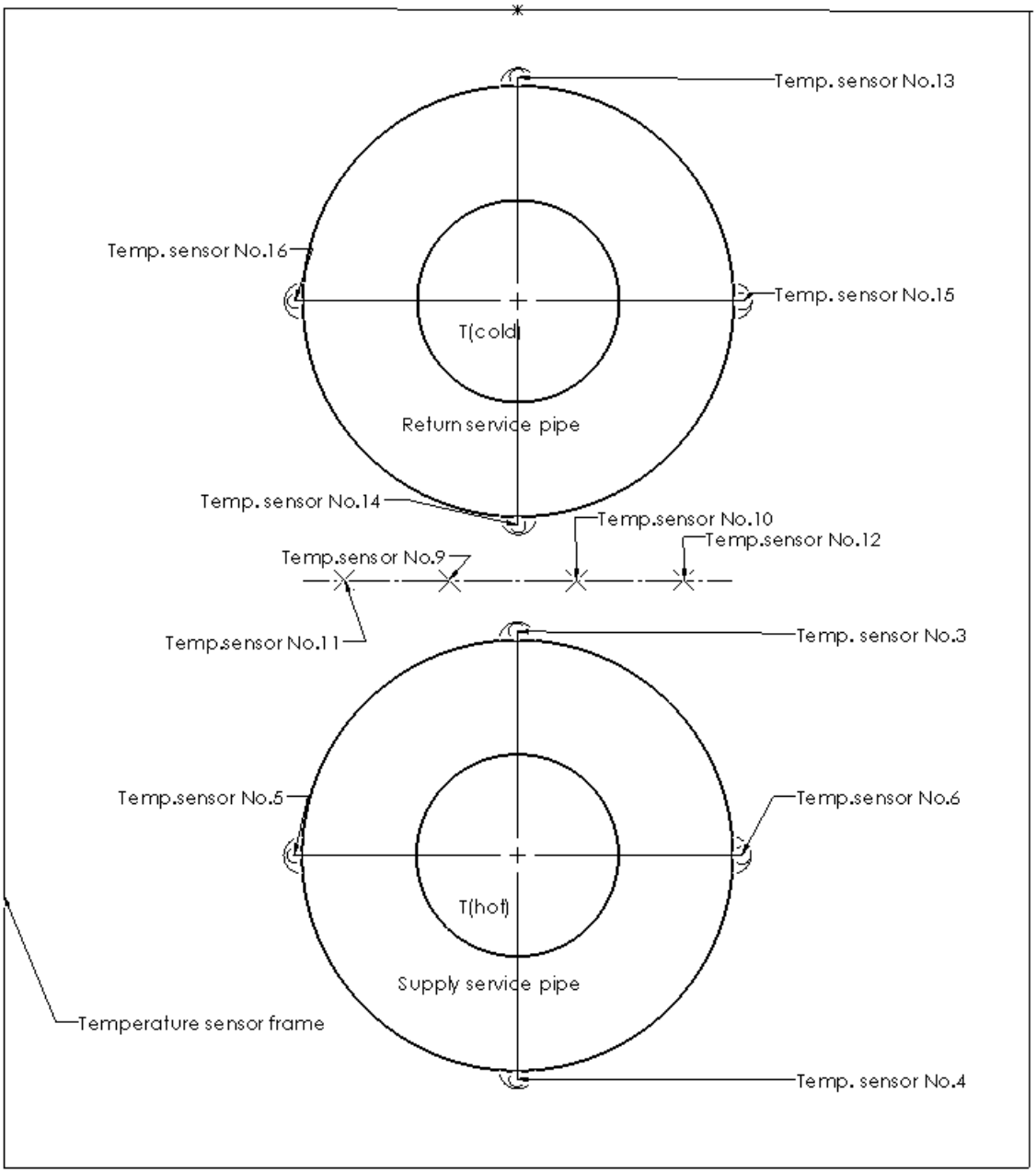

Figure 7.7. Arrangement of DS18B20 temperature sensors for parallel configuration. Sensors No. 3 - No. 6 are sensors recording the temperature on the external surface. Sensors No. 9 - No. 12 are sensors recording the temperature between the supply and return pipes.

7.7. Fluid flow measurement

The tests were carried out with the use of two rotational speeds of impeller pumps. Due to the different internal diameters of the pre-insulated pipes, the supply and discharge lines of the working medium, as well as the inlet and outlet stabs in the accumulative electric heater, it is necessary to measure the flow of the medium in the working system.

Figure 7.8. Turbine digital flow meter US211M used in flow measurements.

For this purpose, a US211M turbine flow meter (Fig. 7.8) was installed in the system. For a system with a higher temperature (the equivalent of a supply line of a municipal heating network), the flow measurement is performed at the entrance to the pre-insulated pipe. The lower temperature system was measured on the section between the outlet from the pre-insulated pipe and the return stub of the electric storage heater. The main parameters of this flow measurements is presented in Table 7.1

Table 7.1 Selected parameters of US211M of used in flow measurements.

Flow sensor connection type	BSPP G 3/4 " male thread
Working voltage	5-18V DC
Repeat error	± 1 %
Temperature range	-20 / - 80 °C
Flow range	2 – 45 l / min
Accuracy	+/-5%

7.8. Opened water system

Heat carrier (or heating medium), a substance thanks to which energy is transported in the form of heat from its source to recipients [72]. The basic requirements for heating factors are:

- High "heat content" when heated
- Low energy loss during transport

- Non-aggressive to the environment
- Price and availability

Water and steam meet the above requirements. Water is a heat carrier used in heating networks with low and high parameters (up to 115 ° C). It is the most widely used heating medium in Poland. The use of steam in heating networks is most often dictated by economic and technical conditions or specific applications, e.g. vulcanization in autoclaves. In a direct simplified comparison of the above two heat carriers (Tab. 7.2)

Table. 7.2 Main advantages and disadvantages of heating factors used in district heating.

	Advantages	Disadvantages
Steam	– Transport via own internal energy	– Lower unit enthalpy: – Water vapor: 241.82 kJ/mol – Steam heat networks have greater heat losses than water losses
Water	– Greater unit enthalpy: Water: 285.83 kJ/mol – Effective transport of refrigerant over longer distances – High heat capacity: 4.2 kJ / kg K	– Additional external energy required for transport

Demineralized water was used in the measuring device. The process of filling the hot and cold system (equivalents of the supply and return systems in the heating network) should start from the upper tanks with a capacity of 25l each. After starting the circulation pump, check the liquid level in the tank by refilling the heating medium. Repeat the procedure until the liquid level in the tank is constant. Following the above algorithm, we fill the system from the lowest level, thanks to which the amount of air in the pipeline and the electric heater is kept to a minimum. The main functions of the tanks (1, 2) shown in Figure 7.9 are as follows:

- Filling the system in such a way as to minimize the amount of air in the system
- Water replenishment necessary due to the replacement of the tested pre-insulated pipes with other ones
- Generation of hydrostatic pressure required for the operation of circulation pumps

– Refilling heat carrier due to leakage

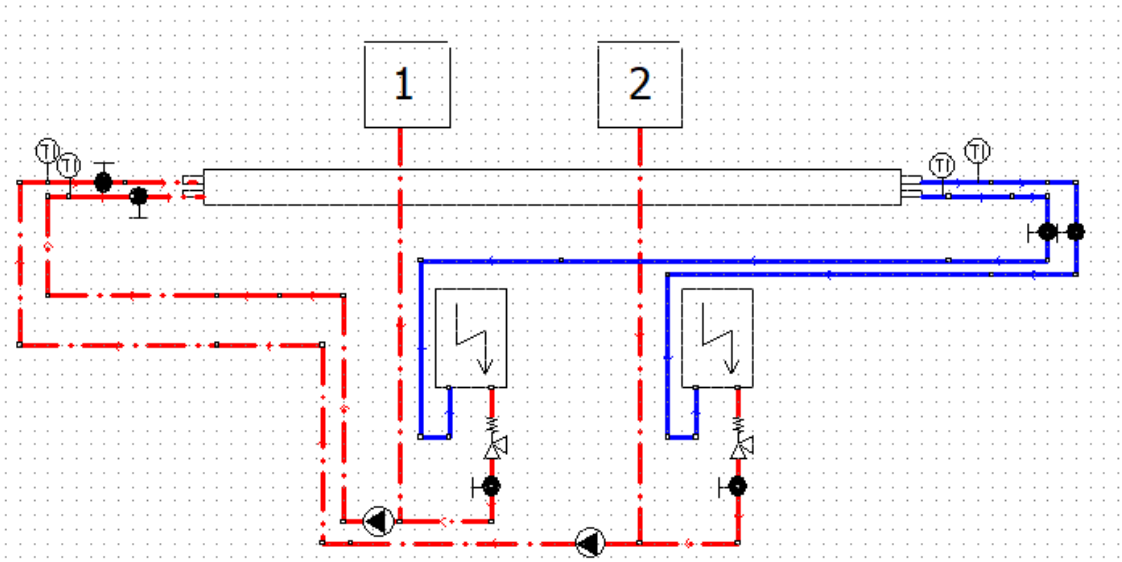

Figure 7.9 Scheme of the circulating water system in a TwinPipe system.

Electric centrifugal pumps were used to force circulation of the medium, one for each transmission line. The performance characteristics of the system are presented in Fig. 7.10.

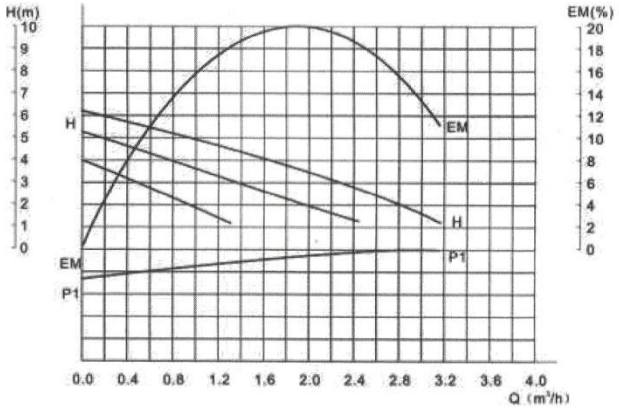

PUMPMODEL OHI	POWER [W]	MAX.FLOW [L/MIN]	MAX.HEAD [M]	INLET/OUTLET [IN]	GW [KG]
25-60-180(high)III 25-60-130(high)III	93	55	6	1 ½" (1" 15-60/130)	2.4
25-60-180(middle)II 25-60-130(middle)II	67	38	5	1 ½" (1"15-60/130)	2.4
25-60-180(low)I 25-60-130(low)I	46	22	3	1 ½" (1"15-60/130)	2.4

Figure 7.10. Table of performance characteristics of the circulation pump of the systems.

All measurements were made in two modes of operation. The first pump gear (Low) and the third gear (high), the theoretical maximum flows are respectively 22.0 and 55.0 [l/min].

8. Statistics

The collecting data had started at the moment of achieving thermal equilibrium (in average after 250 minutes – depending on exterior temperature). The maximum values of temperatures are shown in histograms below (Fig. 8.1 – 8.6). In the tables the statistical information are included Data presented in histograms and tables refer to steady state thermal equilibrium. Calculations are based on 600 probes. The standard deviation, mean, maximum and minimum values are shown. The measurement uncertainty is calculated by following formula:

$$\rho(x) = \frac{1}{\sigma\sqrt{2\pi}} e^{\left[\frac{(x-\mu)^2}{2\sigma^2}\right]}, -\infty < x < \infty, \tag{8.1}$$

where:

μ – is expected value and maximal point on the curve

$\sigma -$ is standard deviation of the results from μ

$\rho(x) -$ is probability density of measured results

The probability value is expressed as a percentage (confidence level). The probability that the normally distributed random variable x is contained in the interval $[x_1, x_2]$ is [30-35], where the Gauss error function is expressed by following formula:

$$erf(u) = \frac{2}{\sqrt{\pi}} \int_0^u e^{(-t^2)} dt = 2\varphi\left(\frac{u}{\sqrt{2}}\right) - 1 \tag{8.2}$$

The table xx below shows confidence level for probability calculated by following formula:

$$P(x_1 \le x \le x_2) = F_{(x_2)} - F_{(x_1)} = \Phi\left(\frac{x_2-\mu}{\sigma}\right) - \Phi\left(\frac{x_1-\mu}{\sigma}\right) = \frac{1}{2}\left[erf\left(\frac{x_2-\mu}{\sqrt{2}\sigma}\right) - erf\left(\frac{x_1-\mu}{\sqrt{2}\sigma}\right)\right] \tag{8.3}$$

Table. 8.1 Table of confidence level $\mu - \Delta x \le x \le \mu + \Delta x$ for calculated probability

Confidence level	Probability $P[\%]$
$\mu - \sigma \leq x \leq \mu + \sigma$	63.8
$\mu - 1.96\,\sigma \leq x \leq \mu + 1.96\,\sigma$	95.0
$\mu - 2\,\sigma \leq x \leq \mu + 2\,\sigma$	95.5
$\mu - 2.58\,\sigma \leq x \leq \mu + 2.58\,\sigma$	99.0
$\mu - 3\,\sigma \leq x \leq \mu + 3\sigma$	99.7

The graphic interpretation of formula (x) and (x) is surface under the plot of the function $\rho(x)$.

Considering the table x attached above, for the level of confidence $\mu - 1.96\,\sigma \leq x \leq \mu + 1.96\,\sigma$, 95 % of the real measured values are contained in range.

The statistics results for P = 95% of probability for supply pipe ”hot pipe” for a single pre-insulated pipe and TwinPipe system (Tab 8.2).

Table. 8.2 The results of probability for P = 95% in two analysis systems (single pipe and TwinPipe) – for supply pipe

Variable		DN pipe	95% CI, for μ
SINGLE PRE-INSULATED PIPE SYSTEM	Inlet hot	DN 40	(74.61, 74.62)
	Outlet hot	DN 40	(72.78, 72.79)
	Inlet hot	DN 50	(80.31, 80.33)
	Outlet hot	DN 50	(77.41, 77.43)
	Inlet hot	DN 65	(79.04, 79.05)
	Outlet hot	DN 65	(74.84, 74.86)
TWIN PIPE SYSTEM	Inlet hot	DN 40 + DN40	(82.81, 82.81)
	Outlet hot	DN 40 + DN40	(78.15, 78.16)
	Inlet hot	DN 50 + DN 50	(78.85, 78.86)
	Outlet hot	DN 50 + DN 50	(76.61, 76.62)
	Inlet hot	DN 65 + DN 65	(74.60, 74.61)
	Outlet hot	DN 65 + DN 65	(72.74, 72.76)

The statistics results for P = 95% of probability for return pipe ”cold pipe” for a single pre-insulated pipe and TwinPipe system.

Table.8.3 The results of probability for P = 95% in two analysis systems (single pipe and TwinPipe) – for return pipe

Variable		DN pipe	95% CI, for μ
SINGLE PRE-INSULATED PIPE SYSTEM	Inlet cold	DN 40	(46.97, 46.99)
	Outlet cold	DN 40	(46.08, 46.09)
	Inlet cold	DN 50	(49.79, 79.80)
	Outlet cold	DN 50	(49.03, 49.04)
	Inlet cold	DN 65	(47.47, 47.48)
	Outlet cold	DN 65	(45.12, 45.13)
TWIN PIPE SYSTEM	Inlet cold	DN 40 + DN40	(47.22, 47.23)
	Outlet cold	DN 40 + DN40	(44.39, 44.40)
	Inlet cold	DN 50 + DN 50	(47.01, 47.02)
	Outlet cold	DN 50 + DN 50	(45.62, 45.63)
	Inlet cold	DN 65 + DN 65	(47.55, 47.57)
	Outlet cold	DN 65 + DN 65	(46.35, 46.37)

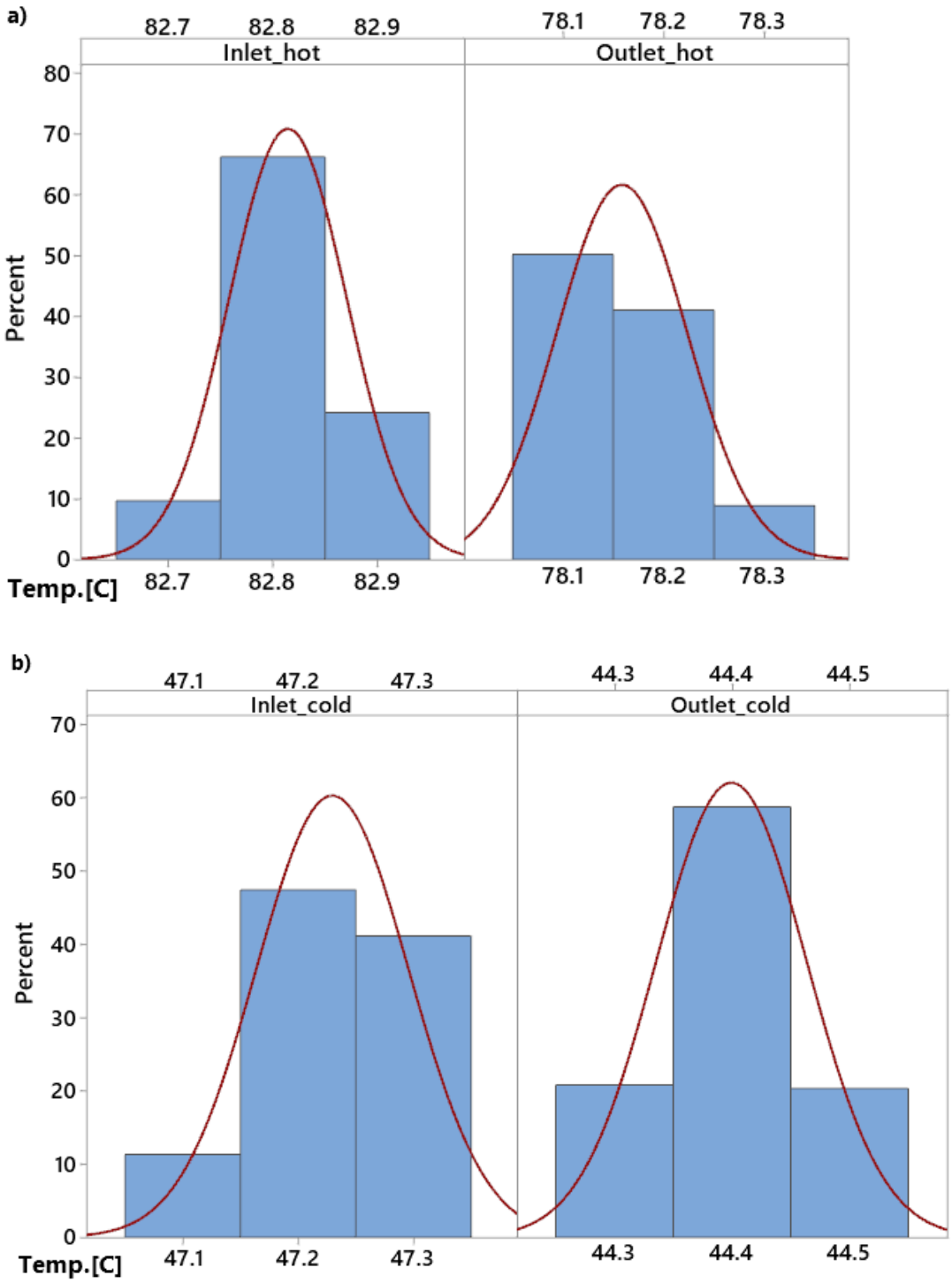

Figure 8.1. Statistical data from the measurement system. Percentage of obtained temperature values for TwinPipe configurations – DN40 supply (a) and return (b) pipe

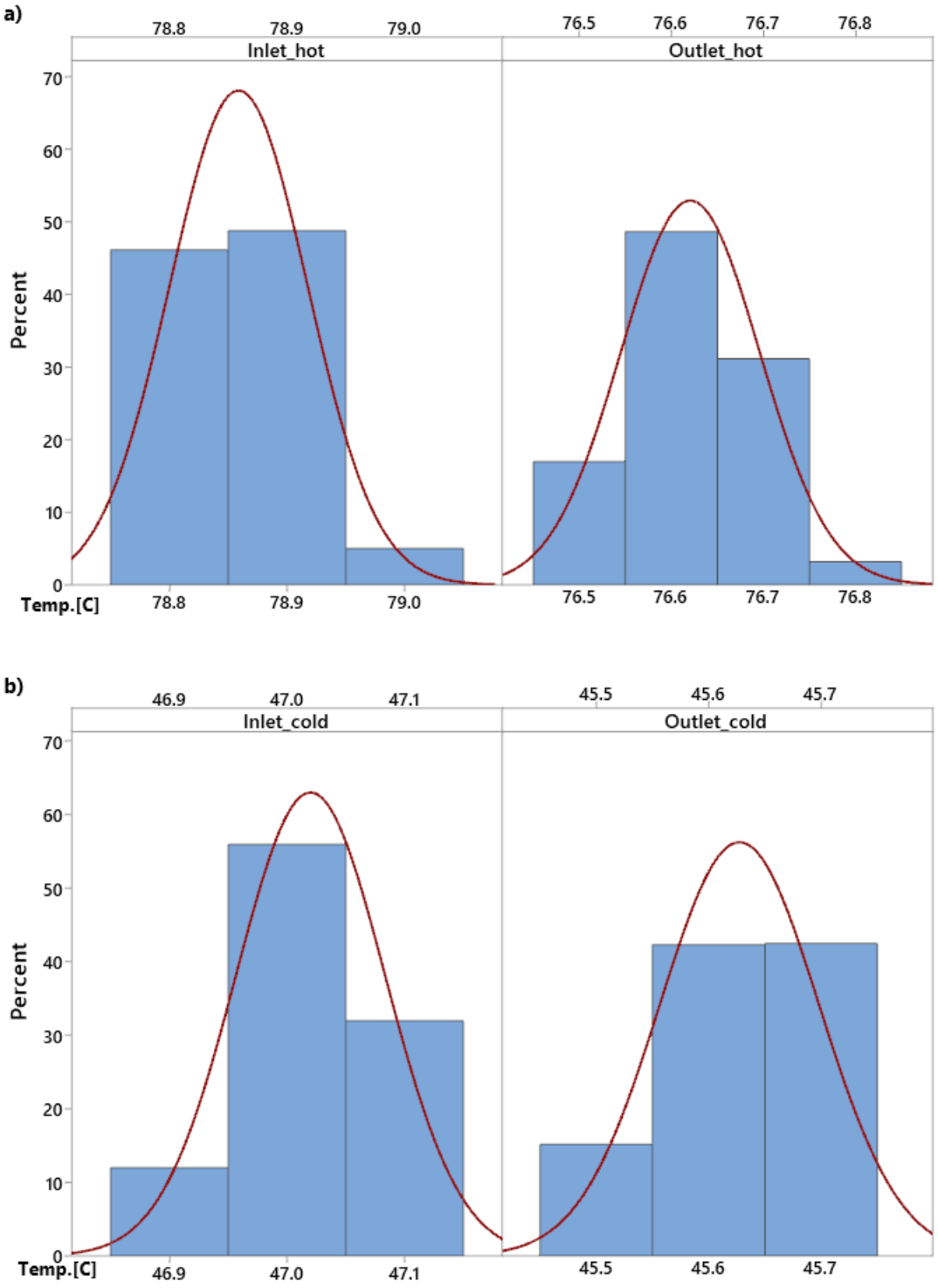

Figure 8.2. Statistical data from the measurement system. Percentage of obtained temperature values for TwinPipe configurations – DN50 supply (a) and return (b) pipe

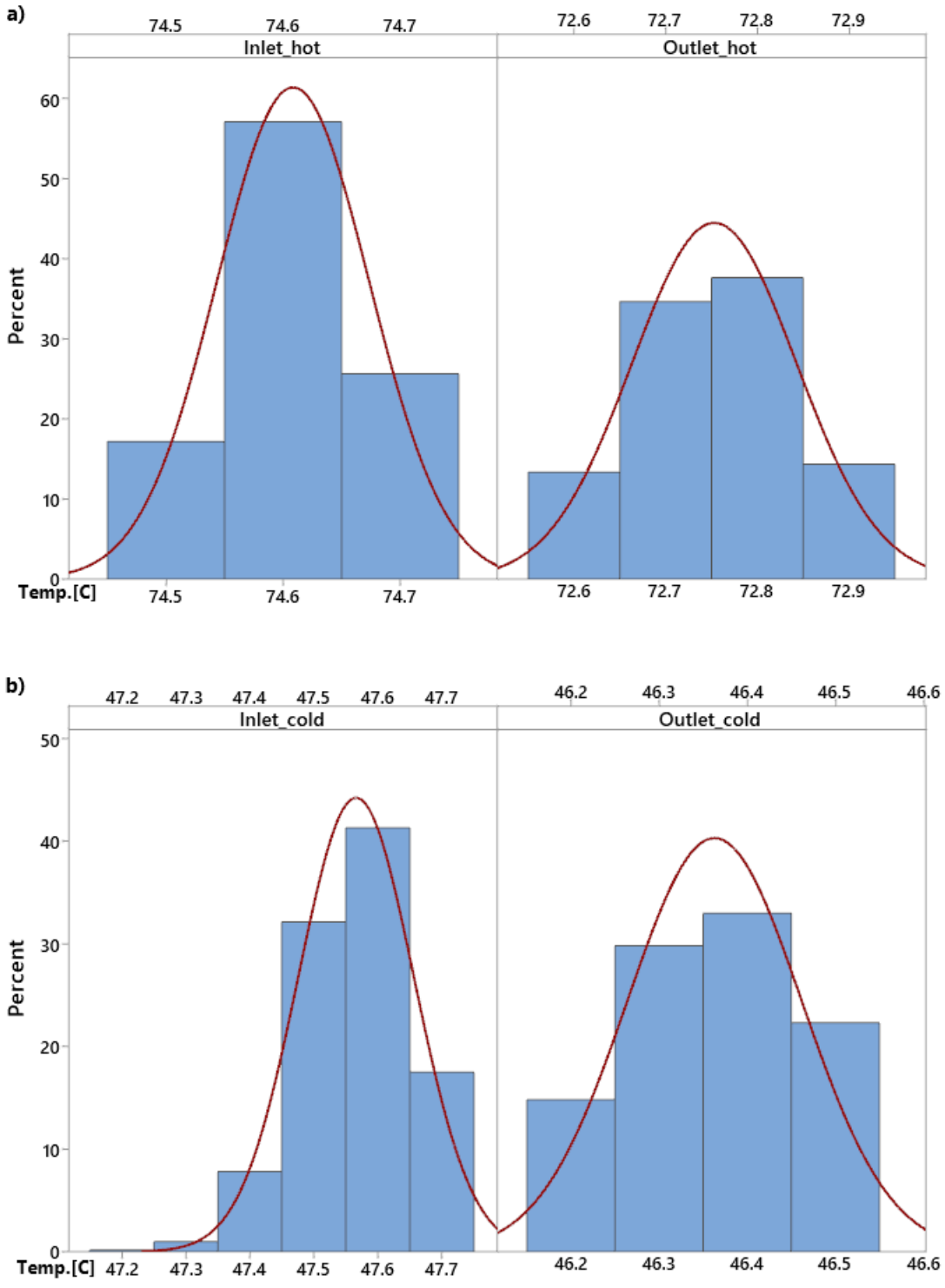

Figure 8.3. Statistical data from the measurement system. Percentage of obtained temperature values for TwinPipe configurations – DN65 supply (a) and return (b) pipe

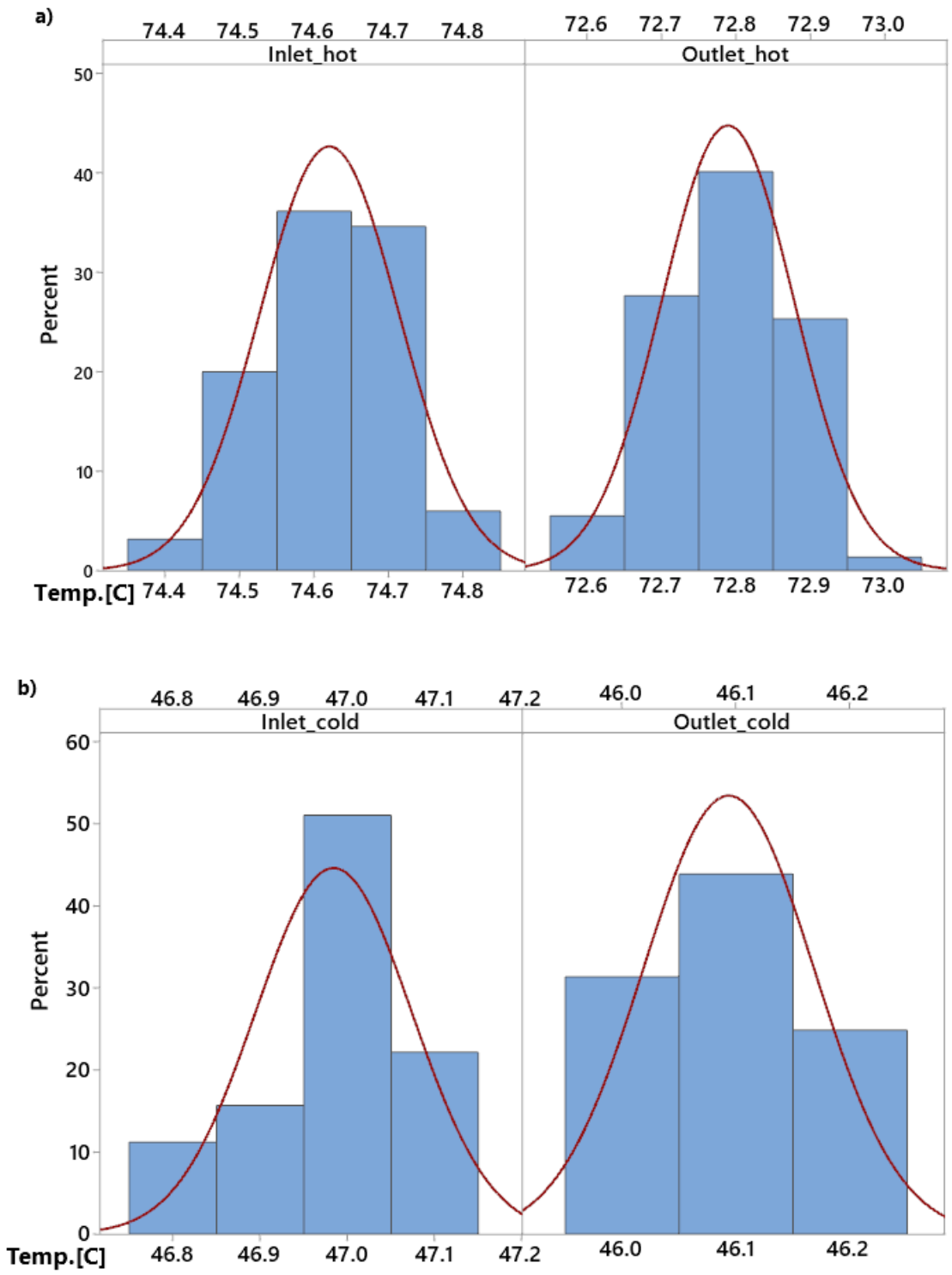

Figure 8.4. Statistical data from the measurement system. Percentage of obtained temperature values for one-single pipe configurations – DN40 supply (a) and return (b) pipe.

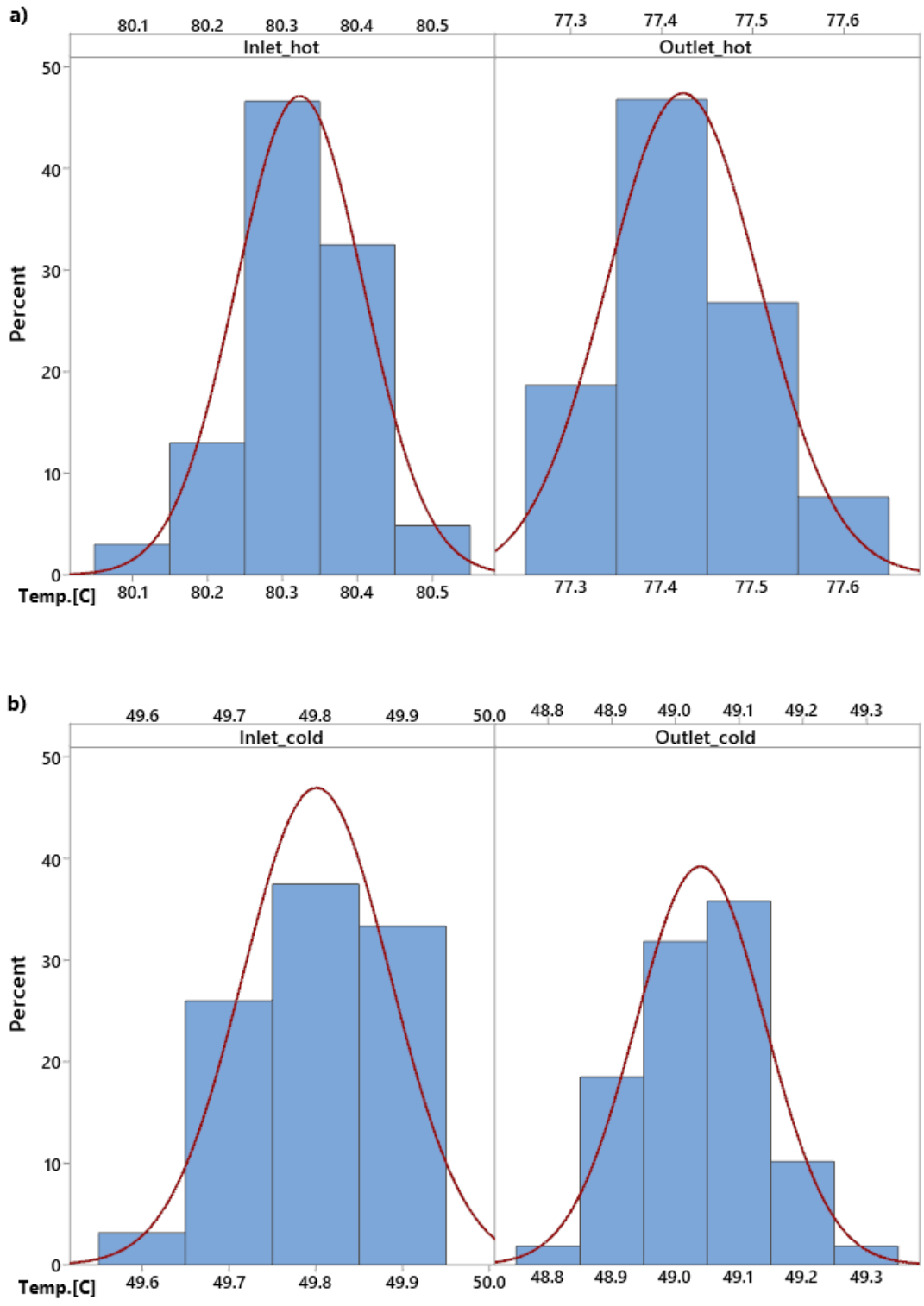

Figure 8.5. Statistical data from the measurement system. Percentage of obtained temperature values for one-single pipe configurations – DN50 supply (a) and return (b) pipe.

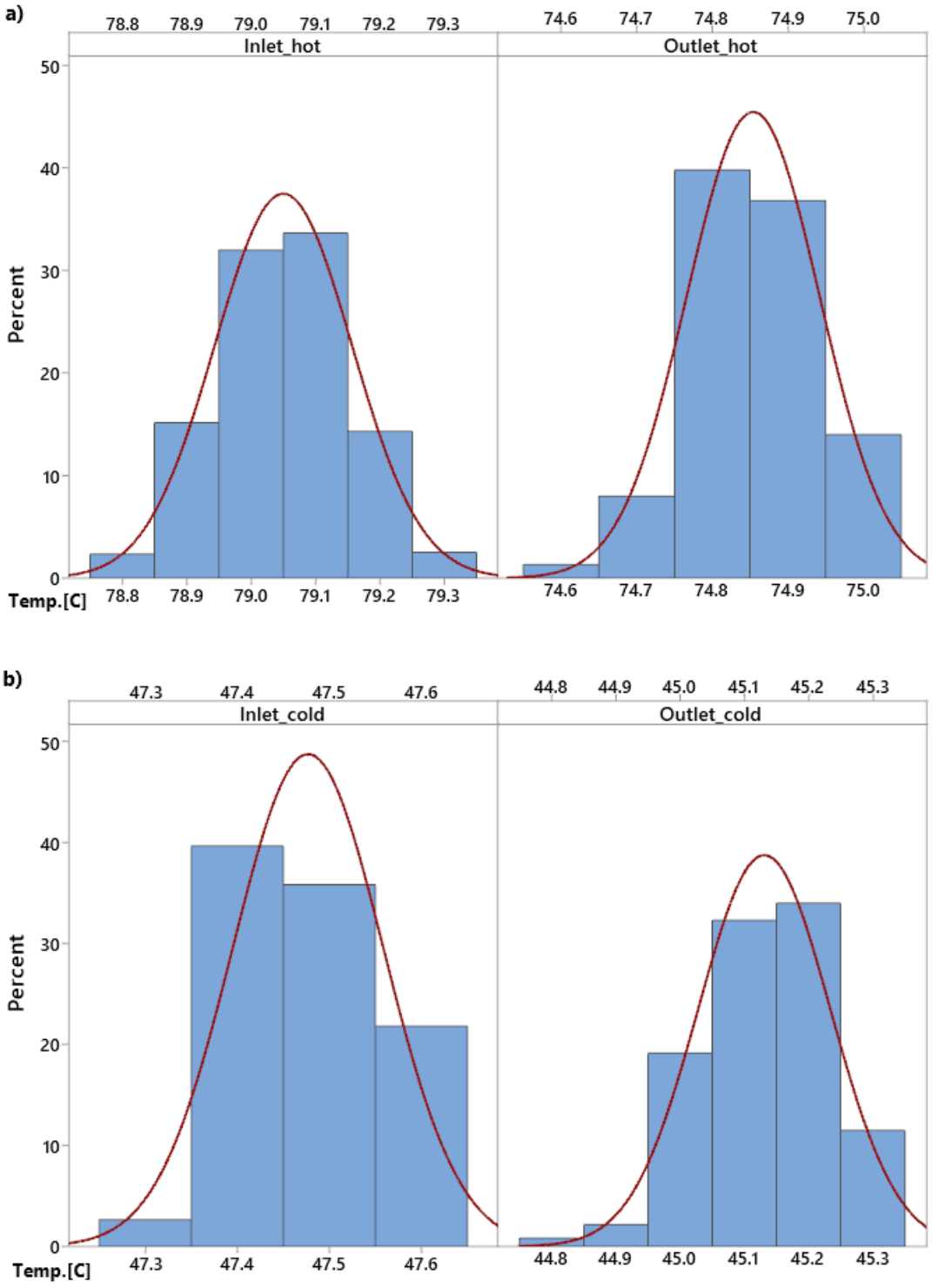

Figure 8.6. Statistical data from the measurement system. Percentage of obtained temperature values for one-single pipe configurations – DN65 supply (a) and return (b) pipe.

The standard deviation (standard uncertainty) of the expected value was calculated from Equation (24):

$$\sigma = \sqrt{\frac{\sum_{i=1}^{n}(x_i - \bar{x})^2}{n(n-1)}} \tag{8.4}$$

where:

x_i –a value of the i-th measurements

$\bar{x}$ - arithmetic mean of measurements

n – number of measurements

The *min* value is the minimum temperature value obtained from the measurements, the *max* is the maximum temperature value measured, *mean* the average value for a set of measurements. The median, on its part, is the middle value. Table 8.4 collects the statistical characteristics of the results for the supply pipe ”hot pipe” for a single pipe and the TwinPipe.

Table 8.4. The results of the temperature measurement errors in the supply side of pipes were obtained for different nominal diameters DN.

Variable		DN pipe	Mean, °C	StDev	Min, °C	Median, °C	Max °C
PRE-INSULATED PARARRALEL PIPE SYSTEM	Inlet hot	DN 40	74.6	0.0935	74.4	74.6	74.8
	Outlet hot	DN 40	72.7	0.0891	72.6	72.8	73.0
	Inlet hot	DN 50	80.3	0.0846	80.1	80.3	80.5
	Outlet hot	DN 50	77.4	0.0841	77.3	77.4	77.6
	Inlet hot	DN 65	79.0	0.106	78.8	79.1	79.3
	Outlet hot	DN 65	74.8	0.0877	74.6	74.9	75.0
TWIN PIPE SYSTEM	Inlet hot	DN 40 + DN40	82.8	0.0564	82.7	82.8	82.9
	Outlet hot	DN 40 + DN40	78.1	0.0648	78.1	78.1	78.3
	Inlet hot	DN 50 + DN 50	78.9	0.0585	78.8	78.9	79.0
	Outlet hot	DN 50 + DN 50	76.6	0.0753	76.5	76.6	76.8
	Inlet hot	DN 65 + DN 65	74.6	0.0649	74.5	74.6	74.7
	Outlet hot	DN 65 + DN 65	72.7	0.0897	72.6	72.8	72.9

In Table 8.5 is collected the statistical characteristics of the results for return pipe ”cold pipe” for a single pipe and TwinPipe system.

Table 8.5. The results of the temperature measurement errors in the return side of pipes were obtained for different nominal diameters DN.

	Variable	DN pipe	Mean , °C	StDev	Min, °C	Median, °C	Max, °C
SINGLE PRE-INSULATED PIPE SYSTEM	Inlet cold	DN 40	46.9	0.0895	46.8	47.0	47.1
	Outlet cold	DN 40	46.0	0.0814	46.0	46.1	46.2
	Inlet cold	DN 50	49.8	0.0849	49.6	49.8	49.9
	Outlet cold	DN 50	49.0	0.1020	48.8	49.0	49.3
	Inlet cold	DN 65	47.4	0.0818	47.3	47.5	47.6
	Outlet cold	DN 65	45.1	0.103	44.8	45.1	45.3
TWIN PIPE SYSTEM	Inlet cold	DN 40 + DN40	47.2	0.0661	47.1	47.2	47.3
	Outlet cold	DN 40 + DN40	44.4	0.0642	44.3	44.4	44.5
	Inlet cold	DN 50 + DN 50	47.0	0.0633	46.9	47.0	47.1
	Outlet cold	DN 50 + DN 50	45.6	0.0709	45.5	45.6	45.7
	Inlet cold	DN 65 + DN 65	47.5	0.901	47.2	47.6	46.5
	Outlet cold	DN 65 + DN 65	46.3	0.098	46.4	46.4	46.5

Table 8.6 presents the temperature value taken for the calculations of the heat losses.

Table 8.6. The results of the temperature measurements on the supply and return side

	DN pipe	T_{hot_in}, °C	T_{hot_out}, °C	T_{cold_in}, °C	T_{cold_out}, °C
SINGLE PRE-INSULATED PIPE SYSTEM	DN 40	74.63	72.78	46.97	46.07
	DN 50	80.33	77.42	49.80	49.03
	DN 65	79.04	74.85	47.47	45.13
TWIN PIPE SYSTEM	DN 40 + DN 40	82.85	78.15	47.26	44.47
	DN 50 + DN 50	78.95	76.62	47.05	45.66
	DN 65 + DN 65	74.63	72.76	47.58	46.35

Based on information included in Table 8.6 and Equations (5.1)-(5.23), the unit heat transfer loss (q) for a single pre-insulated pipe and TwinPipe is calculated and presented in Figures 9.6-9.10 for nominal diameters DN40, DN50 and DN65.

9. Calculation and results

In this section is presented the results of the experimental bench measurements, the results of the analytical and numerical model calculations. The validity of the models used is compared with the measured results. All calculations were carried out for the two district heating network systems analysed: parallel pre-insulated pipes and TwinPipe.

In addition, calculations were carried out using CFD simulation to analyse the temperature distribution in the ground in the vicinity of the district heating network. The results were also compared with experimental results.

9.1 Parameters of the soil, linear dimensions single parallel pre-insulated system and TwinPipe system

The parameters of the soil used on experimental laboratory stab is presented in following Table 9.1: The presented results refer to average parameters of the soil used in trials. The parameters were checked before heating up activity. Pure sandy soil is characterized by high proportion of the sand and little clay. They are quicker to worm up in comparison to clay soil but tends to dry in summer. The pure clay soil remain wet and coil in winter, clay soil contains has ability to keep high amount of water. In order to that worming up take longer. The estimated proportion of the clay and sandy soil in compound is 50/50. The thermo-physical characteristics obtained in trial measurements are in the good agreement with experimental researches at [73]. The greatest impact on coefficient of heat conductivity have:

- density of the soil
- humidity

Tab. 9.1 The main parameters of the soil

Type of the soil	Density ρ $\left[\frac{kg}{m^3}\right]$	Degree of the moisture [%]	Thermal conductivity coefficient λ_{gr} $\left[\frac{W}{mK}\right]$
Compound of the soil (clay and sandy soil)	1800	24	2.2

Based on the research [73] the soil with 5% of humidity comparing to the soil with 15% of humidity gives 50% higher heat transfer coefficient respectively 0.62 and 1.2 $\left[\frac{W}{mK}\right]$.

Dependence of heat conductivity coefficient on the density (respectively 1000 and 2000 $\left[\frac{kg}{m^3}\right]$) of soil for humidity of 20% is respectively 0.5 and 1.4 $\left[\frac{W}{mK}\right]$.

The experimental laboratory stab was designed based on information included in standards [36, 37]. Parameters of pre-insulated pipes system and linear dimensions are shown as follow (Fig. 9.1 and Table 9.2):

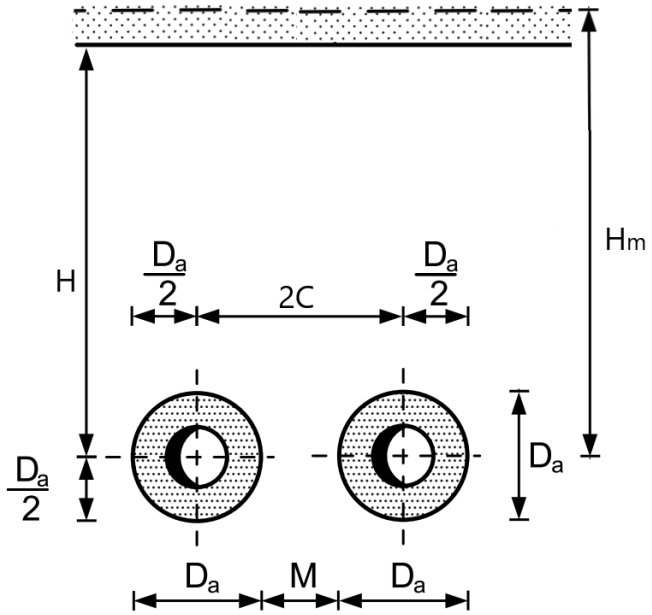

Figure 9.1. Scheme of the underground a pre-insulated single parallel pipe system

Linear dimensions are included in Table 9.2 as shown:

Table. 9.2 The parameters of underground a pre-insulated parallel pipe system for DN 40, DN 50, DN65

–	**DN65**	**DN50**	**DN40**
$2C\ [mm]$	170	170	170
$M\ [mm]$	30	45	60
$D_a\ [mm]$	140	125	110
$H\ [mm]$	455	455	455
$\frac{D_a}{2}\ [mm]$	70.0	62.5	55.0

Material and insulation (polyurethane rigid foam insulation – PUR) properties meets requirements included in norm [74] and [75]

Parameters of TwinPipe system and linear dimensions are shown as follow (Fig. 9.2 and Table 9.3):

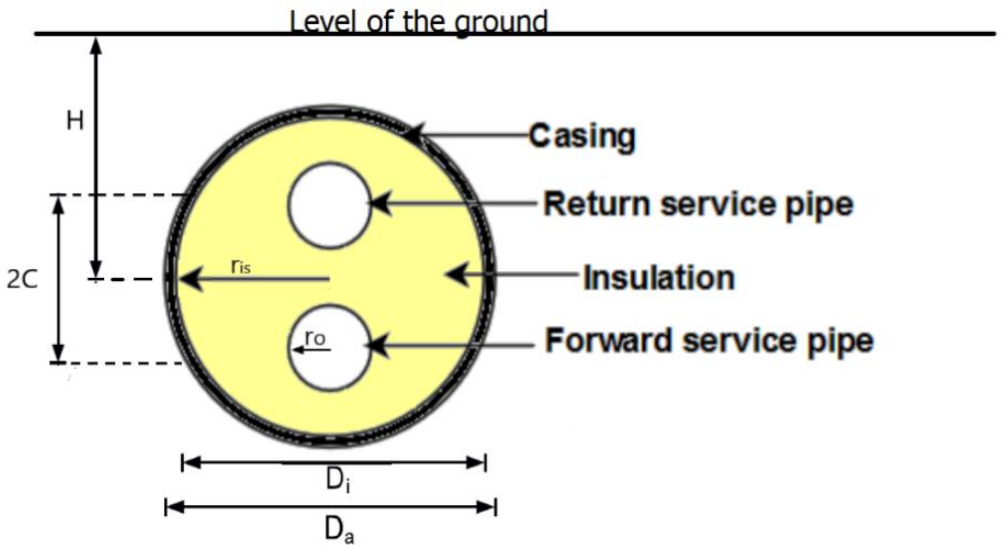

Figure. 9.2. Scheme of the underground a TwinPipe system

Linear dimensions are included in Table 9.2 as shown:

Table. 9.3 The parameters of underground a TwinPipe system for DN 40, DN 50, DN65

–	**DN65**	**DN50**	**DN40**
***2C* [mm]**	48.05	40.15	34.15
D_i **[mm]**	220	195	155
D_a **[mm]**	225	200	160
***H* [mm]**	385	392.5	400
r_{is} **[mm]**	108.3	95.8	75.8
r_o **[mm]**	38.05	30.15	24.15

9.2 Results of analytical, numerical and experimental model

This section presents the results of the steady-state inlet and outlet temperature distribution of the pipe for the two type of configuration (TwinPipe and single pre-insulated

pipes) of pre-insulated pipes depending on different nominal diameters. The temperatures of the water flowing in the pipes and soil temperature are collected by 16 sensors. Temperatures obtained are presented in Table 9.4. The results shown below are the average temperature achieved at the steady state. The measurement interval is 2 s.

The thermal equilibrium (600 cycles) for single pipe configurations is shown in Fig. 9.3., for TwinPipe configurations Fig. 9.4. The plot includes real temperature measurements for the supply section of the pipes. The set temperature values correspond to the supply side of pipes for the third-generation District Heating System (< 100 °C). The lines represent temperatures measured at the beginning and at the end of the examined pre-insulated steel pipe (with a length of 3 m).

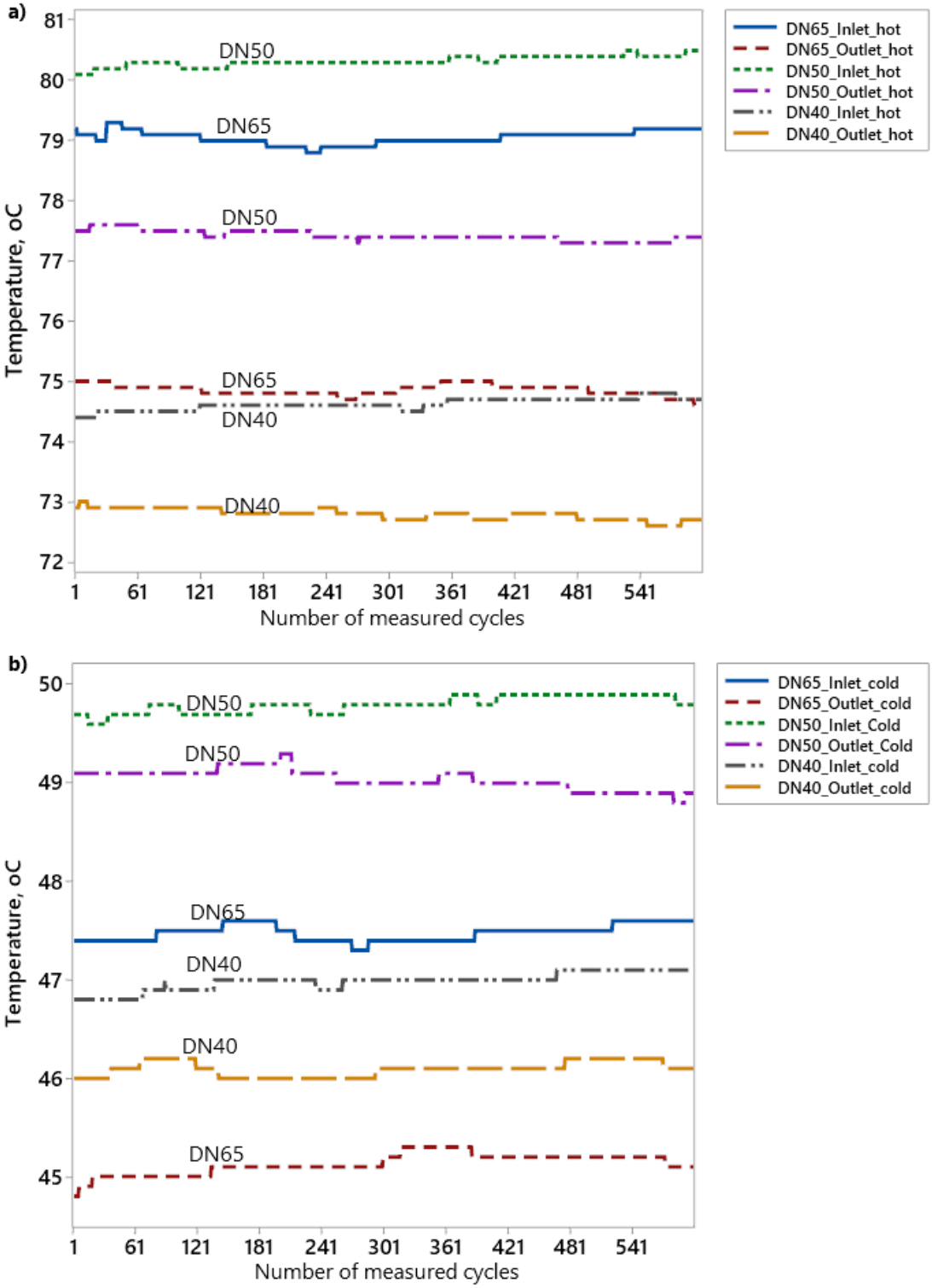

Figure 9.3. Temperature measurements from measurements obtained on single pipe configurations for supply (a) and return (b) pipe.

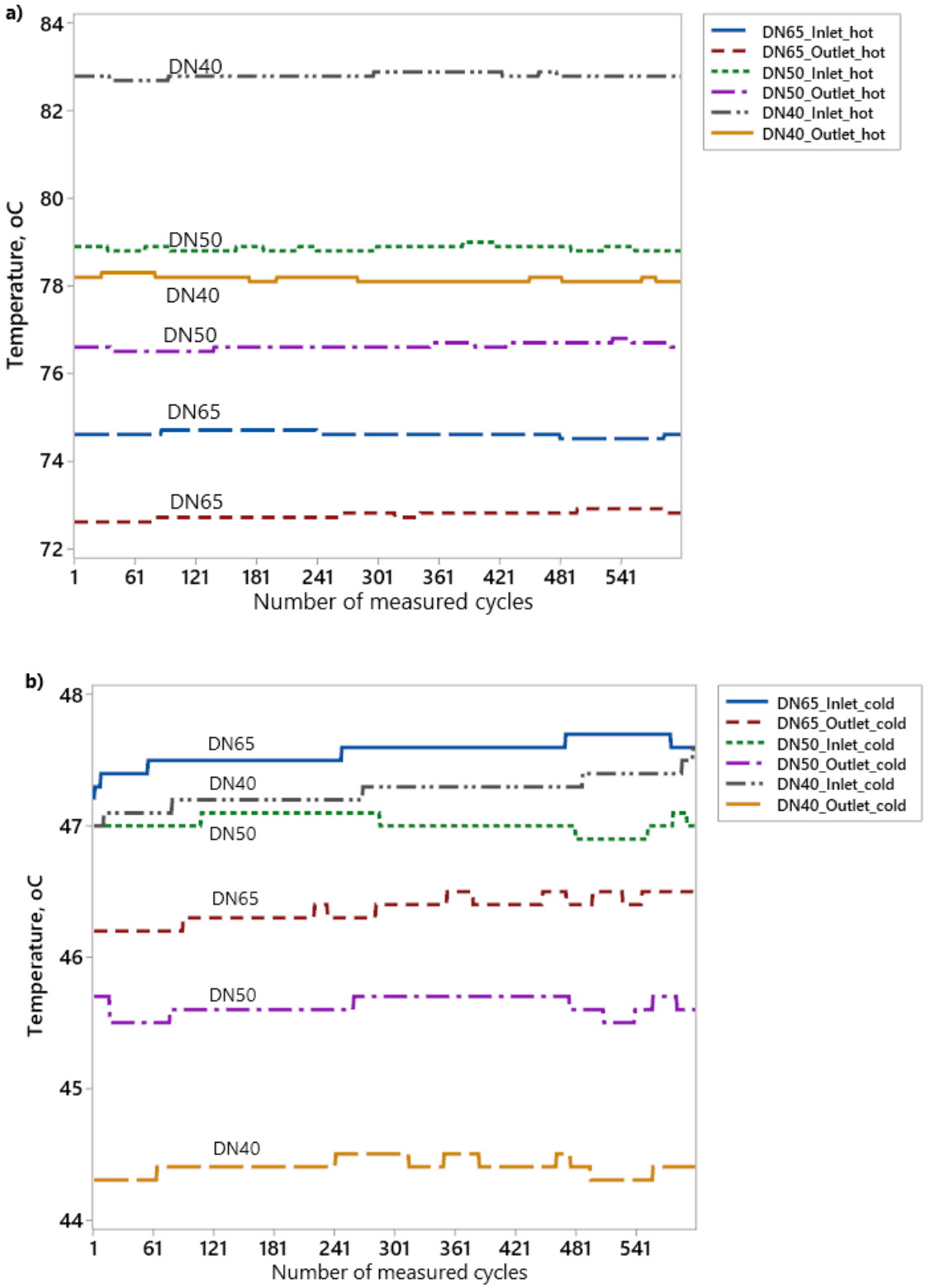

Figure 9.4. Temperature measurements from measurements obtained on TwinPipe configurations for supply (a) and return (b) pipes.

The experimental results

The calculations of experimental model include the value of the measured temperature

Calculation temperature for supply and return pipeline is from equation:

$$T_M = \frac{T_{VL}+T_{RL}}{2} - T_E \tag{9.1}$$

The temperature in supply and return pipeline of analyzed nominal diameter: DN 40, DN 50, DN65 for pre-insulated parallel pipe system in Tab 9.4.

Table. 9.4 The temperature in supply (T_{M_S})and return (T_{M_R}) pipeline of a pre-insulated parallel pipe system for DN 40, DN 50, DN65

Temperature [℃]	DN40	DN50	DN65
$\boldsymbol{T_{M_S}}$	49.905	54.800	56.253
$\boldsymbol{T_{M_R}}$	22.726	26.222	26.602

Heat losses calculation per one meter of pre insulated parallel pipe system pipeline is calculated from eq 9.2 and the value of diameter DN 40, DN 50, DN65 is presented in Tab 9.5. The value of $\sum R$ is calculated from eq. 5.2 (chapter 5).

$$q = \frac{T_M}{\sum R} \tag{9.2}$$

Table. 9.5 The heat losses per unit in supply (q_S)and return (q_r) pipeline of a pre-insulated parallel pipe system for DN 40, DN 50, DN65

q $\left[\frac{W}{m}\right]$	DN40	DN50	DN65
$\boldsymbol{q_s}$	15.42	18.95	22.98
$\boldsymbol{q_r}$	7.02	9.09	10.87
$\boldsymbol{q_s + q_r}$	22.44	28.04	33.85

Heat losses calculation per for one meter of TwinPipe system pipeline is calculated from eq 9.4 and the value for diameter DN 40, DN 50, DN65 is presented in Tab 9.6. The value of h_s is calculated from eq. 5.22 (chapter 5). The value of at the beginning of the pipe (T_1) and at the end (T_2) is from measurement.

$$q_t = 4\pi\lambda h_s \left(\frac{T_1+T_2}{2} - T_0\right) \tag{9.3}$$

Table. 9.6 The heat losses per unit in supply (q_S) and return (q_r) pipeline of a TwinPipe system for DN 40, DN 50, DN65

$\mathbf{q}\left[\frac{W}{m}\right]$	**DN40**	**DN50**	**DN65**
$\boldsymbol{q_s}$	7.84	7.22	7.54
$\boldsymbol{q_r}$	1.70	1.75	1.43
$\boldsymbol{q_s + q_r}$	9.54	8.97	8.97

The analytical results

The analytical calculation of heat loses per one meter of pre insulated parallel pipe system for DN65, DN50, DN40 are calculated from eq. 5.14 (chapter 5) – for supply pipe and eq. 5.15- for return pipe and presented in Tab 9.6.

Table. 9.6 The heat losses per unit in supply (q_s) and return (q_r) pipeline of a pre-insulated parallel pipe system for DN 40, DN 50, DN65

$\mathbf{q}\left[\frac{W}{m}\right]$	**DN40**	**DN50**	**DN65**
$\boldsymbol{q_s}$	16.93	20.77	25.07
$\boldsymbol{q_r}$	7.87	9.98	9.65
$\boldsymbol{q_s + q_r}$	24.80	30.75	34.72

The analytical calculation of heat loses per one meter of TwinPipe system for DN65, DN50, DN40 are calculated from eq. 5.16 (chapter 5) – for supply pipe and eq. 5.17 for return pipe and presented in Tab 9.7.

Tab. 9.7 The heat losses per unit in supply (q_s)and return (q_r) pipeline of a TwinPipe system for DN 40, DN 50, DN65

$\mathbf{q}\left[\frac{W}{m}\right]$	**DN65**	**DN50**	**DN40**
$q_s + q_r$	9.75	8.34	9.65

The numerical results

The scheme of the computational domain is shown in Fig. 5. The heat transfer is assumed to be two dimensional and steady-state.

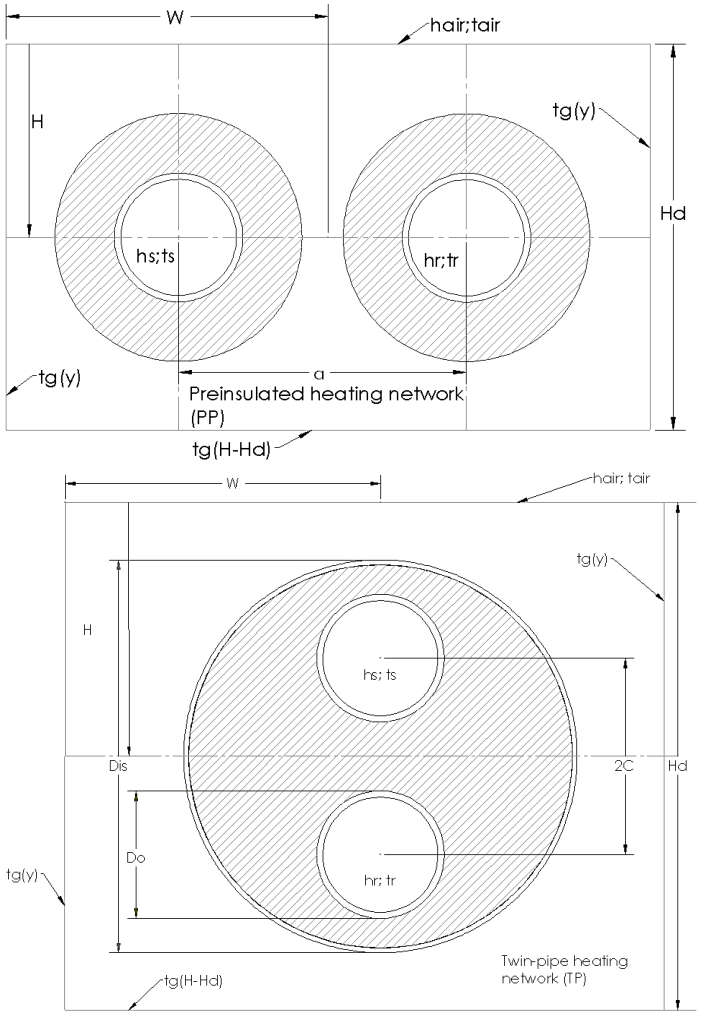

Figure 9.5. Scheme of the computational domain for modeling of pre-insulated heating network

The numerical calculation of heat loses per one meter of a pre insulated parallel pipe system for DN65, DN50, DN40 are calculated from eq. 5.16 (chapter 5) – for supply pipe and eq. 5.17 for return pipe and presented in Tab 9.8.

Table 9.8 The heat losses per unit in supply (q_s) and return (q_r) pipeline of a pre-insulated parallel pipe system for DN 40, DN 50, DN65

q $\left[\frac{W}{m}\right]$	DN40	DN50	DN65
$\boldsymbol{q_s}$	17.49	20.11	24.97
$\boldsymbol{q_r}$	8.52	9.85	11.24
$\boldsymbol{q_s + q_r}$	**26.01**	**29.96**	**36.21**

Table 9.9 The heat losses per unit in supply (q_s)and return (q_r) pipeline of a TwinPipe system for DN 40, DN 50, DN65

q $\left[\frac{W}{m}\right]$	DN40	DN50	DN65
$\boldsymbol{q_s}$	8.31	7.52	7.85
$\boldsymbol{q_r}$	2.66	2.30	2.35
$\boldsymbol{q_s + q_r}$	**9.64**	**8.67**	**9.02**

The comparison of the results of the laboratory test, analytical method and numerical method

The analytical solution results, the numerical solution results and measurement results of heat losses for pre-insulated parallel pipes system at the supply side are presented in Figure 9.6.

The percentage differences between laboratory measurements and the analytical solution results are up to 8.92%, 8.76 %, 8.34 %.

The percentage differences between laboratory measurements and the numerical solution results are up to 14.33 %, 5.77 %, 7.97 %.

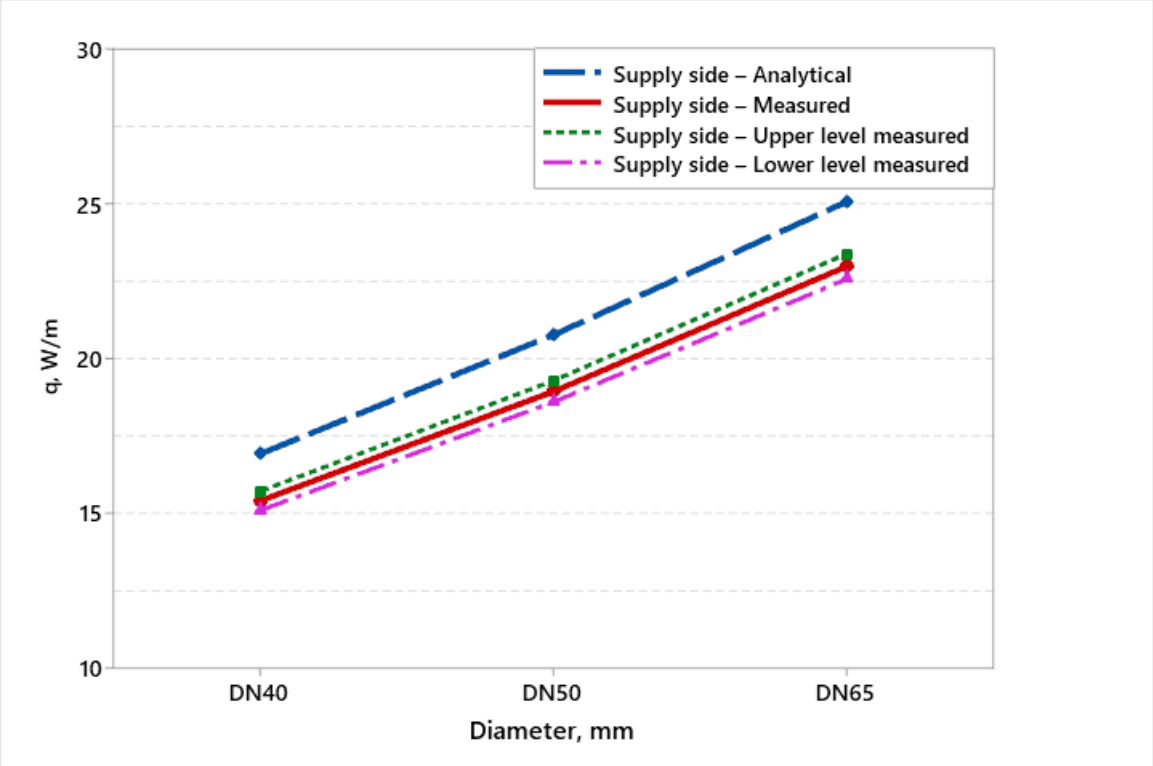

Figure 9.6. Overall heat transfer loss for pre-insulated parallel single pipe – supply side

The analytical and laboratory heat loss comparison for the pre-insulated parallel pipes system at the return side is presented in Figure 9.7.

The percentage difference between laboratory devices and analytical solution results is up to 10.80%, 8.92% and 12.64%.

The percentage difference between laboratory devices and numerical solution results is up to 20.86%, 7.72% and 3.29%.

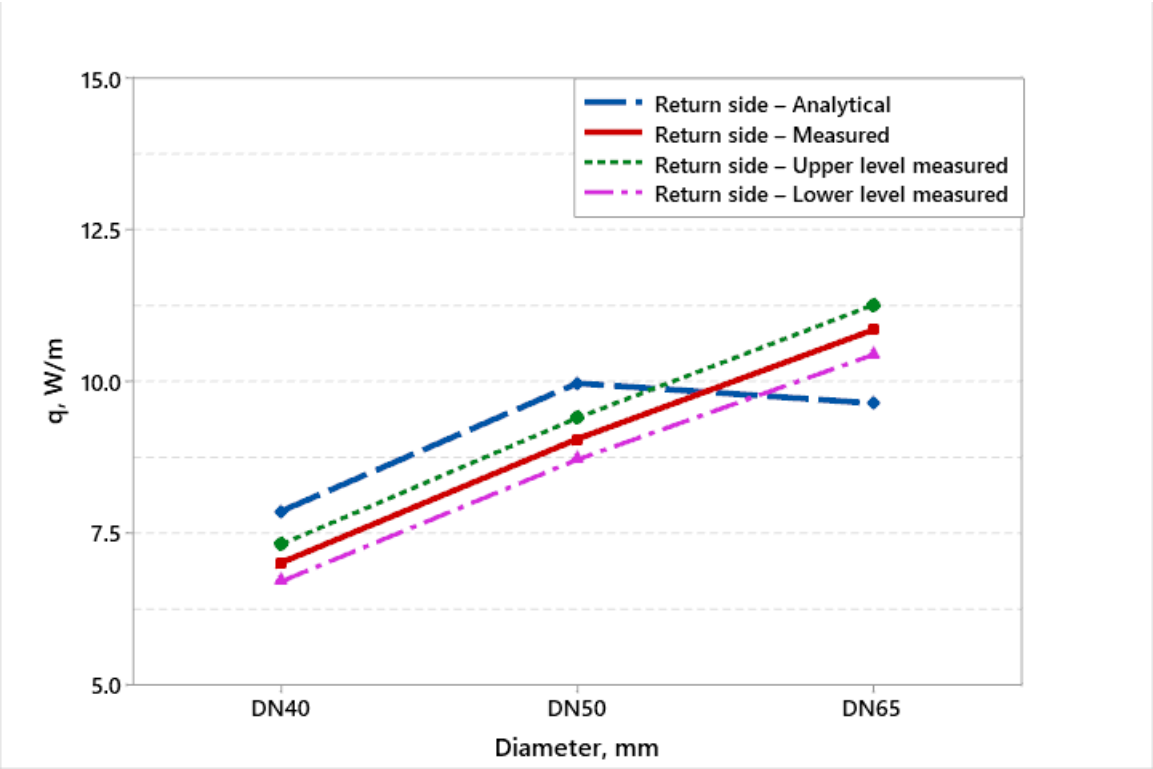

Figure 9.7. The comparison of the results of heat losses for pre-insulated parallel single pipe for various pipe nominal diameter – return pipe

The analytical and laboratory heat loss comparison for the pre-insulated parallel system is presented in Figure 9.8.

The percentage difference between measurements and the analytical solution is to 9.56 %, 8.81 % and 2.51 %

The percentage difference between laboratory devices and numerical solution results is up to 16.56%, 6.41% and 6.52%.

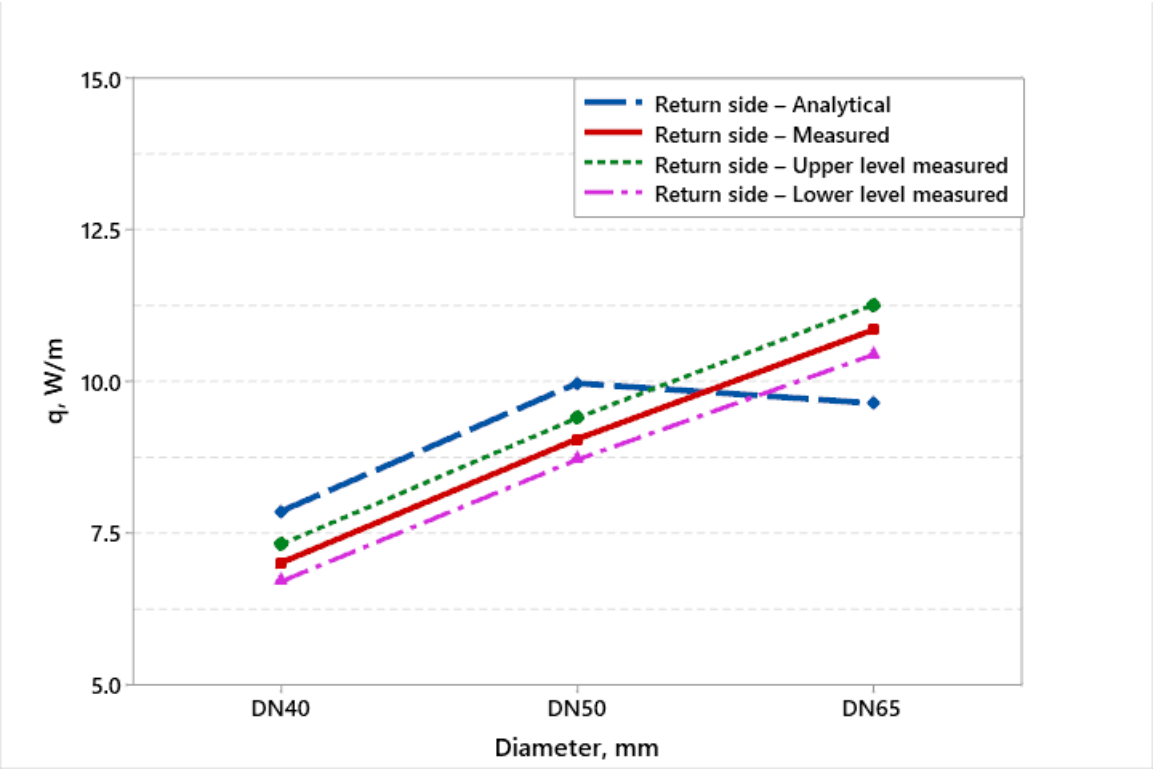

Figure 9.8. The comparison of the results of heat losses for pre-insulated parallel single pipe for various pipe nominal diameter – return pipe

The analytical and laboratory heat loss comparison for the TwinPipe system is presented in Figure 9.9.

The percentage difference between measurements and the analytical solution is to 2.26 %, 6.71 % and 7.05 %

The percentage difference between laboratory devices and numerical solution results is up to 5.65%, 2.77% and 6.95%.

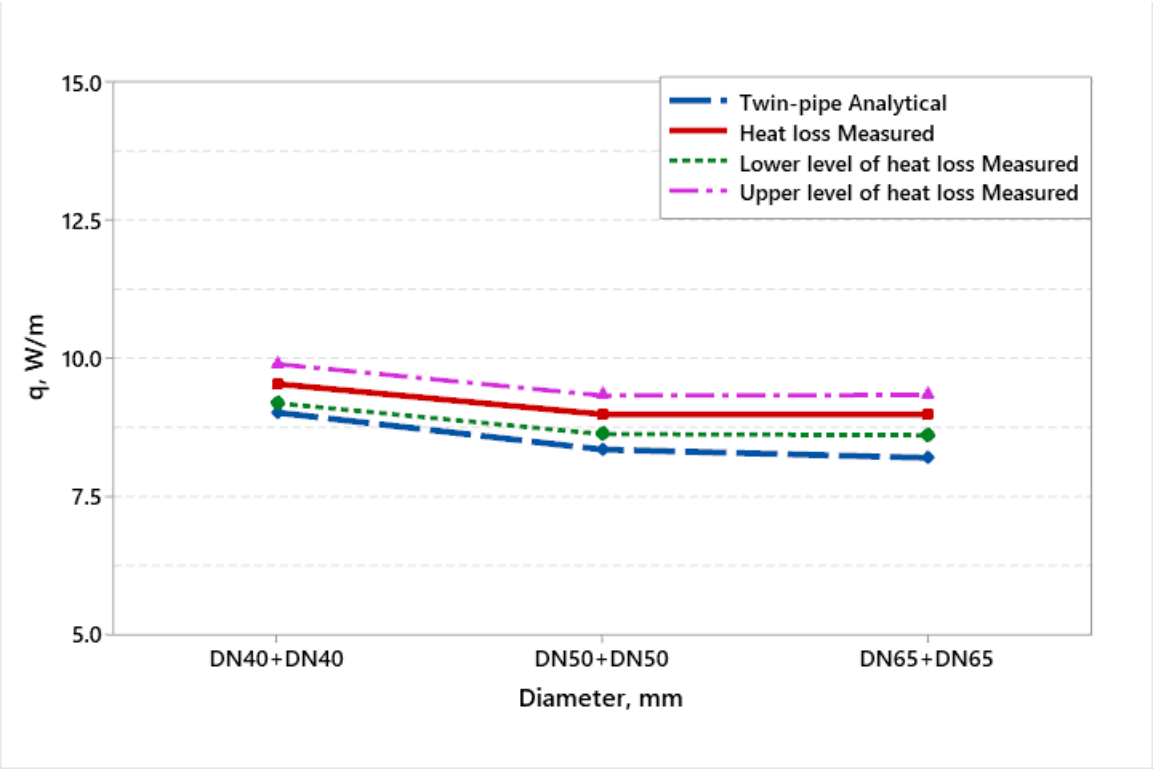

Figure 9.9.The analytical solution results and measured heat loss for the pre-insulated TwinPipe solution

A comparison of the results of the heat losses per one meter from laboratory tests (q_{l_LT}) with the results from analytical method (q_{l_AM}) and numerical method (q_{l_NM}) is given in Table 9.10. and Figure 9.10

Table 9.10. The results of the heat losses with an analytical method and laboratory test

	DN	q_{l_LT}, W/m	q_{l_AM}, W/m	q_{l_NM}
PRE-INSULATED PARALLEL SYSTEM	DN 40	22.43	24.80	26.88
	DN 50	28.00	30.75	29.96
	DN 65	33.84	34.72	36.21
TWIN PIPE SYSTEM	DN 40 + DN40	9.53	9.01	9.02
	DN 50 + DN 50	8.90	8.34	8.67
	DN 65 + DN 65	8.97	8.19	9.64

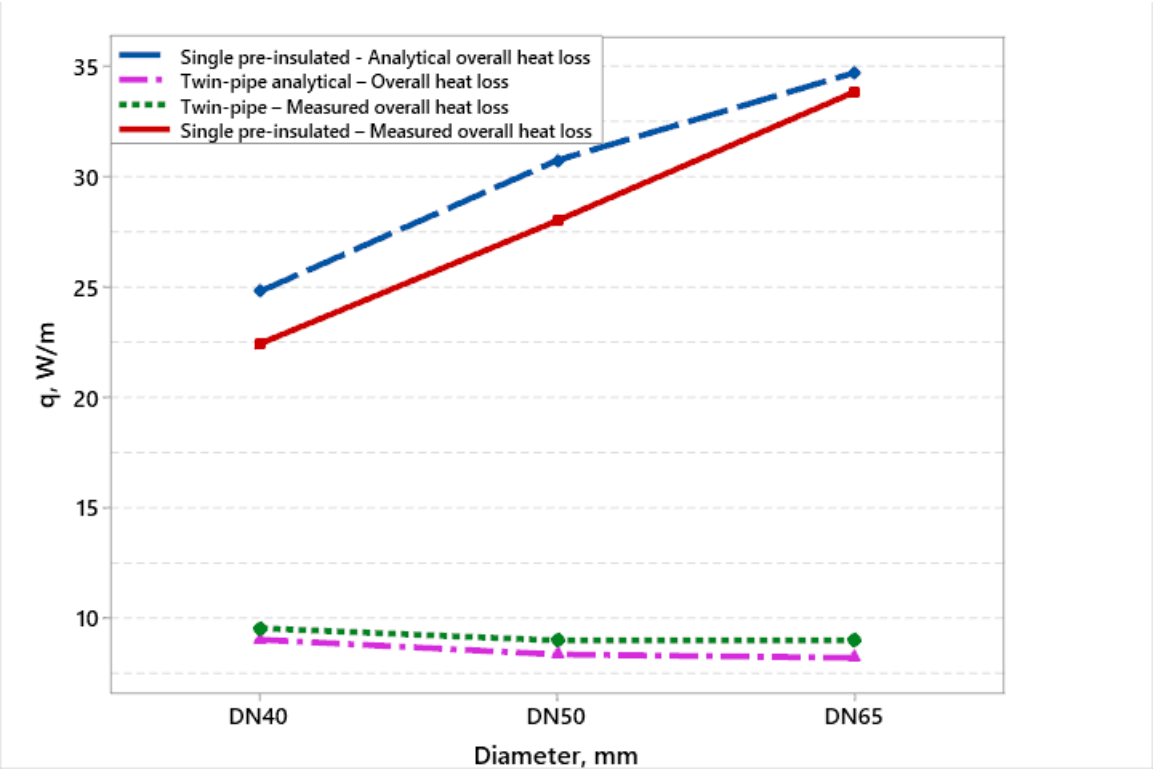

Figure 9.10. Comparison of the analytical solution results and measured heat losses for pre-insulated and TwinPipe systems.

This Figure shows that the analytically calculated heat loss for single pre-insulated and TwinPipes are in good agreement with results obtained during the laboratory tests. The difference between results is up to 5 % for a single pre-insulated pipe system and up to 10 % for a TwinPipe configuration.

9.3 CFD simulation

In this section is presented the results of measurements, computations, and comparisons, covering three measurement series for different size of preinsulated pipes in single parallel and TwinPipe configurations. The thermal conductivity of the insulation had been verified separately for each case. Temperature results are from steady state thermal condition (approx. after 3.5h of heating up). The initial temperature of the soil was used in CFD simulation as a input data.

9.3.1 Bondary conditions

The boundary conditions on geometry prepared in Design Modeler module. The geometry and mesh discretization is shown in Fig. 9.11. The multizone method with hexagonal mapping was applied. The minimum edge length is 0.13163 m. The number of nodes and elements are 68488 and 58265 respectively. The element size defined: 0.008 m.

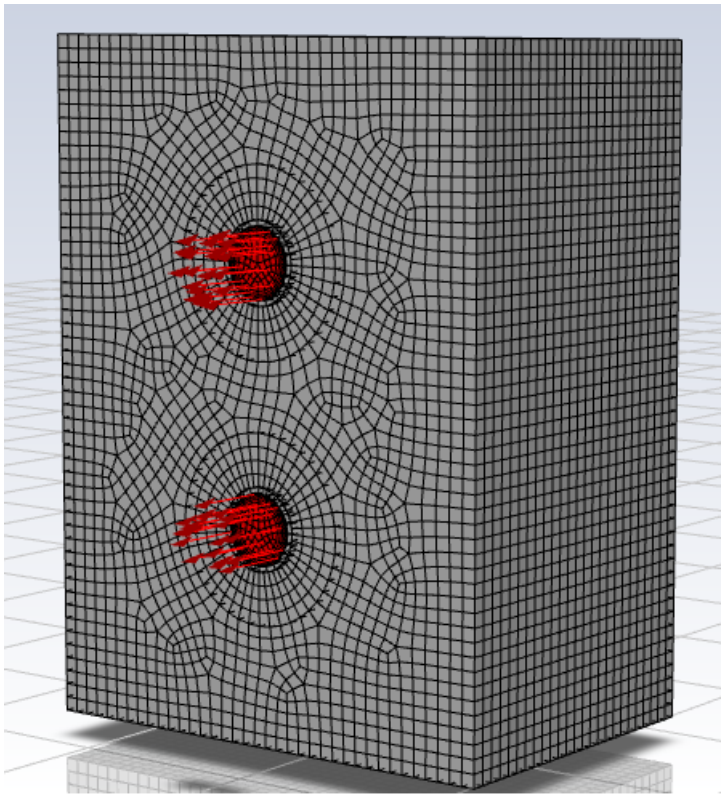

Figure 9.11. The 3D geometry model after discretization process used in CFD simulation.

Applied boundary conditions on geometry are acc.to temperature, thermal conductivity, fluid flow as follows:

- Inlet_1:
  - Velocity magnitude: 1.0 [m/s]
  - Fluid temperature: 85 [°C]
- Inlet_2:
  - Velocity magnitude: 1.0 [m/s]
  - Fluid temperature: 45 [°C]

- Soil_clay:
  - Temperature: 19 [°C]

- Number of iterations: 500.

9.3.2 Single CFD temperature distribution results

In the Figures 9.12 – 9.14 is presented the results of temperature distribution of pre-insulated parallel pipe system for analyzed diameter DN40, DN50, DN65

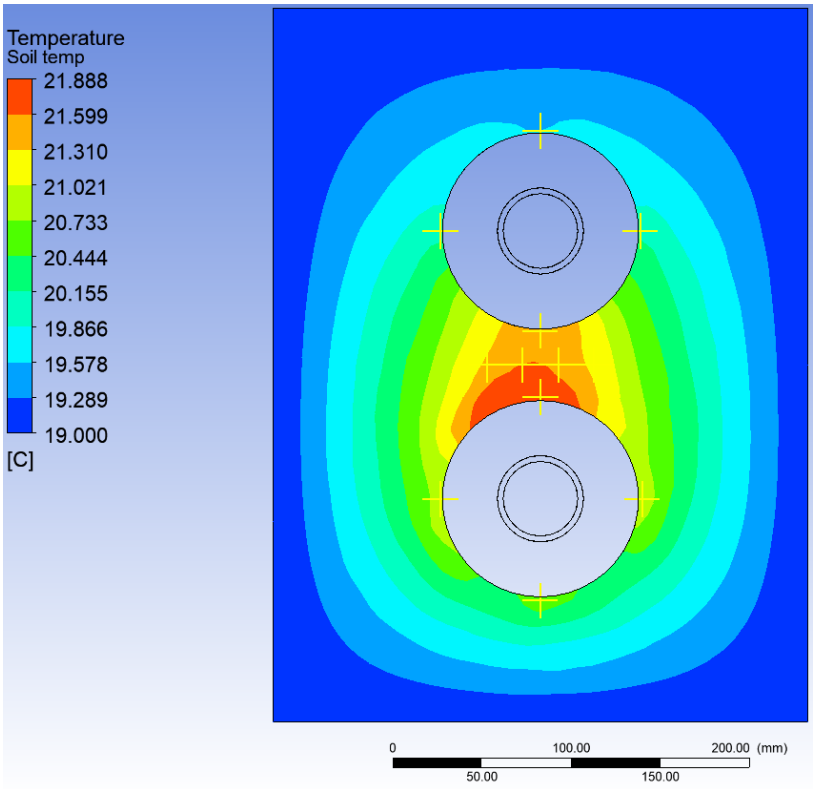

Figure 9.12. Temperature distribution for single configuration – DN40-DN40.

The temperature recorded on sensors 9, 10, 11, 12 are respectively: 21.55°C; 21.55°C; 21.05°C; 21.25°C.

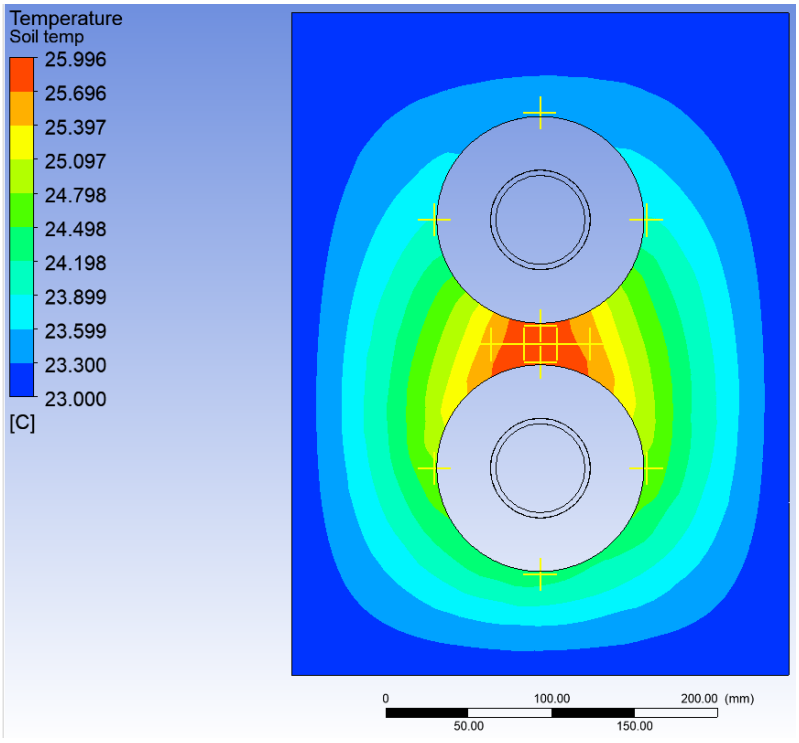

Figure 9.13. Temperature distribution for single configuration – DN50-DN50.

The temperature recorded on sensors 9, 10, 11, 12 are respectively: 25.85°C; 25.85°C; 25.55°C; 25.55 °C;

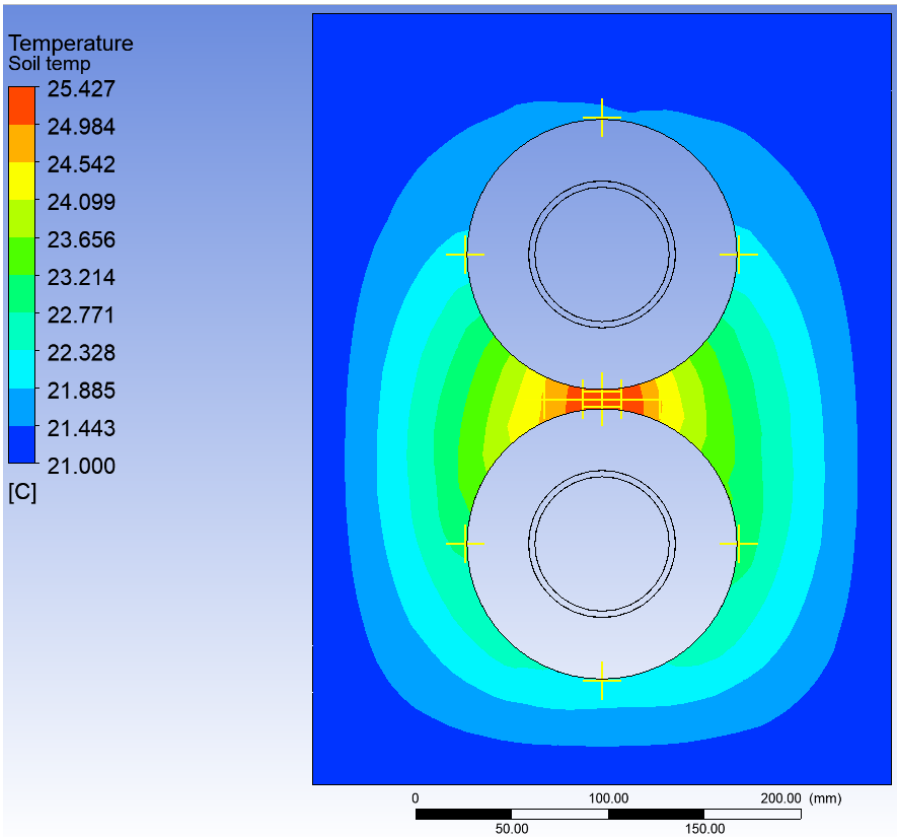

Figure 9.14. Temperature distribution for single configuration – DN65-DN65.

The temperature recorded on sensors 9, 10, 11, 12 are respectively: 25.25°C; 25.35°C; 24.55°C; 24.65°C;

9.3.3 TwinPipe CFD temperature distribution results

In the Figures 9.15 – 9.17 is presented the results of temperature distribution of a TwinPipe system for analyzed diameter DN40, DN50, DN65

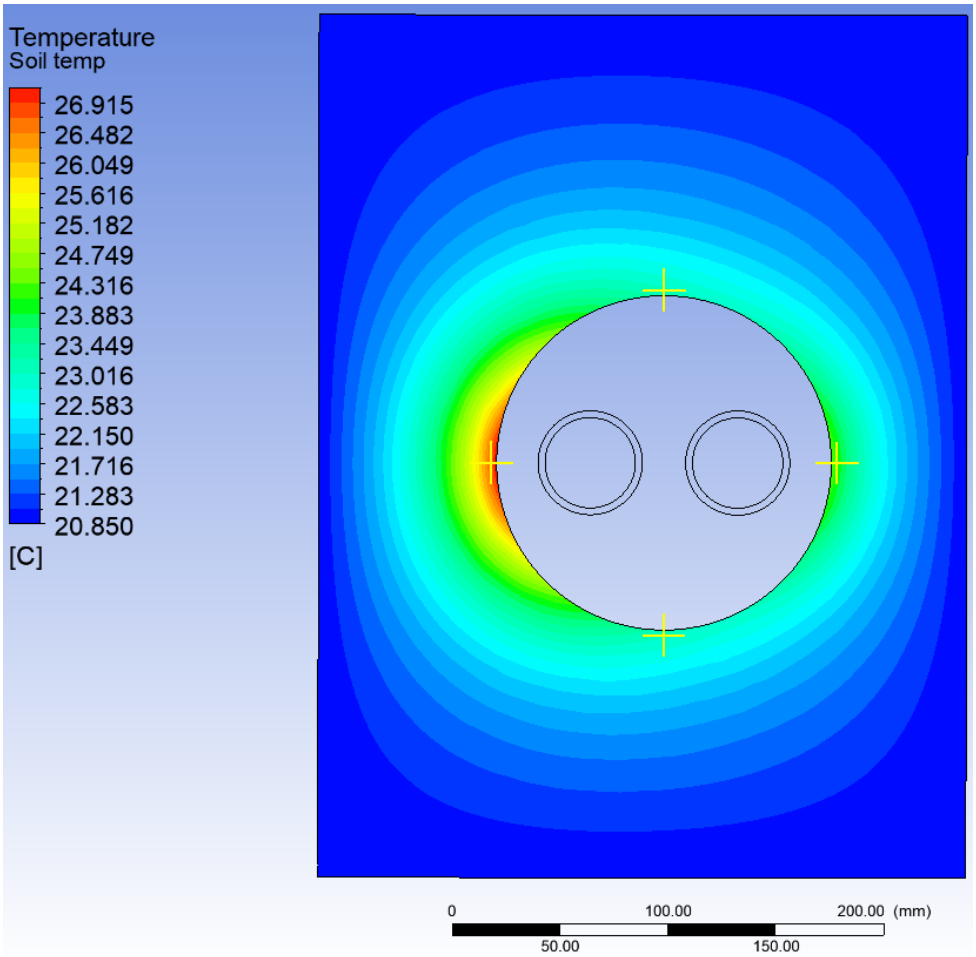

Figure 9.15. Temperature distribution for TwinPipe configuration – DN40-DN40.

The temperature recorded on sensors 3, 4, 5, 6 are respectively: 21.35°C; 21.45°C; 26.75°C; 22.85°C. The average temperature on pipe surface is: 23.1°C.

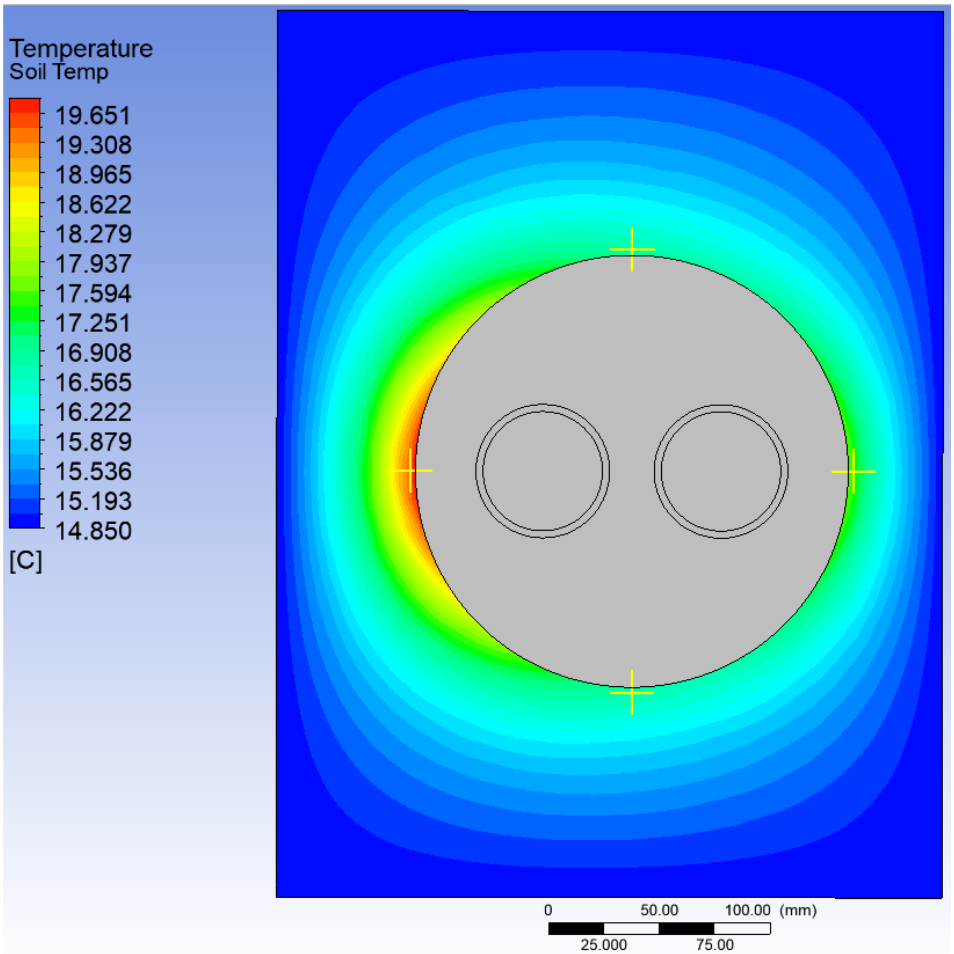

Figure 9.16. Temperature distribution for TwinPipe configuration – DN50-DN50.

The temperature recorded on sensors 3, 4, 5, 6 are respectively: 16.85°C; 16.75°C; 19.55°C; 17.45°C. The average temperature on pipe surface: 17.65°C.

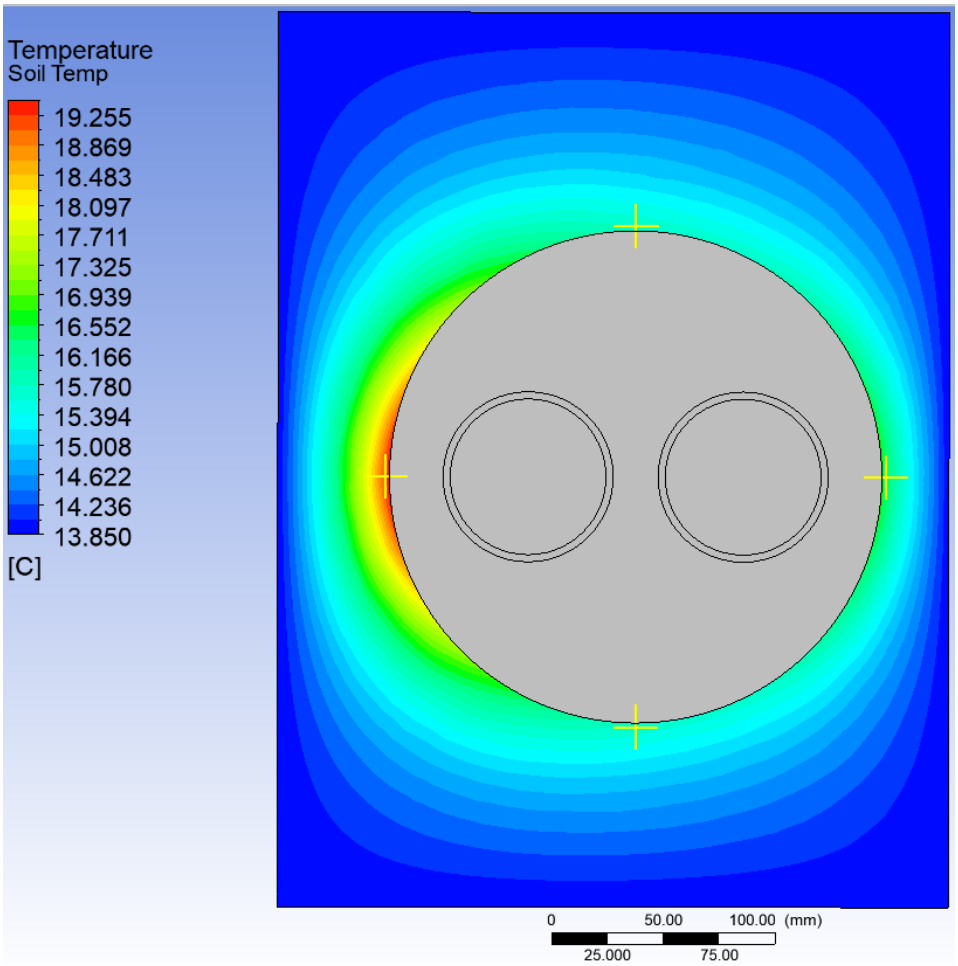

Figure 9.17. Temperature distribution for TwinPipe configuration – DN65-DN65.

The temperature recorded on sensors 3, 4, 5, 6 are respectively: 15.75°C; 15.75°C; 19.05°C; 16.45°C; The average temperature on pipe surface: 16.75°C.

9.3.4 Temperature measurement – results

The heat maps attached below base on temperature measurements during single and TwinPipes examination in the steady state condition. The heat maps are performed in MS excel sheet, temperature cells are calculated using the average of the temperatures values from four neighbouring spots. Maximum number of iterations are limited to 400, maximum change during calculation is limited to 0.001. The area is divided in 3500 cells, the measured values are assigned to excel cells in accordance with sensor arrangement in chapter 7.6

The temperature distributions are presented in Figures 9.18 – 9.20

- Sensors No. 3 - No. 6 are recording the temperature on the outer surface on supply pipe.

- Sensors No. 9 - No. 12 are recording the temperature between the supply and return pipes.
- Sensors No. 13 - No. 16 are recording the temperature on the outer surface on supply pipe.

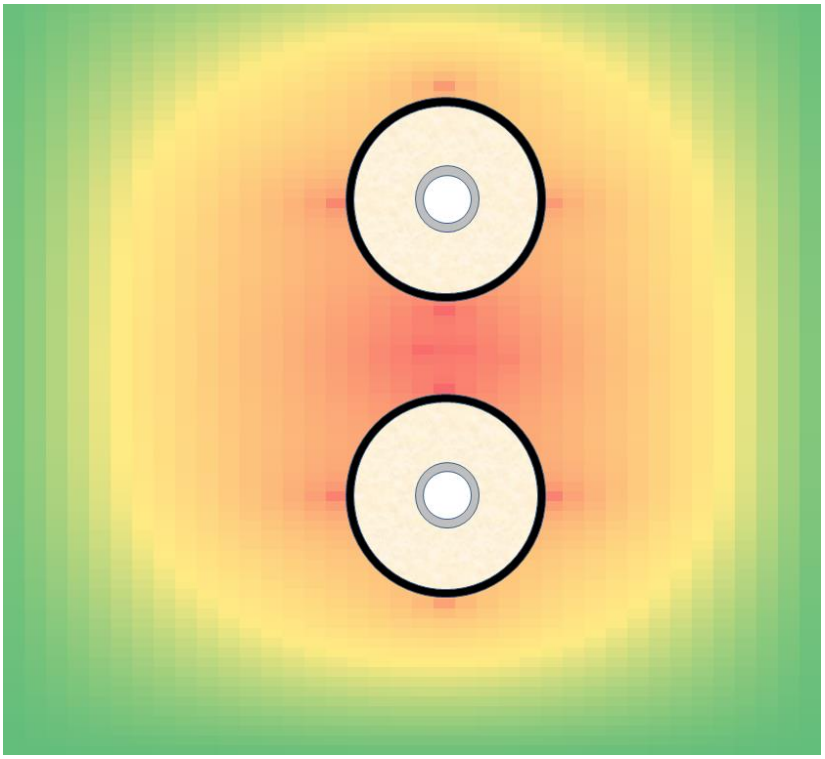

Figure. 9.18 The temperature distribution in the soil for DN40 configuration.

The temperature values DN40 preinsulated pipe system are shown in the Table 9.11.

Table 9.11. The measured temperature from the sensor no 3 – no 16 – DN40

Sensor No.	Measured temperature value [℃]	Arrangement position
No.3	20.5	Supply pipe
No.4	17.0	
No.5	19.2	
No.6	19.3	
No.9	20.3	Distance between supply and return pipes
No.10	19.8	
No.11	18.6	
No.12	18.5	
No.13	17.4	Return pipe
No.14	20.4	
No.15	18.6	
No.16	17.5	

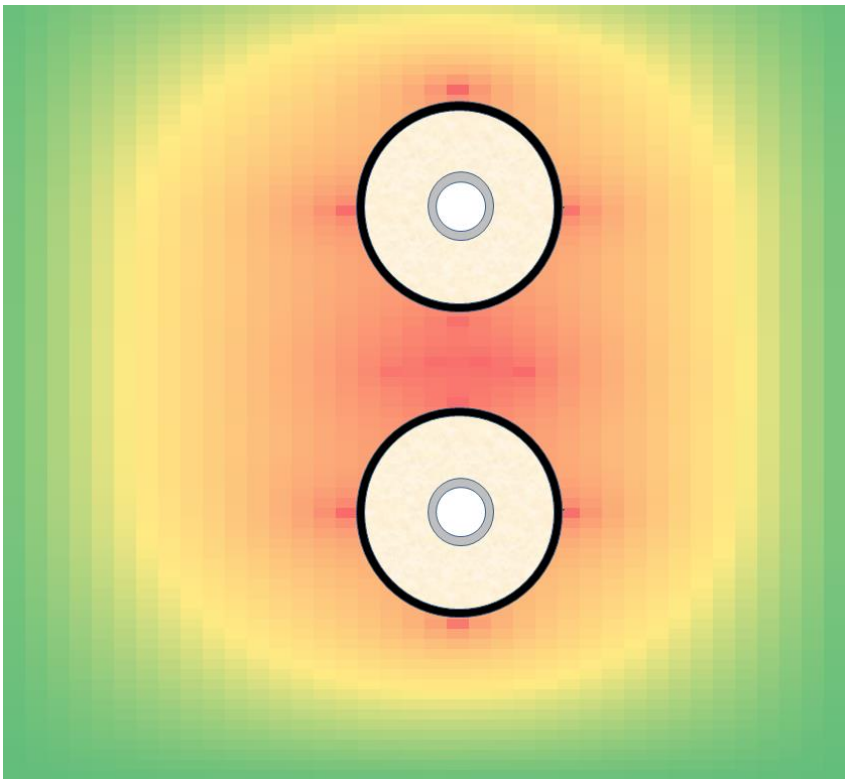

Figure 9.19 The temperature distribution in the soil for DN50 configuration.

The temperature values obtained for DN50 preinsulated pipe system are shown in the Table 9.12.

Table 9.12. The measured temperature from the sensor no 3 – no 16 – DN50

Sensor No.	Measured temperature value [℃]	Arrangement position
No.3	25.5	Supply pipe
No.4	24.3	
No.5	25.1	
No.6	25.6	
No.9	25.3	Distance between supply and return pipes
No.10	25.7	
No.11	25.6	
No.12	24.6	
No.13	25.8	Return pipe
No.14	25.1	
No.15	24.8	
No.16	25.4	

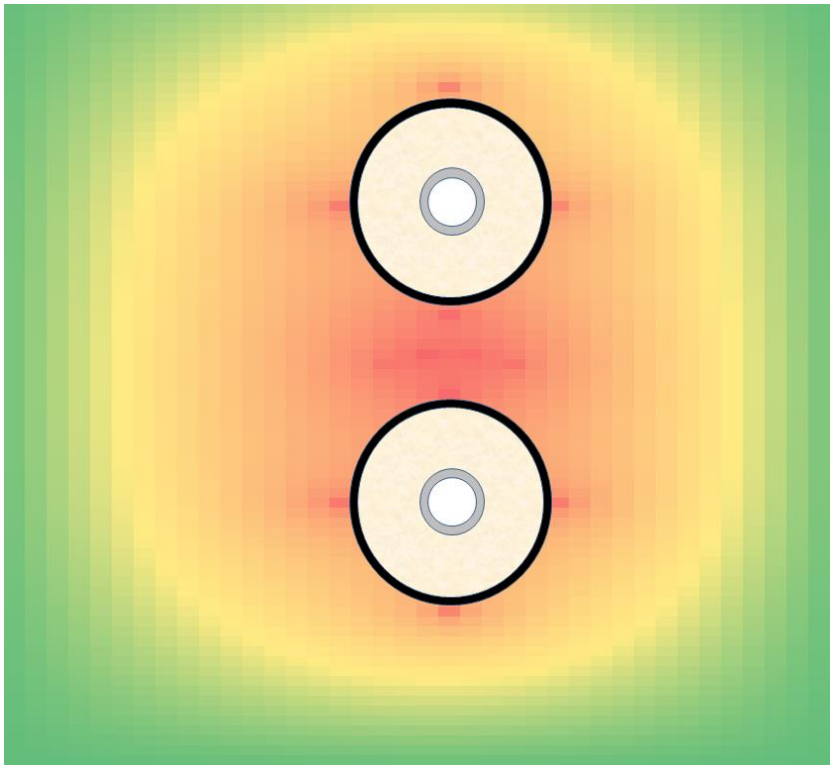

Figure 9.20 The temperature distribution in the soil for DN65 configuration.

The temperature values obtained for DN65 preinsulated pipe system are shown in the Table 9.13.

Table 9.13. The measured temperature from the sensor no 3 – no 16 – DN65

Sensor No.	Measured temperature value [℃]	Arrangement position
No.3	24.4	Supply pipe
No.4	22.2	
No.5	22.8	
No.6	23.1	
No.9	24.5	Distance between supply and return pipes
No.10	24.2	
No.11	23.3	
No.12	23.2	
No.13	22.0	Return pipe
No.14	24.1	
No.15	21.7	
No.16	22.7	

The average value of the temperature between supply and return pipe (no.9 – no.12) is 23.8 ℃.

The temperature distributions for TwinPipe systems are shown in Figures 9.21 – 9.23:

Sensors No. 3 - No. 6 are sensors recording the temperature on the outer surface

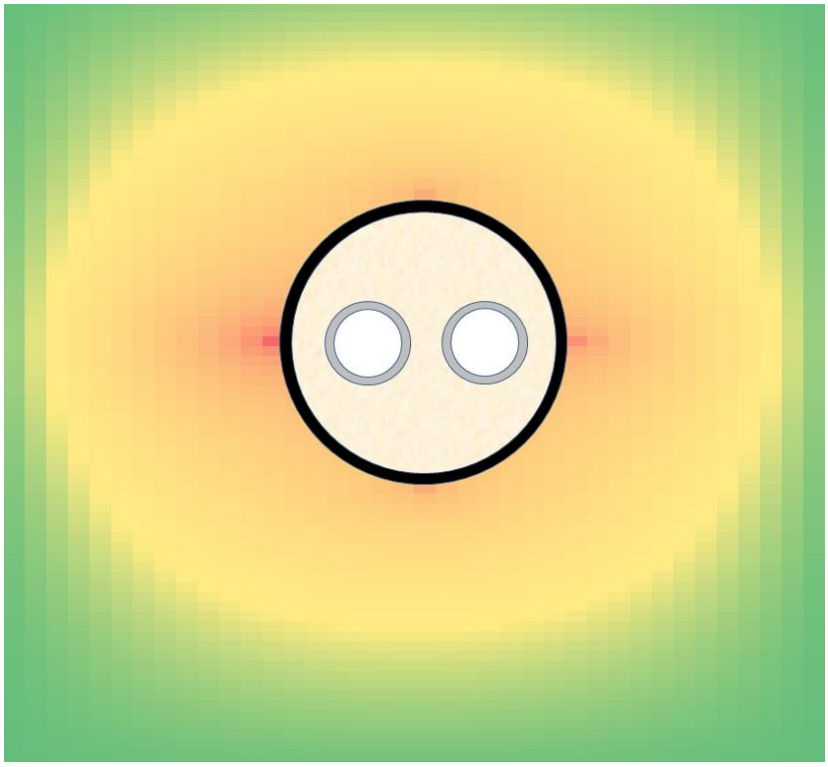

Figure 9.21 The temperature distribution in the soil for DN40 TwinPipe configuration.

The temperature values for DN40 TwinPipe system are shown in the Table 9.14.

Table 9.14 The measured temperature from the sensor no 3 – no 16 – DN40 TwinPipe

Sensor No.	Measured temperature value [℃]	Arrangement position
No.3	20.3	Supply and return pipe
No.4	20.4	
No.5	25.3	
No.6	22.4	

The temperature gradient (5.0 ℃) is between point no.5 (the supply pipe) and no.3 (top of the pipe).

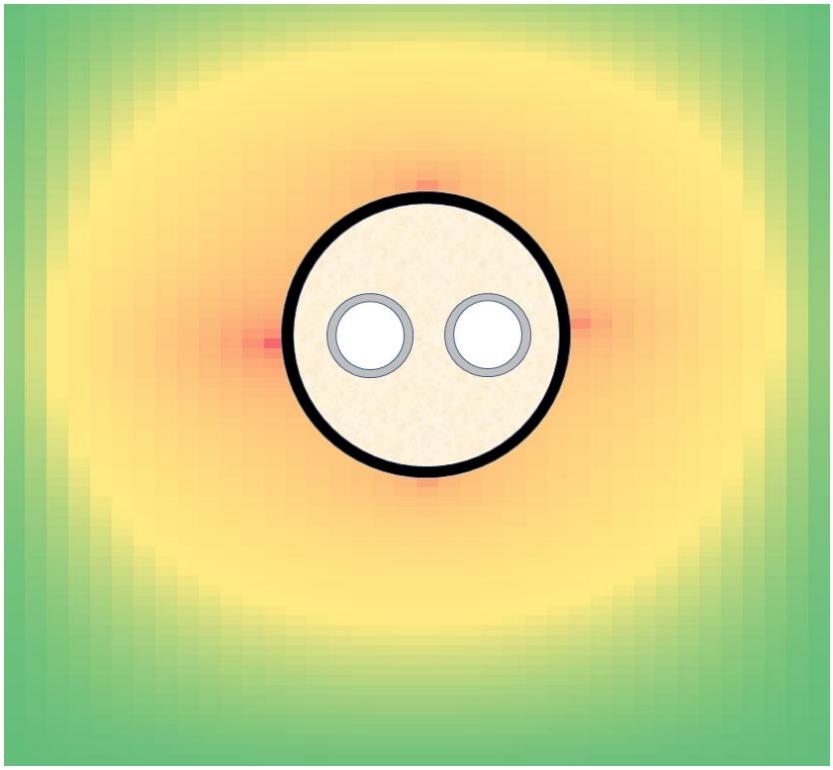

Figure 9.22 The temperature distribution in the soil for DN50 TwinPipe configuration

The temperature values are shown in the Table 9.15.

Table 9.15. The measured temperature from the sensor no 3 – no 16 – DN50 -TwinPipe

Sensor No.	Measured temperature value [℃]	Arrangement position
No.3	15.2	Supply and return pipe
No.4	14.6	
No.5	17.8	
No.6	15.6	

The temperature gradient (3.2 ℃) is between point no.5 (the supply pipe) and no.4 (the return pipe).

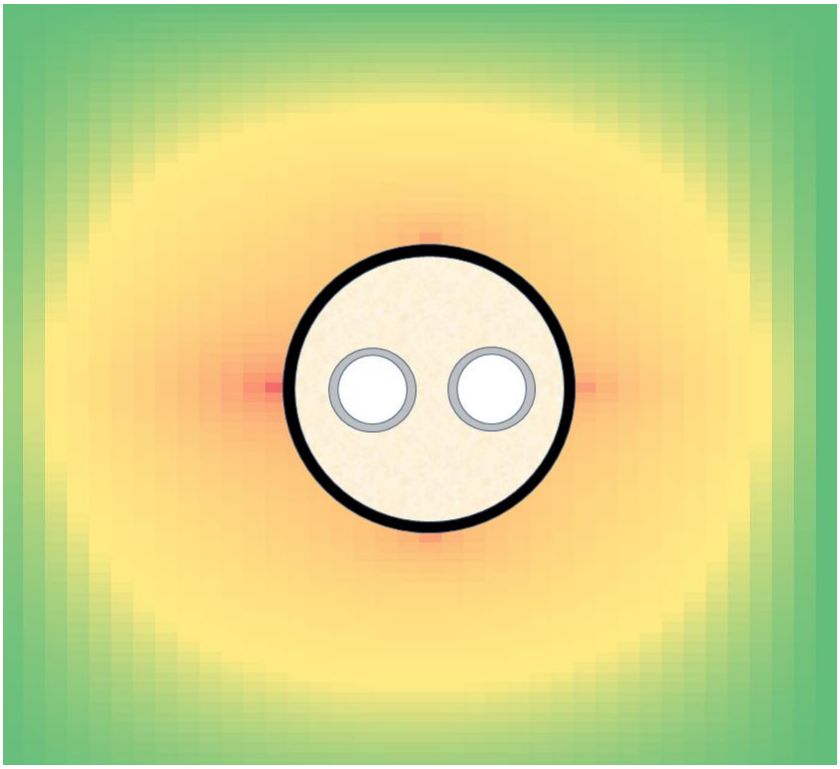

Figure 9.23 The temperature distribution in the soil for DN65 TwinPipe configuration

The temperature values are shown in the following table:

Table 9.16. The measured temperature from the sensor no 3 – no 16 – DN65 -TwinPipe

Sensor No.	Measured temperature value [℃]	Arrangement position
No.3	14.0	Supply and return pipe
No.4	14.5	
No.5	17.3	
No.6	14.7	

The temperature gradient (3.3 ℃) is between point no.5 (the supply pipe) and no.3 (top of the pipe).

9.4 Temperature distribution results comparison

The comparison of temperature distribution results from CFD calculations are comparted with results from laboratory measurements are presented in Tables 9.17 – 9.22

Table 9.17. The average temperature recorded on experimental stand for single configuration (DN40+DN40) compared with CFD simulation

		CFD	Lab. Station	Dev.[%]
Temperature of the soil between pipes [°C]	No.9	21.55	20.80	3.48
	No.10	21.55	20.55	4.64
	No.11	21.05	19.55	7.13
	No.12	21.25	19.90	6.35
Ave. Temp. of soil [°C]	-	21.35	20.75	2.81

Table 9.18. The average temperature recorded on experimental stab. for single configuration (DN50+DN50) compared with CFD simulation

		CFD	Lab. Station	Dev.[%]
Temperature of the soil between pipes [°C]	No.9	25.85	25.30	2.13
	No.10	25.85	25.75	0.39
	No.11	25.55	25.60	-0.20
	No.12	25.55	24.60	3.72
Ave. Temp. of soil [°C]	-	25.70	25.30	1.56

Table 9.19. The average temperature recorded on experimental stab. for single configuration (DN65+DN65) compared with CFD simulation

		CFD	Lab. Station	Dev.[%]
Temperature of the soil between pipes [°C]	No.9	25.25	24.50	2.97
	No.10	25.35	24.25	4.34
	No.11	24.55	23.30	5.09
	No.12	24.65	23.20	5.88
Ave. Temp. of soil [°C]	-	24.95	23.80	4.61

Table 9.20. The average temperature recorded on experimental stab. for TwinPipe configuration (DN40+DN40) compared with CFD simulation

		CFD	Lab. Station	Dev.[%]
Temperature of the soil on the pipe surface [°C]	No.3	21.35	20.30	4.92
	No.4	21.45	20.40	4.90
	No.5	26.75	25.30	5.42
	No.6	22.85	22.40	1.97
Ave. Temp. of soil [°C]	-	23.10	22.70	1.73

Table 9.21. The average temperature recorded on experimental stab. for TwinPipe configuration (DN50+DN50) compared with CFD simulation

		CFD	Lab. Station	Dev.[%]
Temperature of the soil on the pipe surface [°C]	No.3	16.85	15.20	9.79
	No.4	16.75	15.30	8.66
	No.5	19.55	17.80	8.95
	No.6	17.45	15.60	10.60
Ave. Temp. of soil [°C]	-	17.65	16.00	9.35

Table 9.22. The average temperature recorded on experimental stab. for TwinPipe configuration (DN65+DN65) compared with CFD simulation

		CFD	Lab. Station	Dev.[%]
Temperature of the soil on the pipe surface [°C]	No.3	15.75	14.00	11.11
	No.4	15.75	14.50	7.94
	No.5	19.05	17.30	9.19
	No.6	16.45	14.90	9.42
Ave. Temp. of soil [°C]	-	16.75	15.20	9.25

10. Economical analysis

In this chapter, the economic calculations of the use of two analysis in the thesis pipe system will be presented: the single pre-insulated pipe system and the TwinPipe system.

The cost-effectiveness of the TwinPipe system is compared with the single pre-insulted pipe system. The model presented in the previous chapters will determine the heat losses for district heating network pipes under real conditions. The daily heat losses will be determined on the basis of the daily supply and return temperatures (from 1st January to 31st December 2021) in underground heating network. These data were obtained from MPEC (Municipal Heat Distribution Company) in Krakow.

The daily temperature of air, supply and return water in pipe are presented in Fig. 10.1

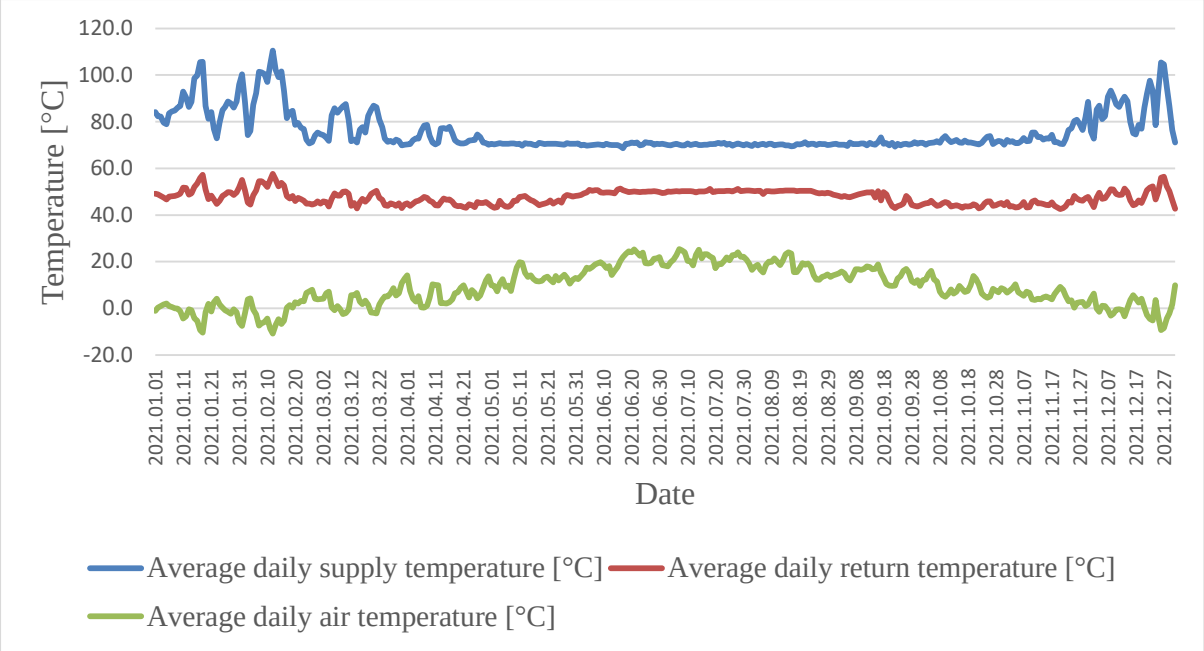

Figure 10.1. The average daily temperature of: air, supply and return of water in the pipe

During the heating period - when the lowest outdoor temperatures are recorded - we can easily observe the highest temperatures.

Economic efficiency indicators can be divided into two types:

- ✓ static (the changing value of money over time is not taken into account) :
  - SPBT (short payback time)
- ✓ dynamic (the changing value of money over time is taken into account)
  - NPV (net present value)
  - NPVR (net present value ratio)
  - IRR (internal rate of return)
  - DPBT (dynamic payback time)

The SPBT is the simplest method to calculated profitability of the investment. It is calculated by:

$$SPBT = \frac{\Delta I}{\Delta E} \quad [-] \tag{10.1}$$

ΔI – investment cost differential [PLN]

ΔE - reducing cost of energy losses [PLN]

The net present value (NPV) method is used to calculate the profitability of the investment. This is a dynamic method. It is based on a discounted cash flow analysis using an assumed discount rate. The NPV value is calculated from equation:

$$NPV = \sum_{i=0}^{t} \frac{CF_i}{(1+r)^t} \quad \text{[PLN]} \tag{10.2}$$

where:

CF_i – cash flow at the time i

r – discount rate

t – number of time periods

Cash flow (*CF*) is the sum of cash outflows and cash inflows for an investment or project over a period of time.
The profitability of the solution analysed is indicated by a positive NPV, and a negative NPV indicates the unprofitability of investing in a more expensive solution.
The ratio of NPV to present value of the investment is called NPVR and is calculated by:

$$NPVR = \frac{NPV}{PVI} \quad \text{[-]} \tag{10.3}$$

PVI - updated value of the investments by time period

The IRR is the discount rate that makes the NPV equal to zero (NPV=0).

$$NPV = \sum_{i=0}^{n} \frac{CF_i}{(1+IRR)^n} = 0 \tag{10.4}$$

The cost-effectiveness of the solution is taken into account if the IRR> cut-off rate. The cut-off rate is usually the interest rate on long-term loans or the rate paid by any borrower. In other words, if the IRR is higher than the cost of raising capital, the greater the difference between the IRR and the cut-off rate, the greater the safety margin and the profitability of a given project. It should be noted that for unusual projects, the IRR may take several values, e.g. if there is a negative cash flow even in the last years and not only in the first years.

The discounted payback time DPBT is defined in a similar way to the static indicator SPBT discussed above. However, it is based on the discounted values of income and expenses. Because of the discounting of cash flows, the payback period is longer in this case, so this indicator provides a more reliable assessment of the profitability of the investment than the static SPBT.

$$DPBT = \frac{\ln(1-r \cdot SPBT)}{-\ln(1+r)} \tag{10.5}$$

Economic calculation results

Three pipe diameters DN40, DN50, DN65 were considered for the economic analysis. Heat losses were calculated using daily flow and return temperatures. The parameters of analysis pipes and ground are presented in section 9.1.

With the aid of the calculation model presented in this paper, the heat loss has been determined for each of the diameters under consideration.

In below Fig. 10.2 – 10.4 is presented daily heat losses in two analysis systems of pipe diameter DN40 (Fig. 10.2) , DN50 (Fig. 10.3), DN65 (Fig. 10.4)

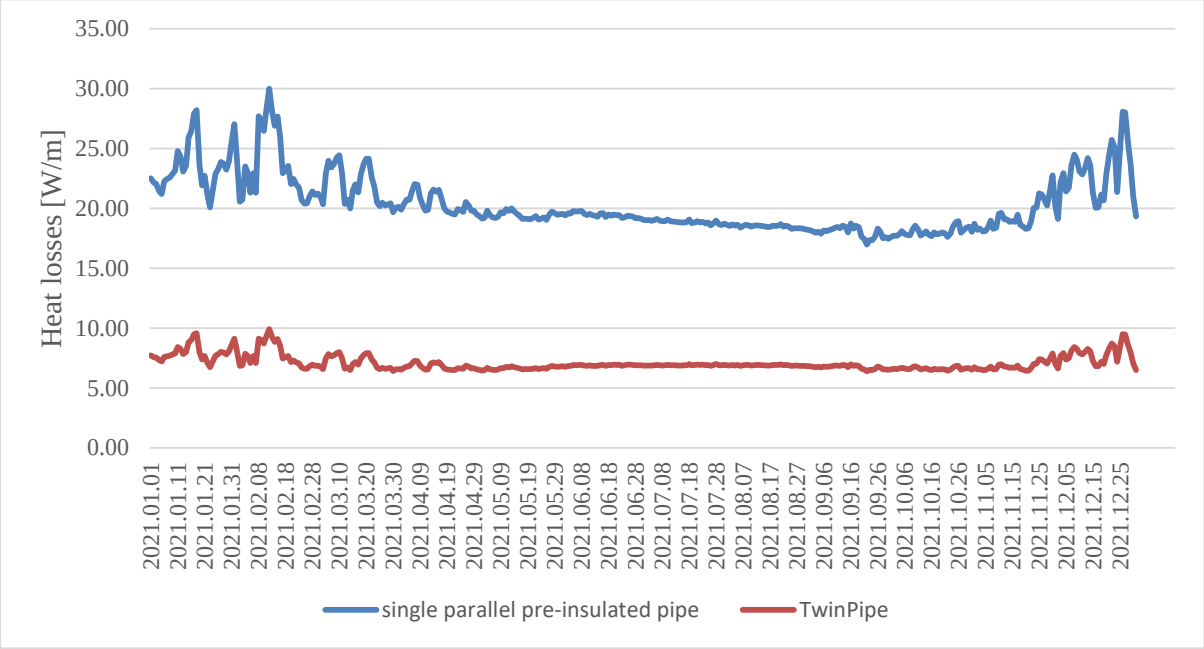

Figure 10.2. The heat losses in single parallel pre-insulated pipe system and TwinPipe system during the year with diameter DN40

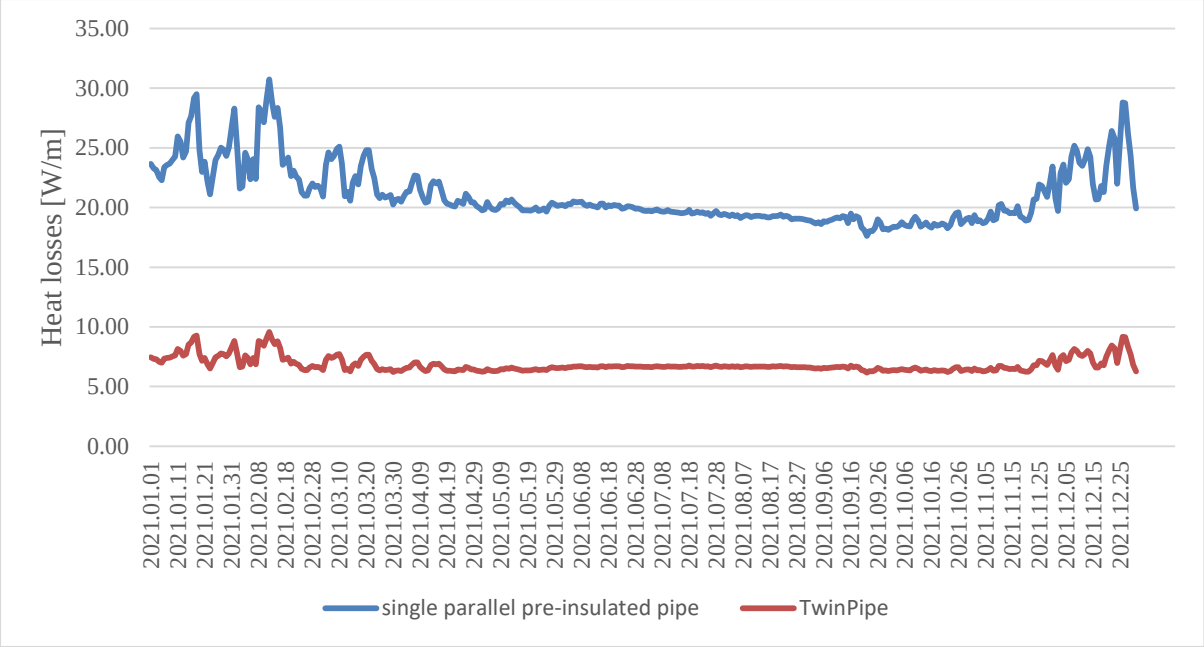

Figure 10.3. The heat losses in single parallel pre-insulated pipe and TwinPipe system during the year with diameter DN50

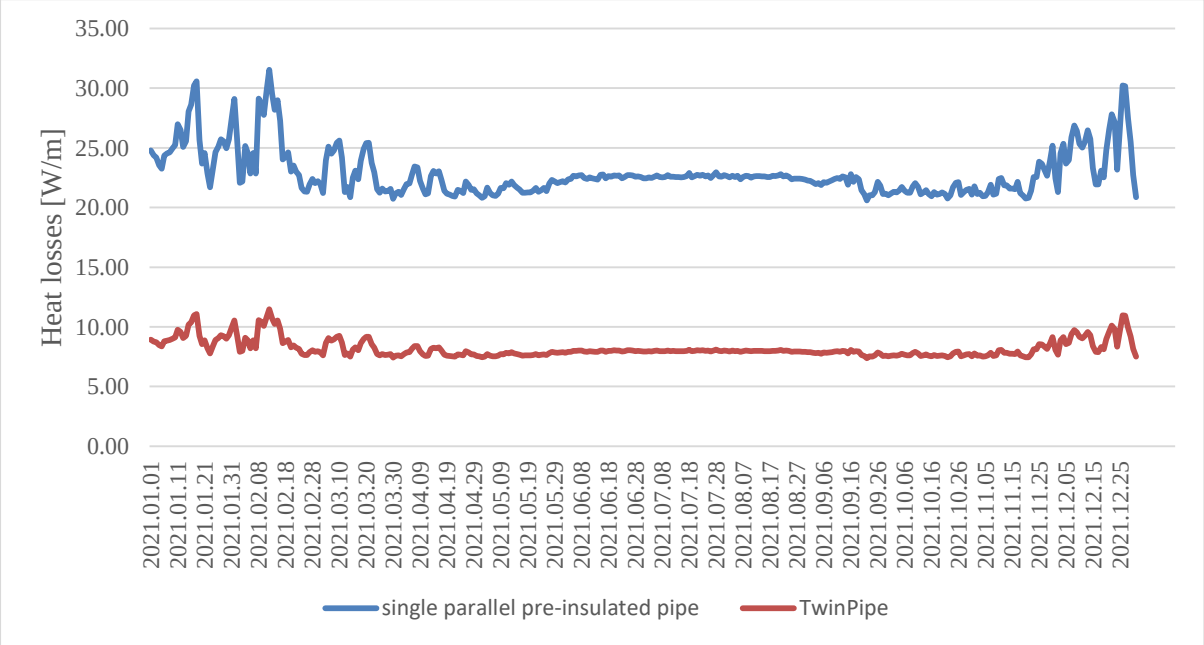

Figure 10.4. The heat losses in single parallel pre-insulated pipe and TwinPipe system during the year with diameter DN65

The total annual heat losses for single parallel system (q_{SP}), for TwinPipe system (q_{TP}) and energy losses for single parallel pre-insulated pipe system (E_{SP}), for TwinPipe system (E_{TP}) are shown in Table 10.1

Table 10.1. The total annual heat and energy losses in pipe diameter DN40, DN50, DN65

DN pipe	q_{SP}, W/m·rok	q_{TP}, W/m·rok	E_{SP}, GJ/ m·rok	E_{TP}, GJ/ m·rok
DN 40	7 673	2 595	0.663	0.224
DN 50	7 858	2 512	0.679	0.217
DN 65	8 401	3 004	0.726	0.260

TwinPipe system shows almost three times less energy loss than single parallel pre-insulated pipe system. The highest heat loss can be seen at DN65 and the lowest at DN40.

The price of heat for further calculations was assumed to be 90 PLN/GJ (in 2023).

The TwinPipe system is a more expensive investment than a single parallel pre-insulated pipe system (from 50% to 100% difference with prices – depends on diameter). The following graphs show how this investment pays off over time for each of the diameters analysed. A discount rate of r = 5% is assumed. The estimated payback period is 15 years.

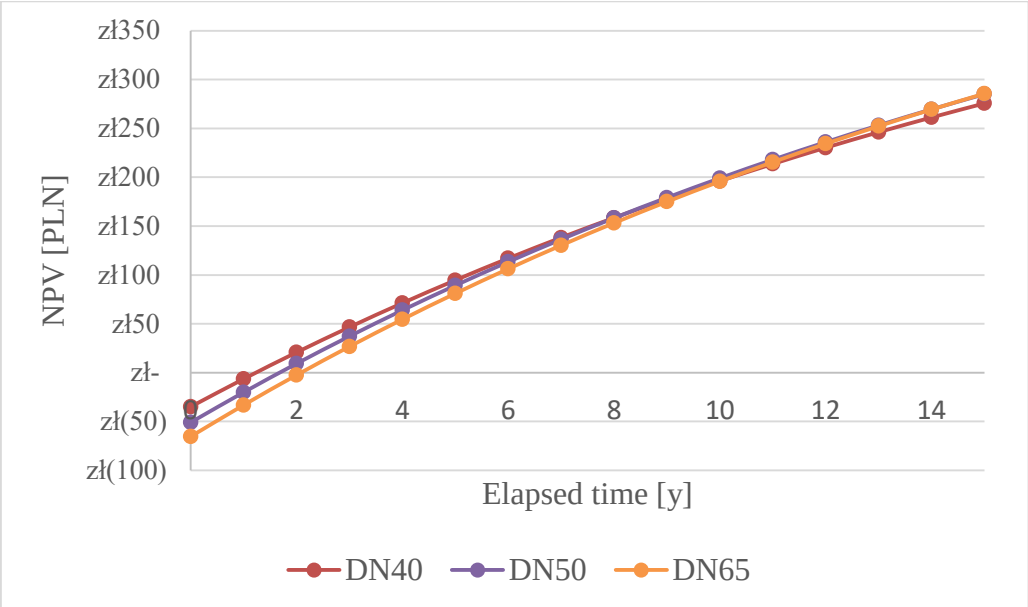

Figure 10.5 The NPV value over the analysis time in different diameter pipe DN40, DN50 and DN65.

The values of economic efficiency indicators are presented in the Table 10.2.

Table 10.2. The value of economic efficiency indicators in pipe diameter DN40, DN50, DN65

DN pipe	NPVR, year	SPBT, year	DPBT, year	IRR, %
DN 40	7.52	0.92	0.93	85.6
DN 50	5.33	1.26	1.33	63.5
DN 65	4.16	1.56	1.66	51.6

The fastest payback time is shown for DN40, slightly longer for DN50 and longest for DN65.It also analyses how the NPV value changes over time with the assumed variable values of the discount rate *r* (Fig. 10.6)

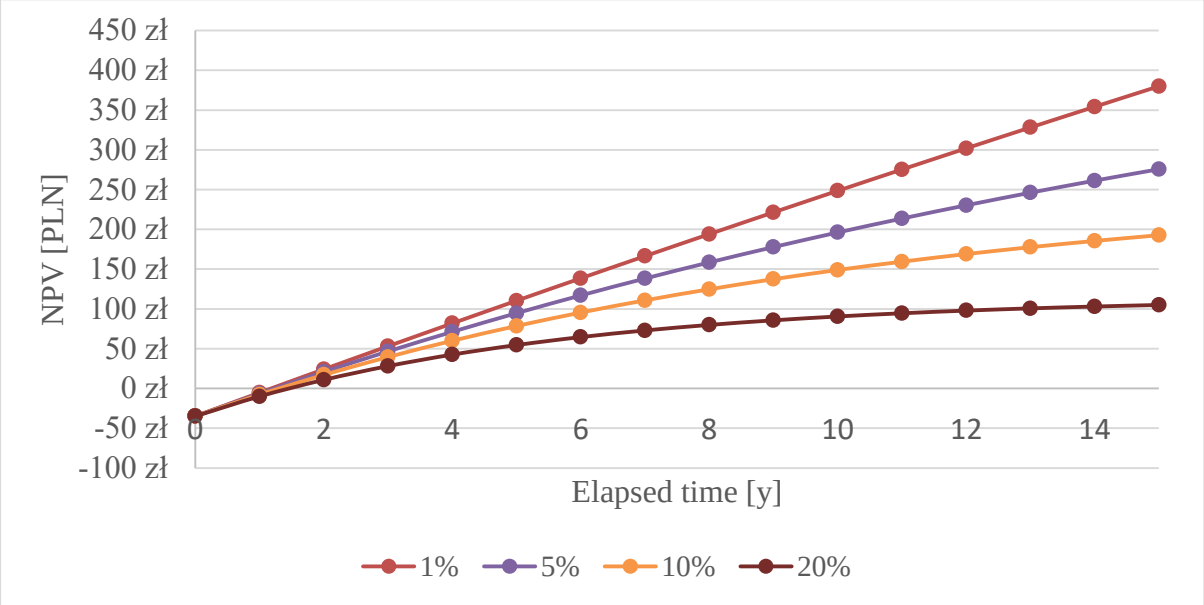

Figure 10.6 The NPV value for replacing single parallel pre-insulated pipe system with TwinPipe system with different discount rate - DN40

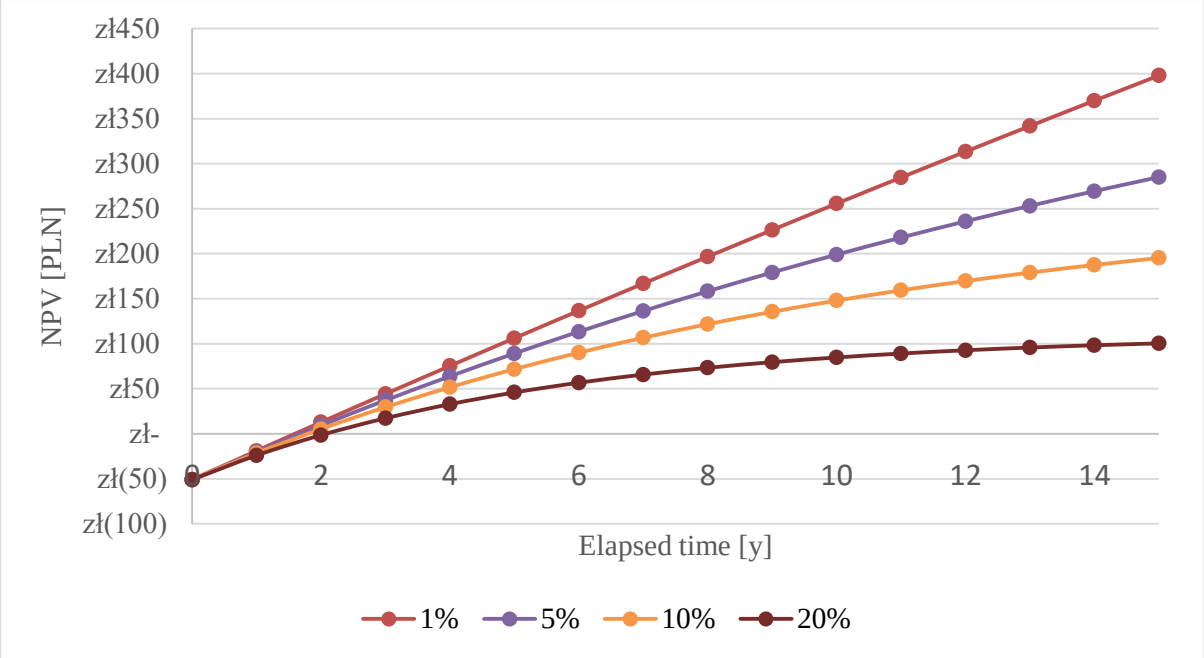

Figure 10.7 The NPV value for replacing single parallel pre-insulated pipe system with TwinPipe system with different discount rate – DN50

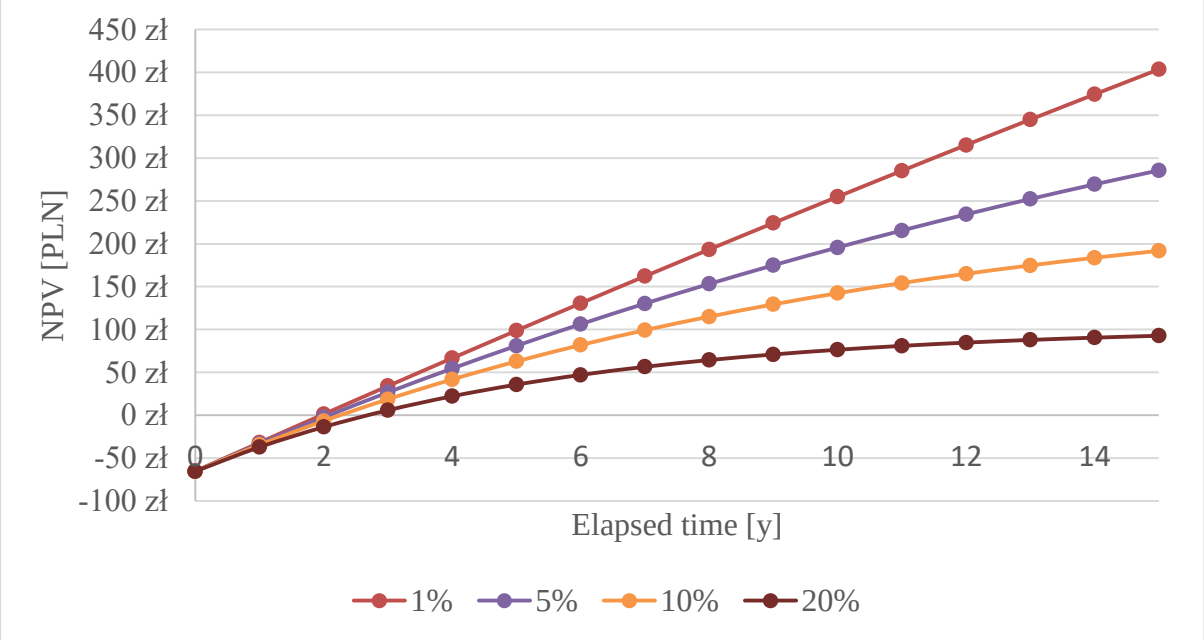

Figure10.8 The NPV value for replacing single parallel pre-insulated pipe system with TwinPipe system with different discount rate – DN65

The changes of NPV value (after the 15 years) with different discount rate with pipe diameter DN40, DN50, DN65 is presented in Fig. 10.9. This indicates an IRR value at a discount

factor value where NPV = 0. The lower the IRR, the higher the net present value and therefore the higher the profit.

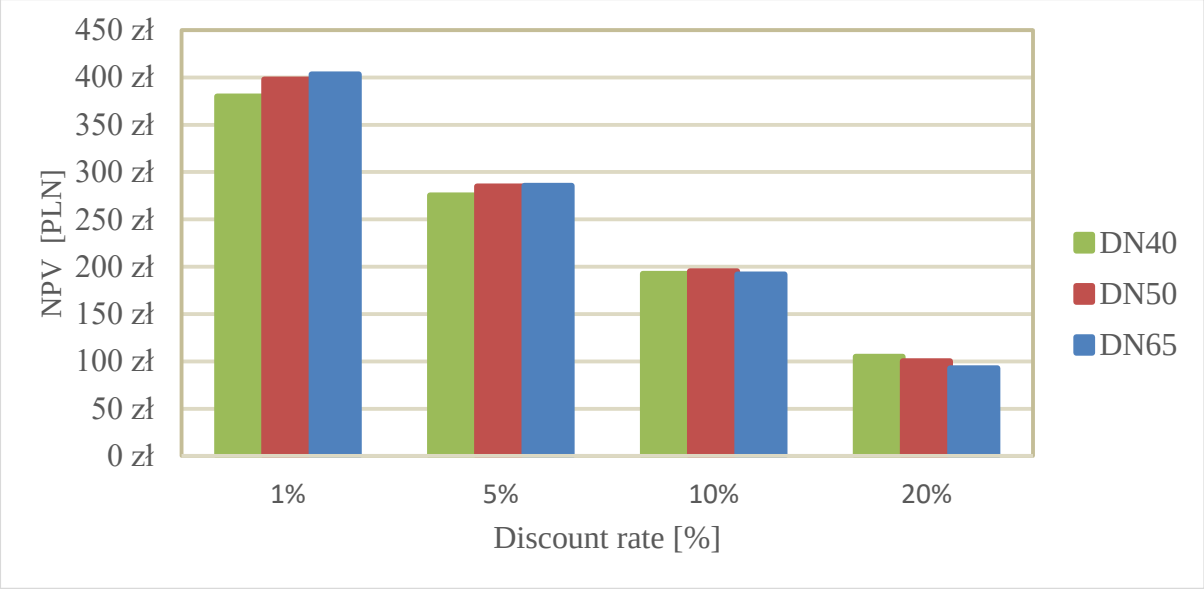

Figure. 10.9 The relationship of NPV value to the discount rate with different DN

The payback time for the TwinPipe system depends mainly on the price of the system. With a parallel single pre-insulated pipe system, you have to buy a supply pipe and a return pipe. TwinPipe is an all-in-one system. As the annual heat loss with this system is almost three times lower than with a parallel single pre-insulated pipe system, the investment is quickly recovered.

11. Summary and conclusions

The thesis proposes mathematical models to simulate heat transfer processes - heat losses in underground district heating networks for two types of systems - a system of single parallel pre-insulated pipes and a TwinPipe system. The proposed model makes it possible to determine the heat losses along the length of these systems and to compare the cost effectiveness of the use of each of the systems analysed.

The first part of the paper presents an analytical (1D) heat transfer model to determine heat losses for district heating networks for both analysed systems. A steady-state (2D) numerical model was then developed using the finite element method. In this model, convective heat flow was added through the finite element boundaries at the surface of both the supply and return pipes. The Kusua and Achenbach model was used as a boundary condition in the heat

transfer simulation for the undisturbed temperature distribution in the ground. The temperature distribution in the surrounding soil was determined by CFD analysis.
The heat loss values from the two models were compared with the test bench measurements. The relative error between the computational and experimental models used is less than 10%. The difference between the analytical approach and the experimental solution is about 7% for the single pre-insulated pipe system and about 5% for TwinPipe system. In contrast, the same relative error between the numerical approach used and the experimental solution is about 9% for the single parallel pre-insulated pipe system and about 5% for the TwinPipe system.

In the last chapter, an economic model is added to determine the profitability of using one of the two analysed underground district heating systems.

The thesis has been achieved. The results of the specific heat losses from the analytical model, a numerical model based on the finite element method, were compared with the experimental results. The agreement of these results was achieved in the range of 3-10%. In addition, the temperature distribution in the ground for both types of heat pipes (single pre-insulated pipe system and TwinPipe) was determined experimentally and by CFD. The results of these calculations also showed good agreement.

The mathematical model of heat losses in the heating network is adopted to select the most economically beneficial solution for the three heating networks connecting the underground storage tank and heat pump for the RESHeat system [76]. The heat exchange model with economic analysis proposed in the paper can be used as an important model for the design of district heating networks, their modernisation and the profitability of using different types of networks. There is even the possibility of extending this to overhead district heating systems.

References

1. Wiltshire R.: *Advanced District Heating and Cooling (DHC) Systems*. Woodhead Publishing (Elsevier), Energy, **2016**
2. Goater A., Squires J.: *Carbon Footprint of Heat Generation*, Number 523 May **2016**, Palimentary office of science & technology
3. Lidberg T., Olofsson T., Ödlund L.: *Impact of Domestic Hot Water Systems on District Heating Temperatures*.
4. Schmidt D., Kallert A., Blesl M., Svendsen S., Li H., Nord N., Sopila K.: *Low Temperature District Heating for Future Energy Systems*. Energy, 116, **2017,** pp. 26-38
5. Lund H., Werner S., Wiltshire R., Svenden S., Thorsen J.E., Hvelplund F., Mathiesen B. V.: *4th Generation District Heating (4GDH): Integration smart thermal grids into future sustainable energy systems*. Energy, 65 April **2014**, pp. 1-11
6. Frederiksen S., Werner S.: *District Heating and Cooling*. Studentlitteratur, Lund **2013**
7. Liescheidt S.: *High Temperature Water Heating Systems*. Course No: M03-006
8. Mathiesen B.V., Lund H., Connolly D.: *Limiting biomass consumption for heating in 100% renewable energy systems.* Energy, 48 (1) Dec. **2012**, pp. 160-168
9. Dobos L, Abonyi J.: *Controller tuning of district heating networks using experiment design techniques*. Energy, 2011, pp. 36:4633
10. Bøhm B., Kristjansson H.: *Single, twin and triple buried heating pipes: on potential savings in heat losses and* costs, International Journal of Energy Research 29, 14, 1301–1312, **2006**.
11. Chen K., Hu, J., Yu L., Zheng M., Sun S., He D., & Lin, J.: *A data-driven model of pipe diameter and insulation thickness optimization for district heating systems.* Paper presented at the Journal of Physics: Conference Series, , 2166(1), **2022**
12. Chicherin S.; Mašatin V.; Siirde A.; Volkova A.: *Method for Assessing Heat Loss in A District Heating Network with A Focus on the State of Insulation and Actual Demand for Useful Energy*. *Energies* **2020**, *13*, 4505.
13. Usman M., & Kim, Y.: *Pipe insulation evaluation for low-temperature district heating implementation in South Korea*. Frontiers in Energy Research, 9, **2022.**
14. Pirouti M., Bagdanavicius A., Ekanayake J., Wu J.; Jenkins N.: *Energy consumption and economic analyses of a district heating network*. Energy **2013**, 57, 149–159.

15. Neirotti F., Noussan M., Riverso S., Manganini G.: *Analysis of different strategies for lowering the operation temperature in existing district heating networks*. Energies **2019**, 12, 321.
16. Nikiforova T., Savytskyi M., Bosschaerts W., Belarbi R.: *Methods and Results of Experimental Researches of Thermal Conductivity of Soils*. Energy, December **2013**, 42, 775 - 783
17. Lund, H. Duic N., Østergaard P.A., Mathiesen B.V.: *Future district heating systems and technologies: On the role of smart energy systems and 4th generation district heating*. Energy **2018,** 165, 614–619.
18. Lund H., Østergaard P.A., Chang M., Werner S. Svendsen S., Sorknæs P., Thorsen J.E.; Hvelplund F., Mortensen B.O.G., Mathiesen B.V.: *The status of 4th generation district heating: Research and results*. Energy **2018**, 164, 147–159.
19. Wirtz M., Kivilip L., Remmen P., Müller D.: *5th Generation District Heating: A novel design approach based on mathematical optimization*. Appl. Energy 2020, 260, 114158.
20. Quaggiotto D., Vivian J., Zarrella A.: *Management of a district heating network using model predictive control with and without thermal storage*, Vol.:(0123456789). Optimization and Engineering 22:1897–191
21. Bilardo M., Sandrone F., Zanzottera G., &Fabrizio E.: *Modelling a fifth-generation bidirectional low temperature district heating and cooling (5GDHC) network for nearly zero energy district (nZED).*Energy Reports, 7, 8390-8405, **2021**
22. Gross M., Karbasi B., Reiners T., Altieri L., Wagner H. Bertsch V.: *Implementing prosumers into heating networks.* Energy, 230, **2021**
23. Zhu T., Ommen T., Meesenburg W., Thorsen J. E., &Elmegaard B.: *Steady state behavior of a booster heat pump for hot water supply in ultra-low temperature district heating network*. Energy, 237, **2021.**
24. Krawczyk, D.A.: *Theoretical and real effect of the school's thermal modernization—A case study*. Energy Build. **2014**, 81, 30–37
25. Krawczyk, D.A., Teleszewski T.J.: *Reduction of heat losses in a pre-insulated network located in centralPoland by lowering the operating temperature of the water and the use of egg-shaped thermal insulation*: A case study. Energies **2019**, 12, 2104
26. Kim J., Kim Y. S., Kim H. Yoon J.: *Effect of operating temperature conditions in 21-year-old insulated pipe for a district heating network*. Case Studies in Thermal Engineering, 27, **2021**,

27. Wang H., Meng H., Zhu T.: *New model for onsite heat loss state estimation of general district heating network with hourly measurements*, Energy Conversion and Management 157:71-85, **2018.**
28. Sartor K., Dewalef P.: *Experimental validation of heat transport modelling in district heating networks*, Energy, **2017**, vol. 137, issue C, 961-968
29. Zhang S., Gu W., Lu H., Qiu H., Lu S., Wang D., Liang J., Li W.: *Superposition-principle based decoupling method for energy flow calculation in district heating networks*. Applied Energy, 295, **2021**
30. Teleszewski T.J., Krawczyk D.A.; Rodero *A.*: *Reduction of Heat Losses Using Quadruple Heating Pre-Insulated Networks: A Case Study*. Energies 12 (24):4699, **2019**
31. Zhang Z., Wang P., Jiang P., Liu Z., & Fu L.: *Energy management of ultra-short-term optimal scheduling of integrated energy system considering the characteristics of heating network*. Energy, 240, **2022.**
32. Triebs M. S.,Tsatsaronis, G.: *From heat demand to heat supply: How to obtain more accurate feed-in time series for district heating systems*. Applied Energy, 311, **2022**
33. Zheng X., Sun Q., Wang Y., Zheng L., Gao X., You S., Zhang H., Shi K.: *Thermo-hydraulic coupled simulation and analysis of a real large-scale complex district heating network in Tianjin*. Energy, 236, **2021**
34. Nowak-Ocłoń M., Ocłoń P.: *Thermal and economic analysis of preinsulated and twin-pipe heat network operation,* Energy, Volume 193**, 2020**.
35. Ocłoń P, Nowak-Ocłoń M., Vallati A., Quintino A., CorcioneM.: *Numerical determination of temperature distribution in heating network*, Energy, Volume 183, Pages 880-891, **2019.**
36. Szkarowski A. Łatowski L.: Ciepłownictwo. Wydawnictwo WNT **2014**
37. Kersten M.S.: *Thermal Properties of Soils. Bulletin 28, Engineering Experiment Station,* Minneapolis: University of Minnesota, **1949**.
38. Gemant, A.: *How to compute thermal soil conductivities*. Heating Piping and Air Conditioning, **1952**
39. Van Rooyen M., H. Winterkorn, *Structural and Textural Influences on Thermal Conductivity of Soils* in Highway Research Board Proceedings, vol. 39, 576, **1957**
40. de Vries DA *Thermal properties of soils*. In: van Wijk WR.: (ed) Physics of plant environment. North-Holland Publishing Company, Amsterdam, pp 210–235, **1963**

41. Johansen O.: *Thermal conductivity of soils*. University of Science and Technology Trondheim, **1975**
42. Campbell GS.: *Soil physics with BASIC*. Elsevier, Amsterdam, pp 221–234, **1985**
43. Ewen J, Thomas HR.: *The thermal probe-a new method and its use on an unsaturated sand*. Géotechnique 37(1):91–105, **1987**
44. Côté J, Konrad JM.: *A generalized thermal conductivity model for soils and construction materials*. Can Geotech J 42(3):443–45, **2005**
45. Lu S. Ren TS, Gong YS, Horton R.: An improved model for predicting soil thermal conductivity form water content at room temperature. Soil Science Society of America Journal 71(1):8-14, **2007**
46. Chen S.X., Thermal conductivity of sands, Heat and Mass Transfer, 44(10), 1241, **2008**
47. Lu YL., Lu S., Horton R., Ren TS. *An empirical model for estimating soil thermal conductivity from texture, water content, and bulk density*. Soil Science Society of America 78(6):1859–1868, **2014**.
48. Nikolaev I.V., Leong W.H. & Rosen M.A. *Experimental Investigation of Soil Thermal Conductivity Over a Wide Temperature Range*. International Journal Thermophys 34, 1110–1129, **2013**
49. Nikoosokhan S., Nowamooz H., Chazallon C.: *Effect of dry density, soil texture and time-spatial variable water content on the soil thermal conductivity*. Geomech Geoeng 11(2):149–158, **2015**
50. Su L.J., Wang Q.J., Wang S., Wang W.H.: *Soil thermal conductivity model based on soil physical basic parameters.* Trans Chin Soc Agr Eng 32(2):127–133 (In Chinese), **2016**
51. He H., Zhao Y., Dyck M.F. et al. *A modified normalized model for predicting effective soil thermal conductivity.* Acta Geotech. 12, 1281–1300, **2017**.
52. Ren J., Men L., Zhang W.: et al. *A new empirical model for the estimation of soil thermal conductivity.* Environ Earth Sci 78, 361, **2019**.
53. Xiong K., Feng Y., Jin H. et al. *A new model to predict soil thermal conductivity*. Science Rep 13, 10684, **2023**.
54. Wallentén P. *Steady-state heat loss from insulated pipes*. Byggnadsfysik LTH, Lunds Tekniska Högskola,. 197 p, **1991.**

55. Kusuda T., Achenbach P.R.: *Earth Temperature and Thermal Diffusivity at Selected Stations in the United States*; DTIC Document AD0472916; National Bureau of Standards: Gaithersburg, MD, USA, May **1965**.
56. Carson J.E.: *Analysis of soil and air temperatures by fourier techniques*. *J. Geophys. Res.* **1963**, *68*, 2217–2232.
57. Penrod, E., Walton W., Terrell D.: *A method to describe soil temperature variation*. *J. Soil Mech. Found. Div.* **1958**, *84*, 1–21
58. Penrod E., Elliott J., Brown W.: *Soil temperature variation (1952–1956) at lexington, kentucky.* Soil Sci. **1960**, *90*, 275–283.
59. Carslaw H.S.; Jaeger J.C.: *Conduction of Heat in Solids*, 2nd ed.; Oxford Clarendon Press: Oxford, UK, 1959.
60. Sepaskhah A., Boersma L. *Thermal conductivity of soils as a function of temperature and water content.* Soil Sci. Soc. *Am. J.* **1979**
61. Yuan Y., Ji H., Du Y.; Cheng B.: *Semi-analytical solution for steady-periodic heat transfer of attached underground engineering envelope*. Build. Environ. **2008**
62. Márquez A., Martínez B., Gómez M., *Ground Thermal Diffusivity Calculation by Direct Soil Temperature Measurement*. *Application to very Low Enthalpy Geothermal Energy Systems. Sensors* **2016**, *16*, 306
63. Ocłoń P. *Numerical modeling of heat transfer and fluid flow processes with Energy engineering applications, monograph, Cracow University of Technology Publishing Press, no. 516, series Mechanics,* **2015**
64. Mohsen M.F.N.: *Some details of the Galerkin finite element method. Applied Mathematical Modelling*,Volume 6, Issue 3, **1982**
65. Fletcher C.A.J.: *Galerkin Finite-Element Methods. In: Computational Galerkin Methods*. Springer Series in Computational Physics. Springer, Berlin, **1984**.
66. Mitsotakis D., Ilan B., Dutykh D.: *On the Galerkin/Finite-Element Method for the Serre Equations*. *J Sci Comput* 61, 166–195, **2014**.
67. Moukalled F., Mangani L., Darwish M.: *The Finite Volume Method in Computational Fluid Dynamics An Advanced Introduction with OpenFOAM and Matlab* Volume 113, Springer **2015.**
68. Hetnarski R., *Encyclopedia of Thermal Stresses* Springer Science, **2014.**
69. Blazek J., Computational Fluid Dynamics: Principles and Applications, Elsevier, **2004.**
70. LeVeque R. J.: *Finite Volume Methods for Hyperbolic Equations*, Cambridge University Press, **2002**.

71. Ferziger J. H., Peric M., *Computational methods for fluid dynamics, 3'rd edition*, Springer, **2003**
72. Chomicz D. *Woda w ciepłownictwie i ogrzewnictwie*. Arkady, Warszawa **1997**
73. Hamdhan I. N., Clarke B. G.: *Determination of Thermal Conductivity of Coarse and Fine Sand Soils*. Proceedings World Geothermal April **2010**
74. EN 15698 – 1: 2020. District heating pipes – Preinsulated bonded TwinPipe systems for directly buried hot water networks – Part 1: Twin pipe assembly of steel service pipe, polyurethane thermal insulation and outer casting of polyethylene
75. EN 13941:2020. Design and intallation of the preinsualted bonded pipe systems for district heating
76. Jakubek D., Ocłoń P., Nowak-Ocłoń M., Sułowicz M., Varbanov P. S., Klemeš J. J.: *Mathematical modelling and model validation of the heat losses in district heating networks*, Energy, Volume 267, **2023**

Summary

The thesis proposes mathematical models to simulate heat transfer processes - heat losses in underground district heating networks for two types of systems - a system of single parallel pre-insulated pipes and a TwinPipe system. The proposed model makes it possible to determine the heat losses along the length of these systems and to compare the cost effectiveness of the use of each of the systems analysed.

The first part of the thesis presents an analytical (1D) heat transfer model to determine heat losses for district heating networks for both analysed systems. A steady-state (2D) numerical model was then developed using the finite element method. In this model, convective heat flow was added through the finite element boundaries at the surface of both the supply and return pipes. The Kusua and Achenbach model was used as a boundary condition in the heat transfer simulation for the undisturbed temperature distribution in the ground. The temperature distribution in the surrounding soil was determined by CFD analysis.

The following section describes the test site. The various components used in the measurements are discussed. In order to reflect to physical heat losses and temperature distribution in the soil, the experimental laboratory stab was designed. The principle of the operation is based on laminar flow of the heat carrier medium (demoralized water) through supply system (hot pipe) and return system (cold pipe) with simultaneous temperature measurement at the beginning and end of the pipe section. For parallel measurements (single pre – insulated pipes) temperature distribution of the soil between these pipes was recorded. Each of the circuits (hot and cold) is equipped with two separate temperature measurement sensors which control the heating systems, centrifugal pumps and venting system. In order to obtain laminar flow each measured pipe was three meter long. Temperature measurement is automatic with an interval of 2 seconds – 16 sensors were used. Before each trial, verification of the temperature sensor was performed using Almemo 2890-9 equipped with T type thermocouple. A detailed error analysis of the measurement results is also presented. The results presented in the plot of the steady-state inlet and outlet temperature distribution of the pipes. Two type of configuration of the pipe was used and compared (TwinPipe and single pre-insulated pipes) Depending on the nominal diameter (DN40; DN50; DN65) the recorded results are different. As a thermal equilibrium is considered 600 cycles (20 min of recording). Results were compered and presented in tables.

The heat loss values from the two models were compared with the test bench measurements. The relative error between the computational and experimental models used is less than 10%. The difference between the analytical approach and the experimental solution is about 7% for the single pre-insulated pipe system and about 5% for TwinPipe system. In contrast, the same relative error between the numerical approach used and the experimental solution is about 9% for the single parallel pre-insulated pipe system and about 5% for the TwinPipe system.

In the last chapter, an economic model is added to determine the profitability of using one of the two analysed underground district heating systems. It is shown the profitability of using TwinPipe system.

The heat exchange model with economic analysis proposed in the paper can be used as an important model for the design of district heating networks, their modernisation and the profitability of using different types of networks. There is even the possibility of extending this to overhead district heating systems.

Streszczenie

W pracy zaproponowano model matematyczny do symulacji procesów wymiany ciepła w tym wyznaczania strat ciepła w podziemnych sieciach ciepłowniczych dla dwóch rodzajów rur ciepłowniczych: rury preizolowanych pojedynczych ułożonych równoległe względem siebie oraz rury typu TwinPipe. Zaproponowany model umożliwia określenie całkowitych strat ciepła na długości tych przewodów oraz porównanie opłacalności zastosowania każdego z analizowanych rodzajów rur

W pierwszej części pracy przedstawiono analityczny jednowymiarowy model wymiany ciepła w celu określenia strat ciepła w sieciach ciepłowniczych dla obu analizowanych przewodów. Następnie opracowano model numeryczny w stanie ustalonym - dwuwymiarowy przy użyciu metody elementów skończonych. W modelu tym konwekcyjny przepływ ciepła został dodany na powierzchni rur zasilających i powrotnych. Model Kusua i Achenbacha został wykorzystany jako warunek brzegowy w symulacji wymiany ciepła dla niezakłóconego rozkładu temperatury w gruncie. Rozkład temperatury w otaczającej glebie został określony za pomocą analizy CFD.

W kolejnej części pracy opisano stanowisko eksperymentalne, w którym zasymulowano pracę rur ciepłowniczych w gruncie w celu wyznaczenia start ciepłą oraz rozkładu temperatury w gruncie. Zasada działania opiera się na laminarnym przepływie nośnika ciepła (wody zdemoralizowanej) przez przewód zasilający („gorąca rura") i przewód powrotny („zimna rura") z jednoczesnym pomiarem temperatury na początku i na końcu odcinka rury. W przypadku pomiarów z rurami preizolowanymi pojedynczymi rejestrowano dodatkowo rozkład temperatury gruntu pomiędzy tymi rurami. Przedstawiono również szczegółową analizę błędów wyników pomiarów. Wyniki przedstawiono na wykresie rozkładu temperatury na wlocie i wylocie rur w stanie ustalonym. Pomiary wykonano dla różnych średnic nominalnych przewodów (DN40; DN50; DN65).

Wyniki obliczeń z modelu analitycznego i numerycznego porównano z wynikami z pomiarów eksperymentalnych. Względny błąd między zastosowanymi modelami obliczeniowymi i eksperymentalnymi jest mniejszy niż 10%. Różnica między podejściem analitycznym a rozwiązaniem eksperymentalnym wynosi około 7% dla pojedynczego systemu rur preizolowanych i około 5% dla systemu TwinPipe. Z kolei ten sam błąd względny między zastosowanym podejściem numerycznym a rozwiązaniem eksperymentalnym wynosi około 9% dla pojedynczego systemu rur preizolowanych i około 5% dla systemu TwinPipe.

W ostatnim rozdziale dodano model ekonomiczny w celu określenia opłacalności korzystania z jednego z dwóch analizowanych rur stosowanych w systemach ciepłowniczych. Wykazano opłacalność stosowania przewodów typu TwinPipe.

Zaproponowany w artykule model wymiany ciepła z analizą ekonomiczną może być wykorzystany jako ważny model do projektowania sieci ciepłowniczych, ich modernizacji i opłacalności korzystania z rodzajów przewodów. Istnieje nawet możliwość rozszerzenia go na napowietrzne systemy ciepłownicze.